

Dynamics Of Heavy Quarks Produced In Relativistic Heavy Ion Collision

By

MOHAMMED YOUNUS

Enrolment No: PHYS04200904004

Variable Energy Cyclotron Centre, Kolkata

A thesis submitted to

The Board of Studies in Physical Sciences

In partial fulfillment of requirements

For the Degree of

DOCTOR OF PHILOSOPHY

of

HOMI BHABHA NATIONAL INSTITUTE



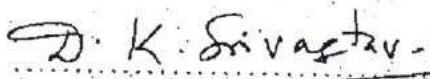
April, 2014

Homi Bhabha National Institute
Recommendation of the Viva Voce Board

As members of the Viva Voce Board, we certify that we have read the dissertation prepared by Mohammed Younus entitled **Heavy Quark Dynamics In Relativistic Heavy Ion Collision** and recommend that it may be accepted as fulfilling the dissertation requirement for the degree of Doctor of Philosophy.

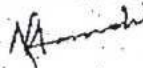

..... Date: 02/4/2014
Chairman- Dr. Rakesh K. Bhandari

..... Date:
Convener/Guide- Dr. Dinesh K. Srivastava

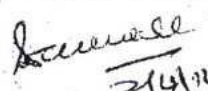

..... Date: 2/4/2014

Member 1- Dr. Asis K. Chaudhuri


..... Date: 2/4/2014

Member 2- Dr. Munshi G. Mustafa 
..... Date: 2/4/2014

..... Date:
Member 3,(External Examiner)- Dr. Sudhir Raniwala

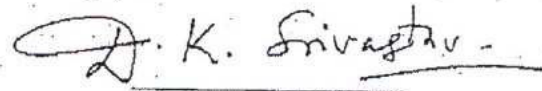

..... Date: 2/4/14

Finally approval and acceptance of this dissertation is contingent upon the candidate's submission of the final copies of the dissertation to HBNI.

I hereby certify that I have read this dissertation prepared under my direction and recommend that it may be accepted as fulfilling the dissertation requirement.

Date: 2/4/2014

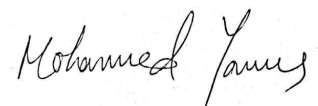
Place: Kolkata


Signature of the Guide

STATEMENT BY AUTHOR

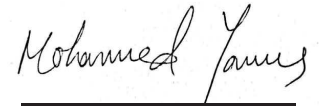
This dissertation has been submitted in partial fulfilment of requirements for an advanced degree at Homi Bhabha National Institute (HBNI) and is deposited in the Library to be made available to borrowers under rules of the HBNI.

Brief quotation from this dissertation are allowable without special permission, provided that accurate acknowledgement of source is made. Requests for permission for extended quotation from or reproduction of this manuscript in whole or in part may be granted by the Competent Authority of HBNI when in his or her judgement the proposed use of the material is in the interests of scholarship. In all other instances, however, permission must be obtained from the author.


Mohammed Younus

DECLARATION

I, hereby declare that the investigation presented in the thesis has been carried out by me. The work is original and has not been submitted earlier as a whole or in part for a degree/diploma at this or any other Institution/University.


Mohammed Younus

Dedicated to the memories of my father, Late Abul kalam Azad

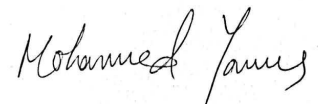
ACKNOWLEDGMENTS

I gratefully acknowledge the constant and invaluable academic and personal support received from my supervisor Dr. Dinesh K. Srivastava throughout my thesis work.

I would very much like to thank, Prof. Bikash Sinha, former Director, VECC and Homi Bhabha Chair, HBNI, DAE, former Director, Prof. Rakesh Kumar Bhandari, VECC, Dr. Santanu Pal, former Head, Theoretical Physics Division, VECC, Dr. Jan-e Alam, VECC, Dr. Sourav Sarkar, VECC, Dr. Munshi G. Mustafa, SINP, Dr. Asis K. Chaudhari, Head, Theoretical Physics Division, VECC, Dr. Tapan K. Nayak, VECC, Dr. Bedangadas Mohanty, NIISER, Dr. A. K. Dubey, VECC, Dr. Subhashish Chattopadhyay, VECC, Dr. Partha Barat, VECC, Prof. Steffen A. Bass, Duke Univ., Prof. Berndt Müller, Duke Univ., US., Dr. Quangyou Qin Wuhan Univ., China, Mr. C. E. Coleman-Smith, Duke Univ., US, Prof. Rainer J. Fries, Texas A&M Univ., Prof. Ralph Rapp, Texas A&M Univ., Texas, US, my colleagues Dr. Umme Jamil, Miss Surasree Mazumder, Mr. Trambak Bhattacharyya, Dr. Nirupam Dutta, Dr. Somanth De and all of my colleagues and predecessors for their useful scientific discussions with me.

I am deeply indebted and grateful to my parents, maternal uncles, grand parents, Mr. Prabir Mazumder, Mrs. Tulana Bhattacharyya, my younger brother and my sisters for their support, love and encouragement during my Ph.D. tenure. Thank you very much. At this moment, I very much remember with gratitude, my father, Late Abul Kalam Azad who was instrumental in building up my limitless confidence and passion for my studies and to produce my best.

I sincerely apologize inadvertent omission of any name from the above list of acknowledgment.


Mohammed Younus



- 1. Name of the Student:** Mohammed Younus
- 2. Name of the Constituent Institution:** Variable Energy Cyclotron Centre
- 3. Enrolment No.:** PHYS04200904004
- 4. Title of the Thesis:** Dynamics of Heavy Quarks Produced in Relativistic Heavy Ion Collisions
- 5. Board of Studies:** Physical Sciences

SYNOPSIS

Introduction:

The interaction of quarks and gluons is governed by the non-abelian gauge theory called Quantum Chromodynamics. Because of the presence of self interaction among gluons and the nature of the strong coupling constant, $\alpha_s(Q^2)$, QCD can be broadly divided into perturbative and non-perturbative regions. The concepts of asymptotic freedom of partons for large Q^2 and infrared slavery at small Q^2 have been some of the most interesting facts of QCD till date.

We now know that in heavy ion collisions, a state of very high temperature and low baryonic density or a state of very high baryonic density and low temperature can be reached, as suggested by Collins & Perry [1]. An extreme condition in which a very small volume in space contains de-confined quarks and gluons and provides us a perfect ground for the application

of QCD. The experiments at RHIC at BNL and LHC at CERN provide opportunities for creating this state of very high temperature and low baryonic density while CBM experiment at FAIR will seek to produce this state at high baryonic density and low temperature. In nature the conditions of the first two experiments were present just a few microseconds after big bang while the last experiment will provide us a peek into the core of neutron stars.

When two heavy nuclei collide with sufficient center-of-mass energies, then the region where they have collided and passed each other or stopped all together, is presumably occupied by matter with energy density $\sim 2-3$ times than nuclear ground state energy density. The region consists of highly energetic de-confined gluons and quarks. The de-confined state of quarks and gluons will perhaps reach a state of thermal equilibrium in a time of order ~ 1 fm/c or less depending on the collision energies. This thermalized state is commonly known as Quark Gluon Plasma. This unique state of matter will survive for a few fermis before collapsing into a state of hadrons. Hence due to such small duration of existence, these experiments pose great difficulties to directly observe and study QGP. However there are some signals which are generated in QGP or probes that travel through this medium and carry the information to us. Theorists on other hand, are using several mathematical calculations and phenomenological models to simulate heavy ion collisions on computing systems and are producing several results and predictions as well as suggesting a few probes such as photons, dileptons, heavy quarks, charged hadrons etc. with signals from QGP like jet quenching, elliptic flow, J/ψ suppression etc. These signals are now being observed with great accuracy by experimentalists and are paving way for future researches. This is certainly a triumph for the QGP scientists all over the world. With a great amount of experimental data already being accumulated and analyzed, the focus is now shifted to accurate theoretical explanations of these results.

Heavy Quark Production:

This thesis is primarily related to heavy quark production and its propagation through QGP. Heavy quarks are mainly produced in very early period of heavy ion collision. Owing to its large mass heavy quark production can be calculated using perturbative QCD techniques. Additionally, the majority of the heavy quarks come from initial gluon fusion during the time of collision. But after the collision and before the deconfined quarks and gluons get thermalized, the secondary partons having large transverse momenta (high p_T jet partons) can interact to produce heavy quark pairs. This may be called jet-jet interaction. Again one of the jets may interact with the thermalized medium to produce heavy quarks. This is called jet conversion in QGP or jet-thermal interaction. Finally, the thermalized partons may interact among themselves to produce heavy quarks, if temperature of the QGP is high and thermal partons possess enough transverse momenta. This may be called thermal production of heavy quark. The production of heavy quark has been calculated using all of these mechanisms [2]. The results showed the relative importance of these secondary mechanisms w.r.t. primary production(initial gluon fusion). However the prompt production of heavy quarks is found to be the dominant process at all collider energies under study. The heavy quark production due to secondary processes was calculated for $\sqrt{s}=200$ GeV/nucleon(RHIC), 2.76 and 5.5 TeV/nucleon(LHC) and comparatively secondary contribution has been found to increase with the increase in collider energies.

As a first step in this thesis, calculation of $Q\bar{Q}$ cross-section has been calculated for proton on proton collision in order to fix the baseline for heavy ion collision. Different partonic structure functions ranging from 'MRS-' series to 'CTEQ-' series have been utilized to check the consistency of calculations. In first place, heavy quark production from proton on proton collision has been calculated with Leading Order pQCD interactions. Subsequently charm and bottom cross-sections have been calculated by including Next-to-Leading order Feynman diagrams. The NLO+LO results are compared with LO contribution multiplied by a k-factor [3]. The comparison between the two are almost identical upto $p_T \approx 20.0$ GeV, for k-factor ranging from 1.5–3.0. While beyond that NLO contribution tend to dominate

the picture and the distributions differ considerably from each other. The LO processes are $gg \rightarrow Q\bar{Q}$, $q\bar{q} \rightarrow Q\bar{Q}$ and while NLO processes included in calculating total $Q\bar{Q}$ cross sections are $gg \rightarrow gQ\bar{Q}$, $q\bar{q} \rightarrow gQ\bar{Q}$, $gq \rightarrow Q\bar{Q}q$ in which one of the final gluons splits (gluon excitation) into heavy quark pair or one of the final Q or \bar{Q} emits gluon (bremsstrahlung).

Heavy Quark Correlation:

This is known that heavy quarks are always produced in pair in agreement with the conservation of flavors in both hadrons and heavy ions collisions. The pairs produced show correlation in rapidity difference of Q and \bar{Q} , $\Delta y = |y_Q - y_{\bar{Q}}|$, or in transverse momentum distribution, $p_{TQ\bar{Q}}$ of pair, or in $\Delta R = \sqrt{\Delta\eta^2 + \Delta\phi^2}$, where one can spot a 'ridge' like structure for $\Delta R < \pi$. Correlation in azimuthal angle difference, $C(\Delta\phi = |\phi_Q - \phi_{\bar{Q}}|)$ of $Q\bar{Q}$, in transverse momentum plane has been also calculated and is one of the possible observable beside transverse momentum distribution and elliptic flow of heavy quark. These features have been initially studied for proton on proton collision. The leading order processes is seen to contribute differently than LO+NLO processes together. Thus, in case of azimuthal correlation, at leading order and zero initial momentum kick, the heavy quark pair would be exactly back-to-back with the correlation function peaking at $\Delta\phi = \pi$ while at NLO, due to emission of gluons either from Q or \bar{Q} or gluon splitting into $Q\bar{Q}$, this back-to-back correlation is lost and the distribution now extends from $\Delta\phi = 0 - \pi$ (from almost collinear to back-to-back $Q\bar{Q}$ pair). In second part, this study has been extended to azimuthal ($\Delta\phi$) correlation of heavy quark pair produced from initial gluon fusion in heavy ion collision. We also know that heavy quark pair is produced in scattering of secondary partons beside its prompt production as discussed in last section. Correlation study has also been extended to $Q\bar{Q}$ produced in secondary mechanisms. It is naively expected that due to azimuthal isotropy of heavy quark distributions in transverse momentum plane (for central collisions only), the correlation distribution must be uniform in entire $\Delta\phi$ region, but the results show exciting correlation patterns instead. Thus the comparison between LO and NLO contributions as well as between pp and AA collision has brought out some interesting features [4].

The study of correlation might provide us a different approach to heavy quark dynamics in QGP and is therefore emerging slowly as one of the most interesting research topic these days.

The effect of QGP medium on charm production and its correlation will now be discussed in the next section.

Medium Effect on Heavy Quark:

Heavy quark can withstand large swarm of light quarks and gluons while passing through QGP and its typical thermalization time has been suggested to be larger than lifetime of QGP. So it is expected that heavy quark can come out with all the effects and information of QGP without itself going much alternations. The experimental results however show that heavy quarks loose energy in QGP almost identically to light quarks and gluons and thus must be subjected to large drag by the medium. Thus studying heavy quark dynamics in QGP is one of the contemporary and most interesting topic in heavy ion collision.

As a first step, effect of flow of the medium on heavy quark correlation has been studied. The model by Cuautle and Paić is based on the effect on a probe particle by the collective flow velocity of the medium and has been implemented in this thesis for heavy quark. For a starter let us consider that a $Q\bar{Q}$ pair is produced at leading order, then both Q and \bar{Q} are exactly back-to-back, moving with momentum, $\vec{p}_{TQ} = -\vec{p}_{T\bar{Q}}$, with velocity $\vec{v}_Q = \pm \vec{p}_{TQ}/M_T$, $M_T = \sqrt{p_T^2 + M_Q^2}$ where M_Q is heavy quark mass. Now if the flow velocity, \vec{v}_f of QGP medium is larger than any of heavy quark velocity, then Q/\bar{Q} whichever is along the flow will be accelerated while one which is opposite might be reversed and back-to-back correlation will be lost. This formalism has been extended to NLO processes included in the calculations. The basic assumption in this calculation is that if heavy quark is thermalized at all, then its azimuthal correlation would be largely affected by the flow of the medium [4]. The calculations have been done by implementing a flow parameter, β_s whose values indicate the

extent of thermalization of heavy quark and has been found to have considerable effect on the correlation distributions.

Next the energy loss by charm has been calculated using two different models. The energy loss by charm has been calculated for both RHIC and LHC temperatures. The first one used is an empirical calculation based on the Wang-Huang-Sarcevic model of energy loss by multiple scattering and has been applied to charm propagating through QGP in this thesis. Two different mechanisms, namely 'BH' and 'LPM' types of energy loss via momentum loss per collision $\propto p_T$ and $\sqrt{p_T}$ respectively, have been implemented in the calculations. Then nuclear modification, ' $R_{AA}(p_T)$ ' and azimuthal anisotropy, $v_2(p_T)$ of charm at RHIC and LHC temperatures and azimuthal correlation, $C(\Delta\phi)$ of charm pair for LHC energies have been calculated. Additionally it is known that light quarks can fragment into one or more types of mesons or baryons, while a charm will mostly fragment into D mesons and finally decay into single non-photonic electron. In experiments, D mesons or non-photonic electrons are observed rather than charm, and thus relevant fragmentation functions based on calculations of C. Peterson et al. and decay functions of Cabibo et al [5]. have been included to give final D mesons and single non-photonic electron distributions. Moreover, this implies a considerable loss in charm energy, and leads to accumulation of charmed mesons in low momentum region giving rise to a characteristic increase in number of low momenta charms, which is unlike the increment due to so called 'Cronin' effect. Our results for R_{AA} & v_2 have been compared with single non-photonic electron data from RHIC and D mesons data from LHC. Consequently the effective drag has been calculated which suggests a large drag experienced by charm quark [6, 7], and this has provided hints that radiative energy loss together with collisional loss might be more applicable than only soft collisions in explaining large charm suppression at RHIC and LHC. In our application of energy loss model in azimuthal correlation study, it has been assumed that charm's direction of propagation does not change much although there is large drag acting on it. Thus integrating over entire momentum region will not show much difference in correlation even if energy loss by charm is considered. However, investigating different p_T regions by imposing cuts, has shown that charms in different

transverse momentum regions show different correlation patterns under similar energy loss conditions.

The second model used is Parton Cascade Model(VNI/BMS) which is based on microscopic Boltzmann transport equation. Now transport equation can be used to transport a system of microscopic particles. The collision term in the transport equation contains invariant matrix elements for all binary scattering ($2 \rightarrow 2$) processes such as $Qg \rightarrow Qg$ and $Qq(\bar{q}) \rightarrow Qq(\bar{q})$, as well as final gluon emission($2 \rightarrow 3$) processes. It helps to describe the full time evolution of QGP as well as any jet particle serving as probe. In this thesis PCM-VNI/BMS calculations have been done and a controlled set of parameters has been implemented which would replicate the probe charm quark evolution in QGP medium. Consequently, energy loss per unit length traversed, dE/dx , momentum broadening or transport coefficient \hat{q} , average energy loss, ΔE , by charm for a temperature ~ 350 MeV, applicable at RHIC energies and also for various charm energies have been calculated. Both collisional energy loss and radiative energy loss (with LPM method) have been included [8]. The resulting average energy loss calculated for charms of various energies can be used to demarcate the radiative and collisional loss sharply. It has been found from the calculations that collisional energy loss due to elastic scattering of gluons and light quarks off charm tends to dominate for lower energy range typically ~ 15 GeV, beyond which radiative loss increase sharply and for larger energetic charm, radiative loss tends to dominate the picture. Moreover, the results for ' dE/dx ' are in good agreement when compared with recent analytical calculations by Shin and Bass, Peigne and Peshier(collisional loss), and R. Abir et al(radiative loss) [9]. The calculations with VNI/BMS has been successfully validated for heavy quark evolution in QGP. Now as next series of calculations, other set of temperatures including those applicable upto highest LHC energies is under progress. Furthermore heavy quark suppression, azimuthal anisotropy and correlation, heavy quark transport coefficients will be calculated in due process.

Bibliography

- [1] J. C. Collins and M. J. Perry, Phys. Rev. Lett. **34**, 1354 (1975).
- [2] Z. Lin and M. Gyulassy, Phys. Rev. C **51**, 512177 (1995); M. Younus and D. K. Srivastava, J. Phys. G: Nucl. Part. Phys., **37**, 115006 (2010).
- [3] U. Jamil and D. K. Srivastava, J. Phys. G: Nucl. Part. Phys., **37**, 085106 (2010).
- [4] M. L. Mangano, P. Nason and G. Ridolfi, Nucl. Phys. B **373**, 295 (1992); M. Younus, U. Jamil and D. K. Srivastava, J. Phys. G: Nucl. Part. Phys., **39**, 025001 (2012); E. Cuautle and G. Paic, arXiv:0604246v2[hep-ph] 2006.
- [5] C. Peterson, D. Schlatter, I. Schmitt and P. M. Zerwas, Phys. Rev. D **27**, 105 (1983); G. Altarelli, N. Cabibo, G. Corbo, L. Maiani and G. Martinelli, Nucl. Phys. B **208**, 365 (1982).
- [6] X-N. Wang, Z. Huang and I. Sarcevic, Phys. Rev. Lett. **77**, 231 (1996); M. Younus and D. K. Srivastava, J. Phys. G: Nucl. Part. Phys. , **39**, 095003 (2012).
- [7] M. Younus and D. K. Srivastava, J. Phys. G: Nucl. Part. Phys. , **40**, 065004 (2013).
- [8] Manuscript titled 'Systematic Study of Charm Quark Energy Loss Using Parton Cascade Model' by M. Younus et al. is under preparation.
- [9] S. Peigné and A. Peshier, arXiv:0802.4362v1[hep-ph] 2008; G. R. Shin, S. A. Bass and B. Müller, J. Phys. G: Nucl. Part. Phys. **37**, 105112 (2010); R. Abir, U. Jamil, M. G. Mustafa and D. K. Srivastava, Phys. Lett. B **715**, 183 (2012).

List of Publications:

a. Published In Journals:

- 1) **Mohammed Younus** and Dinesh K. Srivastava, "Heavy Quark Production from Relativistic Heavy Ion Collisions", J. Phys. **G: Nucl. Part. Phys.**, **37**, 115006 (2010), [arXiv:1008.1120[nucl-th]].
- 2) **Mohammed Younus**, Umme Jamil and Dinesh K. Srivastava, "Correlations of Heavy Quarks Produced at Large Hadron Collider", J. Phys. **G: Nucl. Part. Phys.**, **39**, 025001 (2012), [arXiv:1108.0855[hep-ph]].
- 3) **Mohammed Younus** and Dinesh K. Srivastava, "Empirical Determination of Charm Quark Energy Loss and Its Consequences for Azimuthal Anisotropy", J. Phys. **G: Nucl. Part. Phys.**, **39**, 095003 (2012), [arXiv:1204.5356[nucl-th]].
- 4) **Mohammed Younus** and Dinesh K. Srivastava, "Effect of Energy Loss on Azimuthal Correlation of Charm and Correlated Charm Decay in Collision of lead Nuclei at $\sqrt{s} = 2.76$ A TeV", J. Phys. **G: Nucl. Part. Phys.**, **40**, 065004 (2013), [arXiv:1301.5762[nucl-th]].

b. Preprint/Current Preparations:

- 1) A manuscript titled "Charm Quark Energy Loss in Infinite QCD Matter Using Parton Cascade Model" is under preparation by **Mohammed Younus** and co-authors Prof. Steffen A. Bass and Prof. Dinesh K. Srivastava; arXiv:1309.1276v2[nucl-th] 2013.

c. Conference Proceedings in Journal

- 1) **Mohammed Younus**, Dinesh K. Srivastava and Steffen A. Bass, Proceeding for the talk entitled 'Effects of Quark Gluon Plasma on Charm Quarks Produced in Relativistic

Heavy Ion Collision at SQM-2013, Birmingham, U.K., J. Phys. Conf. Ser. **509**, 012038 (2014).

2) Mohammed Younus and Dinesh K. Srivastava, Proceeding for the poster entitled '**Azimuthal Correlation of Charm Pairs Produced in Heavy Ion Collision**' at SQM-2013, Birmingham, U.K., J. Phys. Conf. Ser. **509**, 012508 (2014).

d.Conference Proceedings:

1) Umme Jamil, Mohammed Younus, and Dinesh K. Srivastava, 'Pair transverse momentum and rapidity correlations of heavy quarks at LHC', Proceedings of the DAE Symposium on Nucl. Phys. **56**, 920 (2011).

2) Mohammed Younus and Dinesh K. Srivastava, 'Azimuthal Correlations of Charm', Proceedings of the DAE Symposium on Nucl. Phys. **56**, 942 (2011).

Contents

Synopsis	ii
List of Figures	xviii
1 Introduction	1
1.1 Fundamental Interactions in Nature	1
1.2 Quantum Chromodynamics	2
1.3 Quark Gluon Plasma	5
2 Signatures of Quark Gluon Plasma	10
2.1 Signals from QGP	10
2.1.1 Photons and Dileptons	10
2.1.2 Strangeness enhancement	12
2.1.3 J/ψ suppression	14
2.1.4 Jet Quenching, Elliptic Flow and Heavy Quarks	15
2.1.5 Correlation and Heavy quarks	18
2.2 Summary	19

3	Heavy Quark Production	23
3.1	Prompt Production	24
3.2	Secondary Production	26
3.2.1	Jet-Jet Interaction	28
3.2.2	Thermal Interaction	29
3.2.3	Free Streaming Interaction	30
3.2.4	Jet Thermal Interaction	31
3.3	Results and Discussions	32
3.4	Summary	33
4	Heavy Quark Correlation	38
4.1	Proton on Proton Collision	43
4.2	Lead Lead Collisions	45
4.2.1	Prompt Interactions	45
4.2.2	Jet-Jet Interaction	46
4.2.3	Jet-Thermal Interaction	47
4.2.4	Thermal Interaction	48
4.3	Results and Discussions	49
4.3.1	Proton Proton Collisions	49
4.3.2	Lead Lead Collisions	54
4.3.3	Effect of Flow	56
4.4	Summary	57

5	Energy Loss Mechanisms of Charm in QGP	67
5.1	Formulation	68
5.1.1	Charm Production	68
5.1.2	Energy Loss	70
5.1.3	Azimuthal Anisotropy	72
5.1.4	Azimuthal Correlation	72
5.2	Results and Discussions	74
5.3	Summary	82
6	Transport of Heavy Quark-Parton Cascade Model	86
6.1	Parton Cascade Model	87
6.1.1	Elastic scattering of charm quark	89
6.1.2	Charm Quark Radiation	90
6.2	Results and Discussions	94
6.3	Summary	100
7	Summary and Outlook	105
	Appendix A:	107
	Appendix B:	112

List of Figures

1.1	Fundamental particles, Forces and Gauge bosons	5
1.2	Comparison of QED and QCD, $\alpha(Q^2)$	6
1.3	(left)Minkowski space-time diagram for Heavy Ion collision evolution.(right)QGP phase diagram.	7
3.1	The p_T distribution for charm production from initial fusion (solid curve), jet-jet (dashed curve), jet-thermal (dash-dotted curve), thermal (stars), and free-streaming (solid circles) processes with initial time 0.147 fm/c, in central collision of gold nuclei at RHIC at $\sqrt{s}=200$ AGeV.	24
3.2	The p_T distribution for charm production from initial fusion (solid curve), jet-jet (dashed curve), jet-thermal (dash-dotted curve), thermal (stars), and free-streaming (solid circles) processes with initial time 0.073 fm/c, in central collision of lead nuclei at LHC at $\sqrt{s}=5500$ AGeV.	25
3.3	The p_T distribution for bottom production from initial fusion (solid curve), jet-jet (dashed curve), jet-thermal (dash-dotted curve), thermal (stars), and free-streaming (solid circles) processes with initial time 0.073 fm/c, in central collision of lead nuclei at LHC at $\sqrt{s}=5500$ AGeV.	26
4.1	Energy dependence of the charm quark production in pp collisions.	39

4.2	(left) Transverse momentum distribution of D^0 -mesons and (right) of D^+ -mesons, in pp collisions for $\sqrt{s}= 2.76$ TeV.	40
4.3	Transverse momentum distribution of single electrons from pp collisions at $\sqrt{s} = 7$ TeV.	41
4.4	Transverse momentum (left panel) and rapidity distribution (right panel) of J/ψ from pp collision at $\sqrt{s}= 7$ TeV, using color evaporation model.	42
4.5	Azimuthal correlation of charm (left panel) and bottom (right panel) quarks at 2.76, 5.5 and 7 TeV for pp collisions. The symbols give the LO values for $d\sigma/d\phi = \sigma_{LO}/\delta(\Delta\phi)$ where $\delta(\Delta\phi)$ is the size of ϕ bin.	43
4.6	Transverse momentum, invariant mass and rapidity distribution of charm and bottom quark pairs at LHC.	58
4.7	Rapidity difference of $\Delta y = y_Q - y_{\bar{Q}}$, of charm and bottom quarks at LO and NLO in pp collisions.	59
4.8	$(\Delta\eta, \Delta\phi)$ correlations of heavy quarks produced in pp collisions at $\sqrt{s}=2.76$ TeV and 5.5 TeV at LO and NLO.	59
4.9	Azimuthal correlation of heavy quarks from prompt interaction for lead on lead collisions at LHC, having different transverse momenta and rapidities close to zero. The symbols give the corresponding LO values, with the same bin-size for $\Delta\phi$. The upper panels are for 2.76 ATeV while the lower panels give results for 5.5 ATeV. The left panels give results for charm quarks while the right panels give the results for bottom quarks.	60
4.10	Azimuthal correlation of heavy quarks from jet-jet interaction for lead on lead collisions at LHC, for different transverse momenta.	60
4.11	Azimuthal correlation of heavy quarks from jet-thermal interaction for lead on lead collisions at LHC, for different transverse momenta.	61

4.12	Azimuthal correlation of heavy quarks from thermal interaction for lead on lead collisions at LHC, for different transverse momenta.	61
4.13	Azimuthal correlation of heavy quarks from prompt interaction for lead on lead collisions at LHC, with flow	62
5.1	R_{AA} and v_2 for non photonic electrons at RHIC. Top: Momentum loss/per collision \propto momentum (left) and \propto square-root of momentum (right). Bottom: Momentum loss per collision= constant (left) and $v_2(p_T)$ for single electrons.	69
5.2	R_{AA} and v_2 for D mesons at LHC. Top: Momentum loss per collision \propto momentum (left) and \propto square root of momentum (right). Bottom: Momentum loss per collision= constant (left) and $v_2(p_T)$ for D-mesons (right).	73
5.3	Comparison of D mesons azimuthal spectrum for two different structure functions.	75
5.4	$dN/d\Delta\phi$ vs $\Delta\phi$ of $c\bar{c}$ pair for $p_T < 2.0$ GeV, and $p_T > 6.0$ GeV.	76
5.5	same as Fig.5.4, $dN/d\Delta\phi$ vs $\Delta\phi$ of $D\bar{D}$ pair for (left) $p_T < 2.0$ GeV, (right) $p_T > 6.0$ GeV.	77
5.6	Invariant mass distribution for di-electron (inset)Increase in di-electron spectrum for $M_{e^+e^-} < 1.0$ GeV, shown in linear scale.	78
6.1	Energy loss for different initial energies after 5 fm/c of propagation.	93
6.2	Energy profile for 16 GeV charm for different time	94
6.3	Energy of probe charm with distance traveled for elastic scattering only	95
6.4	Energy of probe charm with distance traveled for radiative energy loss only	96
B.1	Invariant Matrix elements:(top) $gg \rightarrow Q\bar{Q}$ (bottom) $q\bar{q} \rightarrow Q\bar{Q}$	115

B.2 Invariant matrix elements:(left) $Qq(\bar{q}) \rightarrow Qq(\bar{q})$ (right) $Qg \rightarrow Qg$ 116

Chapter 1

Introduction

1.1 Fundamental Interactions in Nature

The forces or the interactions in nature can be divided explicitly into four categories: Gravitational, Electromagnetic, Weak, and Strong. Since all the matter in the universe is made up of quarks, and leptons, it is obvious that these particles interact only via one or more of these fundamental forces. We also know that such interactions are carried out by vector bosons like photons, gluons, $W^{+/-}$, Z^0 or gravitons(in case of gravitation!).

These grand schemes in our nature are beautifully described by Quantum Field Theories which in turn, are based on Gauge Group Theories [1]. A big part in such theories deals with the strong interactions among quarks via exchange of gluons and is known as Quantum Chromodynamics. The basic degree of freedom for quarks and gluons in this theory is colour charges and is responsible for any strong interaction. We will return to this shortly afterwards.

Let us now look into the experiments. When Rutherford conducted experiments to reveal the structure of atom, he discovered the positively charged protons packed in a small volume called nucleus, which forms only a tiny part of the entire atom. Chadwick discovered electrically neutral neutrons later which also a part of the nucleus alongside protons. The rest of

the atom is filled with electrons revolving around nucleus in specific orbits, as permitted by quantum mechanics. Inside the nucleus positively charged protons can remain stable in spite of a large coulomb repulsion. Several theories rose to explain strong nuclear binding forces. One of them was Yukawa's Mesonic theory which predicts certain screened potential and acts between protons or neutrons or neutron and proton via exchange of vector particles, π mesons. It was then realized that protons and neutrons are not fundamental particles when π mesons were discovered. And soon many types of mesons and hyperons joined the ranks to form a "particle zoo". So, a new set of experiments were conducted called Deep Inelastic Scattering (DIS) [2], which involved highly energetic electrons scattering off protons. This revealed a deep and rich structure for baryons, mesons etc. in a sense that they are formed of quarks, glued together via an extremely strong force through exchange of vector bosons gluons. The gluons like photons don't have electric charge and mass, but have another entirely different quantum number known as colour charge. This colour charge is responsible for strong interaction between quarks and gluons and the gauge theory of Quantum Chromodynamics is used to describe this phenomenon [3].

1.2 Quantum Chromodynamics

QCD is a non-abelian gauge theory belonging to SU(3) gauge group [1, 4]. The lagrangian of a free quark (quark is represented by fermionic field, ψ) can be represented as [5]

$$\mathcal{L}_{QCD} = \bar{\psi}(i\gamma^\mu\partial_\mu - m)\psi \quad (1.1)$$

Now in any gauge theory, the lagrangian must be invariant under local gauge transformation. Suppose

$$\psi(x) \rightarrow \psi'(x) = U(\theta)\psi(x), \quad (1.2)$$

where

$$U(\theta) = \exp\left(\frac{-i}{2}\tau^a\theta_a(x)\right), \quad (1.3)$$

and τ^a are the Gellmann Matrices, the generators of SU(3) group for QCD.

Now the lagrangian \mathcal{L} must be invariant under this transformation of ψ . This prompts one to find a covariant form of $\partial_\mu\psi$ as well. So let us redefine:

$$\partial_\mu\psi \rightarrow D_\mu\psi = (\partial_\mu - ig\tau_a A_\mu^a)\psi \quad (1.4)$$

and we demand that $D_\mu\psi$ transforms in the same manner as ψ under local gauge transformation. Hence we can write

$$(D_\mu\psi)' = U(\theta)D_\mu\psi \quad (1.5)$$

This implies that $\bar{\psi}\not{D}\psi$ is local gauge invariant. Next we can write,

$$\begin{aligned} \left(\partial_\mu - i\frac{g}{2}\tau_a A_\mu^a\right)(U(\theta)\psi) &= U(\theta)\left(\partial_\mu - i\frac{g}{2}\tau_a A_\mu^a\right)\psi, \\ \text{or, } \left[\partial_\mu U(\theta) - i\frac{g}{2}\tau_a A_\mu^a U(\theta)\right]\psi &= -i\frac{g}{2}\tau_a A_\mu^a \psi, \end{aligned} \quad (1.6)$$

And therefore,

$$\frac{\tau_a A_\mu^a}{2} = U(\theta)\frac{\tau_a A_\mu^a}{2}U^{-1}(\theta) - \frac{i}{g}[\partial_\mu U(\theta)]U^{-1}(\theta) \quad (1.7)$$

Now for any infinitesimal transformation,

$$U(\theta) \simeq 1 - i\frac{\tau_a \theta^a(x)}{2}, \quad (1.8)$$

Therefore using eqn 1.8 into eqn 1.7, we can show with slight algebra,

$$\begin{aligned} \frac{\tau_a A_\mu^a}{2} &= \frac{\tau_a A_\mu^a}{2} - i\theta^b A_\mu^c \left[\frac{\tau_b}{2}, \frac{\tau_c}{2}\right] - \frac{1}{2g}(\tau_a \partial_\mu \theta^a), \\ &= \frac{\tau_a A_\mu^a}{2} + F^{abc}\frac{\tau_a \theta^b}{2}A_\mu^c - \frac{1}{2g}(\tau_a \partial_\mu \theta^a), \end{aligned} \quad (1.9)$$

Therefore,

$$A_\mu^a = A_\mu^a + F^{abc}\theta^b A_\mu^c - \frac{1}{g}\partial_\mu \theta^a \quad (1.10)$$

We have used $T^i = \frac{\tau^i}{2}$ and the commutation relation

$$[T^a, T^b] = iF^{abc}T^c \quad (1.11)$$

where F^{abc} is called structure constants for SU(3) group [6].

Hence the full QCD lagrangian can be written as

$$\mathcal{L}_{QCD} = \bar{\psi}_i(i\gamma^\mu\partial_\mu - m)\psi_i + g\tau_a\bar{\psi}_i\gamma^\mu\psi A_\mu^a + \frac{1}{4}F_{\mu\nu}^a F_{a,\mu\nu} \quad (1.12)$$

While the first term gives the lagrangian for the free fermion field, the second term gives the interaction term between the fermion and the gauge boson(gluon). The third term is the free gluonic kinetic energy term and can be expressed by taking the commutation relation of the covariant derivatives of gluonic field shown as:

$$F_{\mu\nu}^a = \partial_\mu A_\nu^a - \partial_\nu A_\mu^a + gF^{abc}A_\mu^b A_\nu^c \quad (1.13)$$

The last term gives gluon self coupling, a unique feature absent in Quantum Electrodynamics(QED). Using this Lagrangian, one can now calculate different conserved quantities and a set of Feynman rules for invariant matrix elements or transition amplitudes for different QCD processes.

Before going into some of the applications of QCD, let us talk a little about two of its unique features called asymptotic freedom and infrared slavery, discovered by David Gross, Franck Wilczek and David Politzer [7]. Because of the colour degree of freedom and the nature of the strong coupling, $\alpha_s(Q^2)$, QCD can be divided into perturbative and non-perturbative regions. The concept of asymptotic freedom of quarks and gluons for large Q^2 and infrared slavery at small Q^2 have been some of the most interesting characteristics of QCD. Mathematically, we can say that QCD differs from QED in terms of behavior of the coupling $\alpha(Q^2)$ which represents the strength of interaction. Due to presence of gluon self coupling in QCD (photon self coupling is absent in QED), α_{QCD} behaves oppositely to that of α_{QED} . One can calculate, $\alpha(Q^2)$ to show [8],

$$\begin{aligned} \alpha_e \equiv \alpha_{QED}(Q^2) &= \frac{\alpha}{1 - (\alpha/3\pi) \ln(Q^2/\lambda^2)} \\ \alpha_s \equiv \alpha_{QCD}(Q^2) &= \frac{\alpha(\mu^2)}{1 + (\alpha(\mu^2)\beta_0/4\pi) \ln(Q^2/\lambda^2)} \end{aligned} \quad (1.14)$$

The difference between QED and QCD is that as Q^2 is decreased, α_e decreases while α_s increases leading to quark and gluon confinement commonly known as infrared slavery. How-

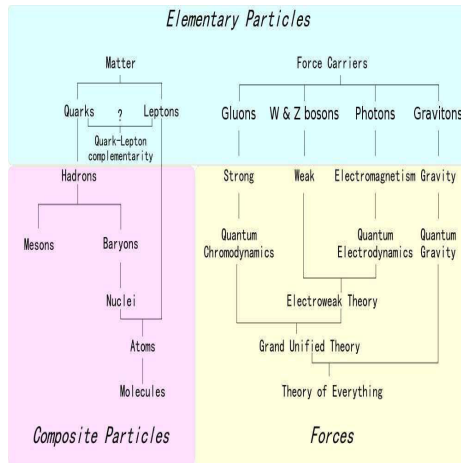


Figure 1.1: Fundamental particles, Forces and Gauge bosons

ever at large Q^2 , α_e gives large coulomb force while α_s diminishes and shows asymptotic freedom for quarks and gluons. This can be observed in the Fig. 1.2

1.3 Quark Gluon Plasma

Now as an application of QCD in practical situations, we move over to heavy ion collisions and the formation of quark gluon plasma. It was suggested that at very high baryonic densities or at very high temperatures, we have quarks and gluons in free state within a larger volume compared to hadronic volumes. This extreme condition can be achieved in heavy ion collision at relativistic energies as suggested, the earliest by [9]. The experiments were conducted at Relativistic Heavy Ion Collider(RHIC), Super Proton Synchrotron(SPS) and Large Hadron Collider(LHC) for achieving such state at very high temperatures and bring us very close to the time when our universe is only few microseconds old and the degrees of freedom are only quarks and gluons. On other hands, experiments at FAIR will give us a state of very high baryonic densities, a condition supposed to be present at the core of neutron stars. Both the extreme cases of these experiments, a system of free quarks and gluons with an energy density $\sim 2-3$ times that of nuclear ground state, is formed within a volume

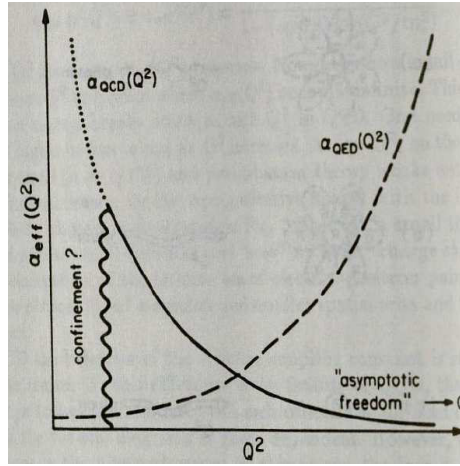


Figure 1.2: Comparison of QED and QCD, $\alpha(Q^2)$

much larger than the hadronic size. This gives us opportunity to study QCD in an ambience of high temperature or high baryonic density [10].

The de-confined quarks and gluons undergo several changes starting just after the collision and finally the hadrons. The entire period of evolution can be divide into several phases: 1) pre-equilibrium phase 2) thermally equilibrated phase (QGP) 3) mixed phase + hadronization [11, 12]. It is suggested that highly energetic partons in pre-equilibrium will interact both elastically and inelastically till they thermally equilibrate locally. This thermal state as known is called quark gluon plasma. The quark gluon plasma expands and cools along, reaching the critical temperature for hadronization. The hadrons, or their decay products finally reach the detectors for further analysis. The critical temperature as predicted by the lattice QCD is about 165-175 MeV, roughly the mass of π meson [13, 14]. The entire system exists for a few microseconds only, which is a very small time to study QGP directly. Alternatively, we choose probes generated in the heavy ion collision and traveling through QGP, before being caught in the detectors. These probes or signals give us an indirect view into the workings of the hot and dense matter.

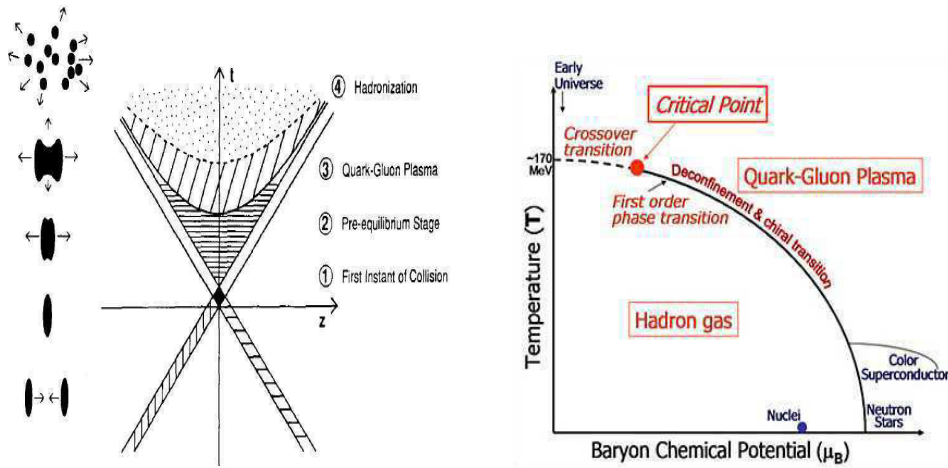


Figure 1.3: (left)Minkowski space-time diagram for Heavy Ion collision evolution.(right)QGP phase diagram.

Outline of the Thesis

The thesis is organized as follows. Chapter 2, deals with the possible signals of QGP like jet quenching, elliptic flow, correlation, J/ψ suppression, strangeness enhancement etc. Chapter 3, deals with heavy quark production from initial fusion gluons followed by calculations of secondary production of heavy quarks. Chapter 4 deals with correlation of heavy quark pairs. In chapter 5, the procedure for the evaluation of energy loss of heavy quarks, the nuclear modification factor, R_{AA} , and the elliptic flow, v_2 using a multiple scattering model calculations. Chapter 6 deals with Boltzmann transport model of charm quark momentum evolution and consequently energy loss per unit length traversed and momentum broadening etc. are calculated. In chapter 7, future prospects on heavy quark study are discussed.

Bibliography

- [1] *Gauge Field Theories*, S. Pokorski, Cambridge University Press (2000); *Gauge Theories of Elementary Particle Physics*, T-P. Cheng, L-F. Li, Oxford Science Publ., Clarendon Press (1982); *Gauge Theories of the Strong, Weak and Electromagnetic Interactions*, C. Quigg, Adv. Book., Publ. West View Press (1997).
- [2] *Quarks and Leptons, An Introductory Course in Modern Particle Physics*, F. Halzen and A. D. Martin, John Wiley and Sons (1987); *Introduction to High Energy Physics*, D. H. Perkins, Cambridge University Press (2000); *Introduction to Elementary Particle Physics*, D. Griffiths, Wiley-VCH Verlag GmbH and Co.kGaA (2004).
- [3] *An Introduction to Quantum Field Theory*, M. E. Peskin and D. V. Schroeder, Addison Wesley Publishing Company (1995); *Quantum Field Theory*, L. H. Ryder, Cambridge University Press (2001); *Quantum Field Theory*, C. Itzykson and J-B. Zuber, McGraw-Hill International Book (1980); *Quantum Field Theory In A Nutshell*, A. Zee, University Press (2005).
- [4] *Gauge Theories in Particle Physics, A Practical Introduction*, Vol. I and II I. J. R. Aitchinson and A. J. G. Hey, Institute of Physics Publications (2004).
- [5] *Quantum Chromodynamics*, W. Greiner, S. Schramm and E. Stein, Springer-Verlag (2007); *Foundation of Quantum Chromodynamics*, T. Muta, World Scientific Publications (2010).

- [6] *Lie Algebras in Particle Physics*, H. Georgi, Levant Books for West View Press (2009).
- [7] D. Gross and F. Wilczek, Phys. Rev. Lett. **30**, 1343 (1973); D. Politzer, Phys. Rev. Lett. **30**, 1346 (1973).
- [8] *Applications of Perturbative QCD*, R. D. Field, Addison-Wesley Publishing Company (1989).
- [9] J. C. Collins and M. J. Perry, Phys. Rev. Lett. **34**, 1354 (1975).
- [10] *The Physics of Quark Gluon Plasma*, B. Müller, Springer-Verlag (1985); *QCD and Collider Physics*, R. K. Ellis, W. J. Stirling and B. R. Webber, Cambridge University Press (2003); *Quark Gluon Plasma*, K. Yagi, T. Hatsuda and Y. Miake, Cambridge University Press (2005).
- [11] *Quark Gluon Plasma, Vols. 1 – 4*, R. C. Hwa and X-N. Wang, World Scientific (2004).
- [12] K. Geiger and B. Müller, Nucl. Phys. **B 369**, 600 (1992).
- [13] *Quantum Chromodynamics on the Lattice*, C. Gattringer and C. B. Lang, Springer (2010); *The Phases of Quantum Chromodynamics*, J. B. Kogut and M. A. Stephanov, Cambridge University Press (2004); *Quarks, Gluons and lattices*, M. Creutz, Cambridge University Press (1983); *Introduction To High – Energy Heavy Ion Collisions*, C. Y. Wong, World Scientific Publishing Co. (1994).
- [14] N. H. Christ, A. E. Terrano, Phys. Rev. Lett. **56**, 111 (1986); S. Muroya, A. Nakamura, C. Nonaka and T. Takaishi, Prog. Theor. Phys. **110**, 615 (2003); Z. Foder and S. D. Katz, JHEP, **04**, 050 (2004).

Chapter 2

Signatures of Quark Gluon Plasma

In relativistic heavy ion collision, the de-confined state of quarks and gluons evolves through different phases before going into final confined state of hadrons. This deconfined medium exists only for a few microseconds. It is nearly impossible to directly observe QGP within this small lifetime. However the detection of various particles in QGP might prove to be useful as signatures and plasma diagnostic tools. It is recognized that there may be no unique signal which will alone lead to the identification of quark gluon plasma. Instead, a number of different signals come out from the medium which may be treated as QGP signatures [1]. Certain probes generated prior to the thermalization of the deconfined state, can bring out information of existence of quark gluon plasma and its properties to us. We will discuss some of these probes and signals of QGP in the following sections.

2.1 Signals from QGP

2.1.1 Photons and Dileptons

Particles having electric charges interact electromagnetically. Photons being the vector belong to interactions of such class of particles and are produced abundantly in heavy ion

collisions. Photon as a probe for QGP has both advantages and disadvantages to its credits, which will be briefly discussed shortly afterwards. First let us look into photon's production mechanisms.

Photons(γ) are produced when any quark(q) annihilate with its own antiquark(\bar{q}) at the lowest order. The processes, $q\bar{q} \rightarrow \gamma\gamma$ (QED, $\mathcal{O}(\alpha_e^2)$) and $q\bar{q} \rightarrow \gamma g$ (QED-QCD, $\mathcal{O}(\alpha_e\alpha_s)$), can be treated as some of the dominant channels for photon production. However the probability ratio for occurrence of QED channel only to QED-QCD channel is about 0.02 [1]. So one can safely neglect the contribution due to QED process. Also, photons can be emitted from Compton like processes ($gq(\bar{q}) \rightarrow \gamma q(\bar{q})$). In relativistic heavy ion collision, depending upon production mechanism, photons can be various types: prompt photons from pre-equilibrium phase, thermal photons from QGP phase as well as photons from conversion of jets in QGP and from hadronic phase . This hadronic photon contribution must be calculated in order to study relative importance of QGP photons with hadronic photons. Some of the channels in hadronic medium are $\pi^+\pi^- \rightarrow \gamma\rho^0$, $\pi^\pm\pi^0 \rightarrow \gamma\rho^\pm$ and $\pi^\pm\rho^0 \rightarrow \gamma\pi^\pm$, etc. The production cross-sections and rates for photon production in heavy ion collision has been extensively calculated in [2, 3].

The advantage of photon as a probe for QGP is that they interact in least possible manner with the QGP medium. Only electromagnetically, they scatter off the medium quarks via compton scattering channels, which can be described by QED diagrams and are very weak when compared to all QCD processes. Consequently, their mean free path is expected to be larger than typical lifetime of QGP. They come out of the system to the detectors almost unscathed carrying information of their production conditions. On the other hand, photon production rate and the photon momentum distribution depends on the distribution of thermal quarks and gluons. Therefore once produced, photons in QGP carry information of the properties of medium from their point of production to detectors and can serve as efficient probes. However the disadvantages are equally troublesome as photons are produced from the time just after the initial collision upto final hadronic decays(eg. $\pi^0 \rightarrow 2\gamma$) and thus it is formidably difficult to differentiate them from different phases of heavy ion collision. Experimental curves for photon distributions cover its entire period of production. However

recent theoretical calculations have been able to roughly distinguish its different region of production and therefore have added interesting features to the study of photon dynamics [4]

Now let us discuss dileptons briefly. Dileptons are produced from initial quark-antiquark annihilations, and also in later hadronic medium (for eg. $\pi^+\pi^- \rightarrow l^+l^-$ or ρ, ω or J/ψ decay). The high energy lepton pairs, in particular e^+e^- but also $\mu^+\mu^-$ are some of the most prominent observables. Other sources for dilepton production beside QGP and hadronic medium is Drell-Yan processes, in which a quark annihilates with an sea antiquark from a nucleon of other nucleus to form a virtual photon which then decays into a lepton pair, ($q\bar{q} \rightarrow \gamma^* \rightarrow l^+l^-$). In this mechanism, nucleonic correlations within a nucleus is not important and the effect can be considered as a collection of independent and uncorrelated nucleon-nucleon collisions. However, hadronic phase production gains importance over Drell-Yan processes as large no. of dileptons are produced from hadronic decays, depending upon the collider energies. The observables with dilepton pair is its pair invariant mass, M_{l+l^-} , pair four-momentum, $p_{l+l^-}^\mu$ and pair transverse momentum, \vec{p}_{Tl+l^-} distributions. The lepton or its antilepton partner travels through the medium where they interact via electromagnetic processes only and hence they are almost unaltered and can bring out information on thermodynamical properties of QGP at the moment of their production. Dileptons also suffer from same disadvantages as those of photons due to its production throughout the entire period of QGP evolution. However when the dilepton spectrum is distributed against the invariant lepton pair masses, then dilepton production from QGP phase can be seen in $\sim 300\text{--}500$ MeV mass region, while the production from hadron phase tends to dominate beyond ≥ 550 MeV. [5, 6]

2.1.2 Strangeness enhancement

Enhancement of strange quarks has been ongoing subject of discussion as a probable signal of QGP. The threshold energy for strange hadrons production is suggested to be 300-400 MeV while for strange anti-baryon threshold is smaller [7]. As QGP lifetime is short for weak decay, strange quarks once produced can only be destroyed by annihilating with an

antistrange quark. This annihilation will occur only if strange quark pairs are abundantly produced in heavy ion collision. Thus the amount of strange particle observed long after the reaction is over can be expected to provide a good signal of the QGP evolution. To find out about strangeness enhancement, one has to study and compare the abundance of strangeness between plasma and hadronic phases.

Let us suppose the threshold energy mentioned earlier be 300 MeV. Therefore, it is known that Fermi Momentum ' p_F ' can be written as $P_F = \mu_B = 300$ MeV, where μ_B is baryonic chemical potential. We know that strange quark mass is around 200 MeV, so $s\bar{s}$ would be around 400 MeV which is close to the threshold energy. Thus it is relatively easy for $s\bar{s}$ production as compared to $u\bar{u}$ and $d\bar{d}$ whose productions are restricted by Pauli's exclusion principle. Again it is more likely that \bar{s} will find a u quark to form $K^+(u\bar{s})$ meson rather than s finding a \bar{u} to form K^- when $\mu_B > 0$. However, s quark may find d and u quark to form $\Lambda(uds)$ hyperons. Thus production of more K^+ and λ will indicate enhanced strangeness production which may be treated as a signal for the formation of deconfined phase. In contrast the threshold energy ' Q ' for strange mesons and hyperons in hadronic phase is around 600 MeV which is larger than $s\bar{s}$ production threshold and thus inhibited. The strange particles from hadronic channels such as $N = N \rightarrow N + \Lambda + K$, $\pi + \pi \rightarrow K + \bar{K}$, is considerably low when compared to partonic phase.

On other hand if we consider a system with high temperature and low baryonic density, then strange quark density is shown to be

$$n_s = n_{\bar{s}} = g_s \int \frac{d^3p}{(2\pi^3)} e^{-\sqrt{p^2+m_s^2}/T} = \frac{3Tm_s^2}{\pi^2} K_2(m_s/T), \quad (2.1)$$

and for non-strange quarks the density is given by

$$n_q = g_q \int \frac{d^3p}{(2\pi^3)} e^{-|p|/T} e^{-\mu_B/T} \quad (2.2)$$

Thus the ratio of strange quarks to non-strange quarks,

$$\frac{n_s}{n_q} = \frac{1}{2} \left(\frac{m_s^2}{T} \right)^2 K_2(m_s/T) e^{\mu_B/3T} \quad (2.3)$$

Thus for $\mu_B > 0$, strange quarks are more abundantly produced than non-strange quarks. In a rapid hadronization the QGP strangeness abundance could almost be conserved and

even stay larger than the hadronic equilibrium abundance. Comparison of ratios of K^+/π with K^-/π and inclusive ϕ, Λ etc. production turned out to be >1.0 [7]. This abundance of multi-strange particles shows that equilibrium might be reached in heavy ion collision. Thus strangeness enhancement may be regarded as one of the possible signature for QGP formation [8].

2.1.3 J/ψ suppression

In QGP, the color charge of a quark is subjected to Debye screening due to the presence of quarks, antiquarks and gluons in the plasma. If we place a J/ψ ($c\bar{c}$ bound state) in a thermal medium, the Debye screening may weaken the interaction between c and \bar{c} . Also because of the distribution of quarks and gluons around $c\bar{c}$, the potential between c and \bar{c} may alter considerably. The combined effect of the two may lead to J/ψ dissociation resulting in its suppression as first suggested by Matsui and Satz [9].

The color potential energy of $c\bar{c}$ system can be written as $-\alpha_{eff}^{QCD}/r$, while the confining potential between them is κr , where κ is the string strength constant. Therefore, the effective Hamiltonian can be written as,

$$H_{eff} = \frac{p^2}{2m} - \frac{\alpha_{eff}}{r} + \kappa r, \quad (2.4)$$

where $\alpha_{eff} = g^2/4\pi$.

If we now place bound charm state in quark gluon plasma, the presence of other thermal quarks, antiquarks, gluons affects the pair in two ways. First, the string tension ' κ ' depends on medium temperature and ultimately goes to zero as temperature increases. Secondly, the presence of thermal distribution leads to the screening of color potential between c and \bar{c} and the Coulomb type potential between them is modified to Yukawa type short range potential:

$$V(r) = \frac{q}{4\pi} \frac{e^{-r/\lambda_D}}{r}, \quad (2.5)$$

where the Debye screening length λ_D is given in pQCD by

$$\lambda_D = \lambda_{QCD} \sim \frac{1}{\mu_D} = \frac{1}{\sqrt{(\frac{N_c}{3} + \frac{N_f}{6})gT}}. \quad (2.6)$$

At high temperature, the range of the attractive interaction becomes so small as to make it impossible for $c\bar{c}$ to remain bound and they dissociate into independent c and \bar{c} and give rise to open charmed meson. Since J/ψ are produced in initial fusion of gluons and quark-antiquark annihilation when temperature is still very high and the system is yet to be equilibrated. Hence J/ψ particles upon interactions with QGP medium may be found to be suppressed when compared to $pp \rightarrow J/\psi$. This suppression can be viewed as a possible signature [10].

On the other hand, the produced J/ψ even after interacting with QGP may remain intact and further proceed to interact with hot hadronic medium. This may also lead to break up. The reaction of J/ψ dissociation in hadronic medium may be shown as $J/\psi + h \rightarrow D + \bar{D} + X$. This might add upto final suppressed J/ψ spectrum [11]. Therefore, the net effect of QGP as well as of hadronic medium on J/ψ may appear as its final suppressed spectra and the effect due to QGP has to be separately evaluated theoretically or extracted from data using experimental techniques.

2.1.4 Jet Quenching, Elliptic Flow and Heavy Quarks

Jet Quenching:

Before going into heavy quarks, let us describe jet quenching and elliptic flow briefly. In relativistic heavy ion collision when a parton of one hadron within an incoming nucleus collide with a parton within another incoming nucleus from opposite direction, then various partons with very high transverse momenta are produced which fly off to all possible directions from collision points and finally fragment into narrow cones of hadrons called jets. These highly energetic secondary quarks, antiquarks and gluons are commonly referred in theory as jet partons. When some of these jet partons enter the thermalized medium, they interact with the medium particles and loose energies and momenta before hadronizing. This loss is observed through a mathematical ratio, is known as nuclear modification factor, ' R_{AA} '. R_{AA} is

defined as

$$R_{AA}(p_T, b) = \frac{\frac{dN_{AA}}{d^2p_T dy}}{T_{AA}(b) \times \frac{d\sigma_{pp}}{d^2p_T dy}} \quad (2.7)$$

This ratio shows the energy loss of any jet parton and commonly called jet quenching. It was first suggested by Bjorken [12] that any jet particle traveling inside a bulk partonic matter must lose a significant part of its energy before hadronizing. The numerator of the ratio shows a single particle transverse momentum distribution of a jet parton produced in nucleus-nucleus collision and traveling through thermal medium. The denominator part has single particle distribution of same species of jet parton produced in proton on proton collision multiplied by nuclear thickness function ' $T_{AA}(b)$ ' which is a proton to nucleus scaling factor (if AA collision is an incoherent superposition of pp collision) and is a function of impact parameter ' b '. If we suppose that no jet quenching has taken place, then the ratio must be unity for all jet momenta. However if the ratio tends to be less than unity, it serves as a definite measure for jet suppression in the medium [13, 14]. This particular mathematical entity is a suitable candidate as a signature of formation of a thermalized medium of deconfined quarks and gluons or QGP.

Theoretically, calculations of R_{AA} is basically model dependent and various formalisms have been developed over the years to estimate this ratio. However, experimental results from LHC and RHIC have shown numerous evidences for the quenching of jet partons when final hadrons momentum spectra are observed.

Elliptic Flow:

For non-central heavy ion collisions, the azimuthal momentum anisotropy is defined as the Fourier expansion in angle ϕ shown in the r.h.s. of the following expression :

$$E \frac{dN}{d^3p} = \frac{1}{2\pi} \frac{dN}{p_T dp_T dy} \left[1 + \sum_{n=1}^{\infty} 2v_n \cos(n\phi) \right], \quad (2.8)$$

where the angle ϕ is the azimuthal angle in the transverse momentum plane and v_n are the Fourier coefficients in the expansion. The second coefficient v_2 is referred to as elliptic flow

and is given by [15]

$$v_2(p_T) = \frac{\int d\phi \frac{dN}{p_T dp_T d\phi} \cos(2\phi)}{\int d\phi \frac{dN}{p_T dp_T d\phi}} \quad (2.9)$$

For central collision, the net elliptic flow should be zero. Also if the nucleus on nucleus collision is the superposition of nucleon collisions then the resulting distribution of partons would be isotropic. In that case v_2 might be zero again. However if the resulting partons scatter among themselves largely then a high transverse flow may develop. In the region of collision where two nuclei overlap with each other a ellipsoidal region in configuration space is developed with pressure gradient higher on the thinner side(minor axis in configuration space but major axis in momentum space). As a result, particles tend to have a large collective flow in the direction of minor axis resulting in anisotropy in the momentum distribution of the partons. The more frequent the rescattering of the partons more is the resultant momentum anisotropy.

Several models including hydrodynamical calculations have been successful in explaining large elliptic flow of partons shown by the data from RHIC and LHC experiments. It is found from hydrodynamical calculations that elliptic flow is very sensitive to initial conditions and equation of states. As large elliptic flow suggests large rescattering among partons, this may also indicates early thermalization of high p_T partons and therefore a strong signature for formation of QGP.

Heavy Quarks:

Heavy quarks are produced in early phases of relativistic heavy ion collision when temperature is still very high and the system is not yet in thermal equilibrium. Their large masses ensures that they are not easily affected by QGP. Also because of their small numbers, they remain isolated from the bulk system and hence may serve as efficient probes for QGP. The details of all mechanisms of heavy quark production and its evolution in quark gluon plasma will be addressed from next chapter onward. For now, it is well known that heavy quark jets suffer suppression even if the magnitude of suppression is slightly smaller than their lighter counterparts. When a heavy quark enters the medium of thermalized quarks and glu-

ons it collides with the medium partons. Because of its large mass, these collisions might not alter their direction of motion considerably. However a series of consecutive collisions might slow down the heavy quark. Recent experimental results for non-photonic electrons at RHIC and D and B mesons at LHC have shown large suppression for heavy quarks, with the order of suppression almost identical to light mesons. This suggests a large effect of the medium on charm momentum. Whether this medium effect can cause heavy quark thermalization is a matter of contemporary interests. However calculations from hydrodynamics also suggested heavy quark equilibration time at RHIC temperatures is larger than lifetime of QGP formed at RHIC energies. This may indicate that heavy quark may not thermalize like light quarks and gluons at RHIC. But it would be interesting to question of heavy quark thermalization at LHC temperatures which are higher than those at RHIC. Consequently, elliptic flow for heavy quarks has also been measured at RHIC and LHC experiments and has emerged as an important observable so far the thermalization of heavy quark is concerned. Various phenomenological and analytical models are being employed to describe these startling results [16].

2.1.5 Correlation and Heavy quarks

Two particle correlation is a relevant quantity in the study of jet quenching and brings out deeper understanding of particle energy loss mechanisms in QGP. The study of two particle correlation is important to determine the flavor dependence of energy loss if the members of a pair belong to two different species. Even particle pairs belonging to same species may be affected in different ways by the medium and their correlation may change. In this context, heavy quarks may serve as efficient observable. Heavy quarks are produced early in collision history, in pairs due to the conservation of heavy flavors in relativistic heavy ion collision. The pair shows correlation in azimuthal angle in transverse momentum plane even in the absence of any medium. However, the heavy quark pair in presence of a dense and hot medium, may suffer considerable energy loss which might alter its correlation, and provide us with information on thermal properties of the QGP. Further if heavy quark pair

scatters with the thermal partons frequently, then its correlation may be deeply affected by the collective flow of the medium particles. Since the collective flow is developed in early phase of QGP, any considerable change in azimuthal correlation of heavy quark pair may indicate formation of quark gluon plasma [17]. Thus correlation of heavy quark pair is slowly emerging as a major QGP signature besides jet quenching and elliptic flow.

2.2 Summary

The calculations on heavy quark production, jet quenching and two particle correlation of heavy quarks as well as heavy quark momentum evolution in quark gluon plasma has been done in this thesis work. I will return to these issues in the following chapters.

Bibliography

- [1] *Introduction to High Energy Heavy Ion Collisions*, C. Y. Wong, World Scientific Publishing Co. (1994).
- [2] J. Kapusta, P. Lichard and D. Siebert, Nucl. Phys. **A 544**, 485c (1992); P. V. Ruuskanen, Nucl. Phys. **A 544**, 169c (1992); S. Raha and B. Sinha, Int. J. Mod. Phys. **A 6**, 517 (1991).
- [3] J. Alam, D. K. Srivastava, B. Sinha and D. N. Basu, Phys. Rev. **D 48**, 1117 (1993); J. Cleymans, E. Quack, K. Redlich and D. K. Srivastava, Int. J. Mod. Phys. **A 10**, 2941 (1995); J. Cleymans, K. Redlich and D. K. Srivastava, Phys. Rev. **C 55**, 1431 (1997); R. J. Fries, B. Muller and D. K. Srivastava, Phys. Rev. Lett. **90**, 132301 (2003); S. A. Bass, T Renk and D. K. Srivastava, Nucl. Phys. **A 783**, 307 (2007).
- [4] R. Chatterjee, D. K. Srivastava and S. Jeon, Phys. Rev. **C 79**, 034906; S. De, D. K. Srivastava and R. Chatterjee, Nucl. Phys. **A 862**, 290 (2011); A. Kumar (ATLAS, CD and D0 Collaborations), EPJ WEB Conf. **49**, 16009 (2013); J. Franz (PHENIX Collaboration), Nucl. Phys. **A 904**, 693c (2013); D. Teaney, Nucl. Phys. **A 904**, 857c (2013).
- [5] P. V. Ruuskanen, Nucl. Phys. **A 522**, 255c (1991); K. Kajantie, J. Kapusta, L. McLerran and A. Mekjian, Phys. Rev. **D 34**, 2746 (1986); E. V. Shuryak, Phys. Lett. **B 78**, 150 (1978); R. C. Hwa and K. Kajantie, Phys. Rev. **D 32**, 1109 (1985); J. Cleymans and J. Finberg, Phys. Lett. **B 168**, 405 (1986); J. Cleymans, J. Finberg and K. Redlich, Phys. Rev. **D 35**, 2153 (1987).

- [6] C. Y. Wong, Phys. Rev. C **48**, 902 (1993); C. Grosso-Pilcher and M. J. Sochet, Ann. Rev. Nucl. Part. Sci. **36**, 1 (1986); N. S. Craigie, Phys. Rep. **47**, 1 (1978); J. C. Collins and D. E. Soper and G. Sterman, Phys. Lett. B **134**, 263 (1984); R. Rapp, arXiv:1306.6394[nucl-th] (2013); M. Martinez, M. Strickland, J. Phys. G **35**, 104162 (2008).
- [7] *The Physics of Quark Gluon Plasma*, B. Müller, Springer-Verlag (1985); J. Rafelski, Phys. Rep. **88**, 331 (1982); S. A. Chin, Phys. Lett. B **78**, 552 (1978); J. I. Kapusta, Nucl. Phys. B **148**, 461 (1979); P. Koch, B. Müller and J. Rafelski, Phys. Rep. **142**, 167 (1982).
- [8] G. Agakishiev *et al.* [STAR Collaboration], Phys. Rev. Lett. **108**, 072301 (2012); B. I. Abelev *et al.* [STAR Collaboration], Phys. Rev. C **77**, 044908 (2008); J. Rafelski and J. Letessier, J. Phys. G **35**, 044042 (2008); J. Aichelin and K. Werner, Phys. Rev. C **79**, 064907 (2009) [Erratum-ibid. C **81**, 029902 (2010)].
- [9] T. Matsui and H. Satz, Phys. Lett. B **178**, 416 (1986).
- [10] E. Eichten *et al.*, Phys. Rev. D **21**, 203 (1980); C. Quigg and J. L. Rosner, Phys. Rep. **56**, 167 (1979); L. D. McLerran and B. Svetitsky, Phys. Rev. D **24**, 450 (1981); H. Satz, Nucl. Phys. A **418**, 447c (1984).
- [11] D. G. Moon (CMS Collaboration), Nucl. Phys. A **904**, 591c (2013); L. Turko, D. Prorok and D. Blaschke, J. Phys. G **37**, 094053 (2010); S. Gavin, hep-ph/9609470 (1996); L. Grandchamp and R. Rapp, Nucl. Phys. A **709**, 415 (2002); T. Lang and M. Bleicher, Acta. Phys. Polon. Supp. **5**, 573 (2012).
- [12] J. D. Bjorken, Fermilab-Pub-82/59-THY, Batavia (1982).
- [13] M. Gyulassy and M. Plümer, Phys. Lett. B **243**, 432 (1990); M. H. Thoma, *QuarkGluonPlasma*, 2. ed, R. C. Hwa, P.51, World Sci. (1995); R. Baier, Nucl. Phys. A **715**, 209c (2003).

- [14] R. Karabowicz (BRAHMS Collaboration), Nucl. Phys. **A 774**, 477 (2006); A. Grelli (ALICE Collaboration), Nucl. Phys. **A 904**, 635c (2013); M. B. Tonjes (CMS Collaboration), Nucl. Phys. **A 904**, 713c (2013).
- [15] S. Shi (STAR Collaboration), J. Phys. Conf. Ser. **422**, 012002 (2012); D. Lohner (ALICE Collaboration), arXiv:1212.3995 (2012); M. Nasim, B. Mohanty and N. Xu, Phys. Rev. **C 87**, 014903 (2013); C. M. Ko, S. H. Lee, T. Song and J. Xu, EPJ Web Conf. **13**, 04001 (2011).
- [16] Y. L. Dokshitzer, V. A. Khoze and S. I. Troian, J. Phys. **G: Nucl. Part. Phys.** **17**, 1602 (1991); A. Shor, Phys. Lett. **B 215**, 375 (1988); A. Adare *et al* (PHENIX Collaboration), Phys. Rev. Lett. **98**, 172301 (2007); D. Caffari, Nucl. Phys. **A 904**, 643c (2013). S. K. Das and A. Davody, arXiv:1211.2925 [hep-ph] (2012).
- [17] N. Xu, X. Zhu, P. Zhuang, Phys. Rev. Lett. **100**, 152301 (2008), N. Xu, X. Zhu, P. Zhuang, J. Phys. **G 36**, 064025 (2009); M. L. Mangano, P. Nason, G. Ridolfi, Nucl. Phys. **B 373**, 295 (1992); S. Frixione, M. L. Mangano, P. Nason, G. Ridolfi, Adv. Ser. Direct. High Energy Phys. **15**, 609-706 (1998). [arXiv:hep-ph/9702287 [hep-ph]].

Chapter 3

Heavy Quark Production

Investigation of the properties of a quark gluon plasma, a deconfined strongly interacting matter, constitutes a major part of research in high energy nuclear physics [1]–[8]. In the last chapter we discussed some of the probable signatures of QGP with an brief introduction to heavy quark as a pertinent candidate for probing this ultra-dense and hot medium. But before going into the details of charm quark evolution in QGP in the subsequent chapters, let us describe in this chapter, various production mechanisms for heavy quarks.

Heavy quarks being produced in early phase of heavy ion collisions when mostly hard scattering processes take place [9], offer some very distinct advantages. They are mainly produced from prompt gluon fusion($gg \rightarrow Q\bar{Q}$) and quark anti-quark annihilations($q\bar{q} \rightarrow Q\bar{Q}$). These processes can be accurately described up to next-to-leading order(NLO) using pQCD. However, there may exist other mechanisms of heavy quark production, e.g., a pre-equilibrium secondary production of heavy quarks due to interaction between partons having a large transverse momenta or due to the passage of a parton with large transverse momentum through thermalized partons or due to interaction among thermalized partons themselves. These processes may show considerable effects if added to prompt production of heavy quarks.

As a first step, we consider production of charm and bottom quarks at RHIC and LHC energies due to prompt interactions, thermal productions, and pre-equilibrium productions due to interaction of two partonic jets and due to the passage of partonic jets through the quark gluon plasma.

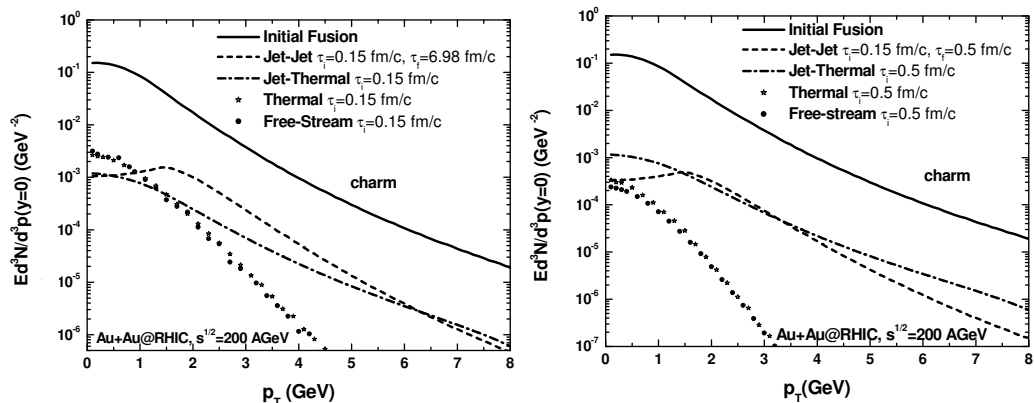


Figure 3.1: The p_T distribution for charm production from initial fusion (solid curve), jet-jet (dashed curve), jet-thermal (dash-dotted curve), thermal (stars), and free-streaming (solid circles) processes with initial time 0.147 fm/c, in central collision of gold nuclei at RHIC at $\sqrt{s}=200$ AGeV.

3.1 Prompt Production

Prompt production of heavy quarks will primarily occur through initial gluon fusion and quark anti-quark annihilations. The flavor excitation processes at NLO order are suppressed as suggested earlier in [10].

The differential cross-section for leading-order processes, $gg \rightarrow Q\bar{Q}$ and $q\bar{q} \rightarrow Q\bar{Q}$ [16] is given by

$$\frac{d\sigma(\hat{s}, \hat{t}, \hat{u})}{d\hat{t}} = \frac{|\mathcal{M}|^2}{64\pi^2\hat{s}^2} \quad (3.1)$$

where the invariant amplitude $|\mathcal{M}|^2$ is shown in Appendix B:

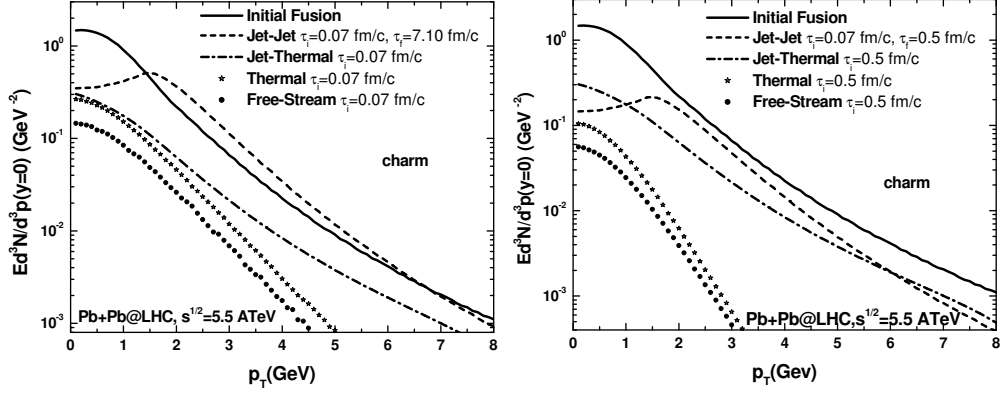


Figure 3.2: The p_T distribution for charm production from initial fusion (solid curve), jet-jet (dashed curve), jet-thermal (dash-dotted curve), thermal (stars), and free-streaming (solid circles) processes with initial time 0.073 fm/c, in central collision of lead nuclei at LHC at $\sqrt{s}=5500$ AGeV.

The running coupling, α_s is taken a constant value of 0.3 for our calculations. The cross-section for the prompt production of heavy quarks from proton-proton collisions at leading order [12] can be shown to be,

$$\begin{aligned} \frac{d\sigma}{dy_1 dy_2 d^2p_T} &= 2x_1 x_2 \sum_{ij} \left[f_i^{(1)}(x_1, Q^2) f_j^{(2)}(x_2, Q^2) \frac{d\hat{\sigma}_{ij}(\hat{s}, \hat{t}, \hat{u})}{d\hat{t}} \right. \\ &\quad \left. + f_j^{(1)}(x_1, Q^2) f_i^{(2)}(x_2, Q^2) \frac{d\hat{\sigma}_{ji}(\hat{s}, \hat{u}, \hat{t})}{d\hat{t}} \right] / (1 + \delta_{ij}), \end{aligned} \quad (3.2)$$

where i and j are the interacting partons and f_i and f_j are the partonic structure functions, and x_1 and x_2 are the momentum fractions of the parent nucleons carried by the interacting partons. For heavy ion collisions the p_T spectrum for heavy quark production is given by

$$\frac{dN}{d^2p_T dy} = T_{AA} \frac{d\sigma}{d^2p_T dy} \quad (3.3)$$

where for central collisions, $b=0$ fm, nuclear thickness, T_{AA} is calculated from Glauber formalism to be 286 fm^{-2} for Au+Au at RHIC and 292 fm^{-2} for Pb+Pb at LHC. We account for higher order ($q\bar{q} \rightarrow gQ\bar{Q}$ and $gg \rightarrow gQ\bar{Q}$), corrections by multiplying a constant K-factor

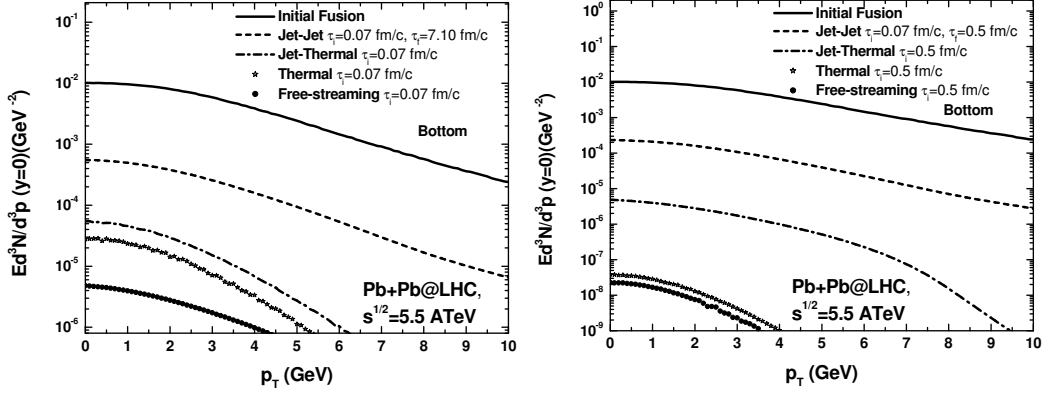


Figure 3.3: The p_T distribution for bottom production from initial fusion (solid curve), jet-jet (dashed curve), jet-thermal (dash-dotted curve), thermal (stars), and free-streaming (solid circles) processes with initial time 0.073 fm/c, in central collision of lead nuclei at LHC at $\sqrt{s}=5500$ AGeV.

≈ 2.5 to leading-order $Q\bar{Q}$ cross-section (see, Ref [11]). The parameterized form of EKS98 nuclear shadowing function [13] has been used to produce shadowing or overlapping effect of parton distributions in a nucleus, especially for low 'Bjorken x ($x < 0.1$)' [14], where the effect is more prominent. CTEQ5L parton distribution function [15] has been used for initial parton distribution in the nucleus for the calculations. More up-to-date structure functions or pdfs can be used and will be addressed in the future. The same formalism(Eqn, 3.2) can be used to calculate the prompt production of gluons and light quarks by taking corresponding matrix elements for massless partons [16].

3.2 Secondary Production

The initial hard scattering between the partons of the two nuclei will result in production of gluons and light quarks having large transverse momenta. These will ultimately fragment and lead to a stream of hadrons into a narrow cone. These quarks and gluons with large transverse momenta are referred as jet particles. Being copious in number, they would interact frequently and may even approach thermalization. However, two gluonic jets or a quark and

anti-quark jet are likely to have sufficient energy to produce a pair of heavy quarks, if they interact. This secondary mechanism for heavy quark pair production is called jet-jet interaction [17]. Again a high p_T jet may enter the thermalized medium and on interacting with the medium particles may produce heavy quark pairs. This is called heavy quark production from jet conversion in QGP or jet-thermal interaction [19, 20, 21]. Also within QGP, any two thermal gluons or a thermal quark and its thermal anti-quark partner may interact to give heavy quark pair, provided the medium temperature is sufficiently high. This may be termed as heavy quark production due to thermal interaction [18]. The general expression for the production of a heavy quark from any of these secondary interaction at central rapidity is given by [17, 22, 9]:

$$\begin{aligned}
E \frac{d^3 N}{d^3 p} \Big|_{y=0} &= \int d^4 x \int \frac{1}{16(2\pi)^8} \frac{d^3 p_1 d^3 p_2 d^3 p'}{\omega_1 \omega_2} \\
&\times \delta^4 \left(\sum p^\mu \right) / E' \\
&\times |M|^2 F(\vec{x}, \vec{p}_1, t) F(\vec{x}_2, \vec{p}_2, t)
\end{aligned} \tag{3.4}$$

where $\sum p^\mu = p_1 + p_2 - p - p'$, p_1 and p_2 are the four-momenta of the incoming partons and p and p' are the same for outgoing heavy quark and an its anti-quark. $F(\vec{x}, \vec{p}, t)$ gives the phase space distribution function for the incoming partons. Integrating over $d^3 p'$, we get for $y=0$ ($p_z=0$, and $p_T=p$), the momenta integration part can be written as(see Appendix A):

$$\begin{aligned}
&\int \frac{d^3 p_1 d^3 p_2 d^3 p'}{\omega_1 \omega_2 E'} \delta^4 \left(\sum p^\mu \right) |\mathcal{M}|^2 F(\vec{x}, \vec{p}_1, t) F(\vec{x}, \vec{p}_2, t) \\
&\approx \int \dots \int dp_{T2} dp_{T1} \frac{\delta(\sum E)}{E'} |\mathcal{M}|^2 \\
&\times F(\vec{x}, p_{T1}, \phi_1, y_1, t) F(\vec{x}, p_{T2}, \phi_2, y_2, t) ,
\end{aligned} \tag{3.5}$$

where

$$\frac{\delta(\sum E)}{E'} = \frac{\delta(p_{T1} - p_{T1,0})}{[p_{T2}(\cosh(y_1 - y_2) - \cos(\phi_1 - \phi_2)) - (E \cosh y_1 - p \cos \phi_1)]} ,$$

and we have

$$p_{T1,0} = \frac{p_{T2}(E \cosh y_2 - p \cos \phi_2)}{[p_{T2}(\cosh(y_1 - y_2) - \cos(\phi_1 - \phi_2)) - (E \cosh y_1 - p \cos \phi_1)]}.$$

3.2.1 Jet-Jet Interaction

For jet-jet interaction, we approximate the phase-space distribution of the gluon, quark, or anti-quark jets produced in initial (prompt) scattering of the partons in a central collision as:

$$\begin{aligned} F(\vec{x}, \vec{p}, t) &= f_{\text{jet}}(\vec{x}, \vec{p}, t) \\ &= \frac{(2\pi)^3}{g_i \tau \pi R_T^2 p_T} \frac{dN_i}{dy d^2 p_T} \delta(y - \eta) \Theta(\tau_f - \tau) \Theta(\tau - \tau_i), \end{aligned} \quad (3.6)$$

with charm $p_T > 2$ GeV. Here $\delta(y - \eta)$ denotes the Bjorken correlation for space-time and energy-momentum rapidities and ' i ' stands for quarks, anti-quarks, or gluons. The degeneracy of quarks and gluons is given by $g_{g/q}$ such that $g_g = 8 \times 2$ and $g_q = 3 \times 2$ [22]. ' $\Theta(\tau)$ ' functions limit the jet-jet interaction between an initial time, $\tau_i \simeq 1/p_T$ and final time τ_f , which is taken as a parameter(see Sec. 3.3). R_T is the transverse radius of the nucleus and $dN_i/d^2 p_T dy$ is the transverse momentum distribution of partons for $p_T > 2$ GeV. We neglect the dependence of this distribution on the momentum rapidity as we are calculating the results for heavy quarks at $y=0$, when only very small values of y_1 and y_2 contribute, and the rapidity dependence is marginal.

The momentum space distribution of the jets at RHIC and LHC are taken from parametrization given earlier [6], where the jet distributions were calculated in LO-pQCD with a K-factor ≈ 2.5 to account for higher-order effects. CTEQ5L structure functions and EKS98 shadowing functions, as discussed in previous section have been used. Thus we have,

$$\begin{aligned} h_{\text{jet}}^i(p_T) &= \frac{1}{g_i} \left. \frac{dN}{dy d^2 p_T} \right|_{y=0} \\ &= \frac{1}{g_i} K \frac{C}{(1 + p_T/B)^\beta}. \end{aligned} \quad (3.7)$$

The parameters C, B, β calculated using CTEQ5L structure function, are shown in Appendix-A. The equation 3.5 is then simplified (see Appendix-A) and can be solved numerically to give heavy quarks production from jet-jet interaction.

3.2.2 Thermal Interaction

Due to multiple scattering among jet partons ($g, u(\bar{u}), d(\bar{d})$) in rapid succession, the deconfined state may form thermally equilibrated medium early and follow hydrodynamics evolution till QGP hadronizes. Heavy quarks may be produced in this thermal medium if the temperature is high [4].

We can estimate the initial temperature by assuming Bjorken hydrodynamics [25] which relates it to the final particle rapidity density, dN/dy by

$$\frac{2\pi^4}{45\zeta(3)\pi R_T^2} \frac{dN}{dy} = 4aT_0^3\tau_0 \quad (3.8)$$

where $a=42.25\pi^2/90$ for massless light quarks and gluons and $R_T = 1.2A^{1/3}$. We take particle rapidity density as 1260 estimated experimentally at RHIC [26] and assumed that the particle rapidity density at LHC is about 5625. Some recent works suggest a smaller value for $dN/dy \approx 3000-3500$ at LHC from considerations of parton saturation [27]. However, larger values used in our calculations have also been suggested [28]. An increase in the particle rapidity densities, which is steeper than expected has also been seen [29].

The time evolution of the temperature of thermalized QGP for a boost-invariant longitudinal expansion is governed by:

$$T_i^3\tau_i = T^3\tau = \text{const.} \quad (3.9)$$

This provides that $\tau_i \approx 0.15 \text{ fm}/c$ is assumed for our calculations. As an alternative, we also considered a much larger time of thermalization [1, 30], $\tau_i \approx 0.5 \text{ fm}/c$, with T_i calculated from Eq. 3.8. For LHC, we have similarly assumed $\tau_i \approx 0.07 \text{ fm}/c$ and $0.5 \text{ fm}/c$. The critical temperature, T_c , is taken to be 170 MeV and τ_c is estimated from Eqn. 3.9, such that thermal interactions would take place between τ_i and τ_f only. We take the phase space distribution

for the thermalized quarks and gluons as,

$$f_{th}^i(p_T, y, \eta) = \exp[-p_T \cosh(y - \eta)/T] . \quad (3.10)$$

Using the thermal parton distribution Eq. 3.10 in Eq. 3.4, we get thermal charm distribution. For details see (appendix)

3.2.3 Free Streaming Interaction

As an extreme, we consider free-streaming partons, as a model of evolution of the system of deconfined quarks and gluons, which completely relaxes the condition of thermalization. The initial distribution at $t = \tau_0$ and $z = 0$ is obtained by assuming maximum entropy, so that

$$f(p, x) = \frac{dN}{d^3p d^3x} = \exp\left(-\frac{E}{T_o}\right) , \quad (3.11)$$

and the condition that needs to be satisfied is

$$p^\mu \frac{\partial f(x, p)}{\partial x^\mu} = 0 . \quad (3.12)$$

We assume boost invariance along the z-axis. The solution which satisfies the differential Eq. A.14 is

$$f(p, x) = \exp\left[-\frac{\sqrt{p_T^2 + (p_z t - E z)^2/\tau_0^2}}{T_0}\right] . \quad (3.13)$$

With certain simplification (see Appendix) Eq. A.16 becomes

$$f(p_T, \eta, y) = \exp\left[-\frac{p_T \sqrt{1 + \tau^2 \sinh^2(y - \eta)/\tau_0^2}}{T_0}\right] . \quad (3.14)$$

Thus the final integration is calculated for heavy quark production from free streaming partons using 3.4 see (appendix) for details

The initial conditions for the free-streaming case are taken to be same as that for the thermal production, whereas the final time is taken as R_T/c , the transverse radius of the nuclei, after which the system would surely expand rapidly along the transverse direction as well and disintegrate.

3.2.4 Jet Thermal Interaction

Now we discuss the production of heavy quarks by passage of light quark and gluonic jets through thermalized QGP. The phase space distributions can be divided into jet partons and thermalized partons. The thermal distribution can be written as

$$f_{th} = \exp[-p_T \cosh(y - \eta)/T] . \quad (3.15)$$

and the jet distribution

$$\begin{aligned} F(\vec{x}, \vec{p}, t) &= f_{\text{jet}}(\vec{x}, \vec{p}, t) \\ &= \frac{(2\pi)^3}{g_i \tau \pi R_T^2 p_T} \frac{dN_i}{dy d^2 p_T} \delta(y - \eta) \Theta(\tau_f - \tau) \Theta(\tau - \tau_i) , \end{aligned} \quad (3.16)$$

We have already discussed τ_i in previous sections, which gives the start of the time from when we consider the system to be in the form of QGP. We define τ_d as the time which a jet takes to reach the surface of the quark gluon plasma. Consider a jet formed at \vec{r} with velocity \vec{v} which travels to the surface of plasma. The distance, d , covered in this process is given by,

$$d = -r \cos \phi + \sqrt{R_T^2 - r^2 \sin^2 \phi} , \quad (3.17)$$

where $\phi = \cos^{-1}(\hat{v} \cdot \hat{r})$, and R_T is the radius of the system. A massless quark or a gluon would take a time

$$\tau_d = d/c \quad (3.18)$$

for this journey and the interaction between jet and thermal partons would take the time, $\tau = \tau_i - \mathbf{min}[\tau_c, \tau_d]$, where τ_c is the freezeout time for QGP. Using these conditions, the Eq. 3.4 can now be simplified to give jet-thermal contribution to heavy quark production (see

Appendix for details).

$$\begin{aligned}
E \frac{d^3 N}{d^3 p} \Big|_{y=0} &= \frac{1}{16(2\pi)^4 \pi R_T^2} \int d\tau r dr d\eta d\phi_1 d\phi_2 dy_1 dp_{T2} \\
&\times \frac{p_{T1,0}}{(p_{T2}(\cosh(y_1 - \eta) - \cos(\phi_1 - \phi_2)) - E \cosh y_1 + p_z \sinh y_1 + p_T \cos \phi_1)} \\
&\times f_{th}(p_{T1,0}, y_1, \eta) \left[g_q^2 N_f h_{\text{jet}}^q(p_{T2}) |M|_{q\bar{q} \rightarrow Q\bar{Q}}^2 + \frac{1}{2} g_g^2 h_{\text{jet}}^g(p_{T2}) |M|_{gg \rightarrow Q\bar{Q}}^2 \right],
\end{aligned} \tag{3.19}$$

3.3 Results and Discussions

In Fig. 3.1 we plot charm p_T distribution at RHIC energies. We see that charm distribution from prompt production dominates at all p_T . Considering initial jet formation time to be 0.15 fm/c, we have used two conditions, one with $\tau_f=R_T/c$ and the other with thermalization time ~ 0.5 fm/c. In any case the time integration is reduced to $\ln(\tau - f/\tau_i)$, and thus one can easily obtain this results for any choice of initial condition.

Our results for RHIC is quite similar to those by Lin and Gyulassy. Also the jet-thermal contribution is found to be comparable to jet-jet interaction. The contribution of thermal production is small at Large p_T but larger by a factor of 3 at lower p_T when compared to jet-jet and jet-thermal contributions. The contribution obtained by free streaming partons with initial conditions similar to that of thermal production is also very small particularly at higher p_T regions.

In Fig. 3.2, we show the results from our calculations of charm p_T distributions at LHC regime. We consider central collision of lead nuclei at $\sqrt{s}=5500$ GeV/nucleon. Other initial conditions have already been discussed. We find that the charm production from initial fusion is about a factor of 10 or more than at RHIC, and of course its fall with p_T is much more slower, as one would expect. We plot our results at LHC, taking formation time of QGP to be 0.07 fm/c. We have assumed the initial time of jet-jet interaction to be from $\tau_i < 0.1$ fm/c to the time until the jet reaches the surface ($\sim \tau_f=R_T/c$) as one of the extremes. The other extreme condition is by taking $\tau_f=0.5$ fm/c, the formation time of equilibrated medium.

We find that the production of heavy quark due to the jet-jet interaction is comparable to the prompt production for $p_T > 2.0$ GeV. However the contribution falls off for $p_T < 2.0$ GeV as we have considered jet partons having momentum > 2.0 GeV. Thermal contribution is about 40% for $\tau_i \sim 0.07$ fm/c and about 20% for $\tau_i \sim 0.5$ fm/c.

The thermal and the free-streaming contributions shown in Figs. deserve more attention. We see that the two contributions for larger initial temperatures at LHC differ by a factor of about 2 or more, while for the smaller initial temperature at RHIC they are of similar magnitude. This, we feel, has its origin in the large initial temperature which enhances the phase-space contribution to the thermal production of charm quarks. This feature is also evident from Figs. 3.3 where we plot the p_T spectra of the bottom quarks production at LHC.

3.4 Summary

Single particle spectra of charm for RHIC and LHC energies and that of bottom at LHC energies only have been calculated and discussed in this chapter. The mechanisms for heavy quark production elaborated here, are initial gluon fusion and secondary multiple scattering processes like jet-jet interaction and thermal interaction and passage of jets through QGP. Two different initial conditions, one with early thermalization time of $\tau \sim 0.1$ fm and other with thermalization time of 0.5 fm have been used. Substantial production of charm, specially at LHC, is seen in addition to the production due to initial fusion.

Another calculation for prompt charm production may be obtained from color glass condensate model [31]. Also, more complete calculations, reported in detail are found in [32] and also reported in Chapter 6.

We conclude that production of charm quarks at LHC and even at RHIC from processes other than initial fusion can be large and can play a significant role in our study of back-to-back correlation(Chapter 2). This may have important implications for the study of the nuclear modification factor R_{AA} as well as large mass dileptons having their origin in the correlated charm decay particularly at top LHC energy of $\sqrt{s}=5.5$ A TeV. However at lower collider

energies, it is seen that prompt production dominates over secondary mechanisms and as a first step one may use the prompt charm distribution only to study QGP properties.

Bibliography

- [1] S. S. Adler *et al.*, [PHENIX collaboration], Phys. Rev. Lett. **91**, 183201 (2003); S. Esumi [PHENIX collaboration], Nucl. Phys. A **715**, 599 (2003); C. Adler *et al.*, [STAR collaboration] Phys. Rev. Lett. **90**, 032301 (2003); *ibid.* **89**, 132301 (2002); *ibid.* **87**, 182301 (2001); P. Huovinen, P. F. Kolb, U. W. Heinz, P. V. Ruuskanen, and S. A. Voloshin, Phys. Lett. B **503**, 58 (2001).
- [2] X. N. Wang, Phys. Rev. C **63**, 054902 (2001); M. Gyulassy, I. Vitev, X. N. Wang, Phys. Rev. Lett. **86**, 2537 (2001); K. Adcox *et al.*, [PHENIX collaboration], Phys. Rev. Lett. **88**, 022301 (2002), J. Adams *et al.* [STAR collaboration], Phys. Rev. Lett. **91**, 172302 (2005).
- [3] R. J. Fries, S. A. Bass, and B. Müller, Phys. Rev. Lett. **94**, 122301 (2005).
- [4] D. G. d'Enterria, D. Peressunko, Eur. Phys. J. C **46**, 451 (2006); R. Chatterjee, L. Bhattacharya, D. K. Srivastava, "Electromagnetic Probes", Lecture notes in Physics, 785 (The Physics of the Quark-Gluon-Plasma), Ed. S. Sarkar, H. Satz, and B. Sinha. (Springer, Berlin, 2010).
- [5] T. Matsui and H. Satz, Phys. Lett. B **178**: 416, (1986)
- [6] R. L. Thews, M. Schroedter, J. Rafelski, Phys. Rev. C **63**, 054905 (2001).
- [7] A. Adare *et al.* [PHENIX Collaboration], Phys. Rev. Lett. **101**, 122301 (2008), A. Adare *et al.* [PHENIX Collaboration], Phys. Rev. Lett. **98**, 232301 (2007), S. S. Adler *et al.* [PHENIX Collaboration], Phys. Rev. C **69**, 014901 (2004).

- [8] R. A. Lacey *et al.*, Phys. Rev. Lett. **103**, 142302 (2009)
- [9] M. Younus and D. K. Srivastava, J. Phys. **G 37**, 115006 (2010). U. Jamil and D. K. Srivastava, J. Phys. **G 37**, 085106 (2010);
- [10] J. C. Collins, D. E. Soper and G. F. Sterman, Nucl. Phys. B **263**, 37 (1986), R. K. Ellis, Report No. FERMILAB CONF 86/35 T, 1986.
- [11] B. L. Combridge, Nucl. Phys. B **151**, 429 (1979).
- [12] E. Eichten, I. Hinchliffe, K. D. Lane and C. Quigg, Rev. Mod. Phys. **56**, 579 (1984) [Addendum-ibid. **58**, 1065 (1986)].
- [13] K. J. Eskola, V. J. Kolhinen, and C. A. Salgado, Eur. Phys. J. C **9**, 61 (1999); K. J. Eskola, V. J. Kolhinen, P. V. Ruuskanen and C. A. Salgado, Nucl. Phys. **A 661**, 645c (1999).
- [14] M. Arneodo, Phys. Rep. **240**, 301 (1994); M. Arneodo *et al.* [NMC Collaboration], Nucl. Phys. **B 481**, 23 (1996).
- [15] H. L. Lai *et al.* [CTEQ Collaboration], Eur. Phys. J. C **12**, 375 (2000).
- [16] J. F. Owens, Rev. Mod. Phys. **59**, 2, (1987).
- [17] Z. W. Lin and M. Gyulassy, Phys. Rev. C **51**, 2177 (1995) [Erratum-ibid. C **52**, 440 (1995)].
- [18] J. Kapusta, L. McLerran, D. K. Srivastava, Phys. Lett. B **283**, 145 (1992).
- [19] R. J. Fries, B. Müller, and D. K. Srivastava, Phys. Rev. Lett. **90**, 13 (2003).
- [20] D. K. Srivastava, C. Gale, R. J. Fries, Phys. Rev. C **67**, 034903, (2003), S. Turbide, C. Gale, D. K. Srivastava, and R. J. Fries, Phys. Rev. C **74**, 014903 (2006).
- [21] W. Liu and R. J. Fries, Phys. Rev. C **78**, 037902 (2008).
- [22] J. Rafelski and B. Müller, Phys. Rev. Lett. **48**, 1066 (1982) [Erratum-ibid. **56**, 2334 (1986)]; P. Koch, B. Müller, J. Rafelski, Phys. Rep. **142**, 167 (1986).

- [23] P. Levai, B. Müller, X. N. Wang, Phys. Rev. C **51**, 6 (1995).
- [24] A. Shor, Phys. Lett. B **215**, 375 (1988), A. Shor, Phys. Lett. B **233**, 231 (1989) [Erratum-ibid. B **252**, 722 (1990)].
- [25] J. D. Bjorken, Phys. Rev. D **27**, 140 (1983).
- [26] See e.g., S. S. Adler *et al.* [PHENIX Collaboration], Phys. Rev. C **71**, 034908 (2005) [Erratum-ibid. C **71**, 049901 (2005)].
- [27] D. Kharzeev, E. Levin and M. Nardi, Nucl. Phys. A **747**, 609 (2005)
- [28] N. Armesto and C. Pajares, Int. J. Mod. Phys. A **15**, 2019 (2000).
- [29] V. Khachatryan *et al.* [CMS Collaboration], JHEP **1002**, 041 (2010), K. Aamodt *et al.* [ALICE Collaboration], Eur. Phys. J. C **68**, 89 (2010), K. Aamodt *et al.* [ALICE Collaboration], arXiv:1004.3514. to appear in Eur. Phys. Jour. C.
- [30] S. Turbide, C. Gale, S. Jeon and G. D. Moore, Phys. Rev. C **72**, 014906 (2005).
- [31] D. Kharzeev and K. Tuchin, Nucl. Phys. A **735**, 248 (2004).
- [32] S. A. Bass, B. Müller and D. K. Srivastava, Phys. Lett. B **551**, 277 (2003), S. A. Bass, B. Müller, D. K. Srivastava, J. Phys. G **30**, 283 (2004), T. Renk, S. A. Bass and D. K. Srivastava, Phys. Lett. B **632**, 632 (2006), D. Y. Chang, S. A. Bass and D. K. Srivastava, J. Phys. G **30**, L7 (2004), D. Y. Chang, S. A. Bass and D. K. Srivastava, J. Phys. G **31**, S1005 (2005).
- [33] J. Uphoff, O. Fochler, Z. Xu and C. Greiner, J. Phys. Conf. Ser. **230**, 012004 (2010), J. Uphoff, O. Fochler, Z. Xu and C. Greiner, arXiv:1003.4200 [hep-ph].

Chapter 4

Heavy Quark Correlation

In previous chapter, we discussed in details on calculations of various mechanisms of heavy quark production (also see Refs. [1]–[4]) and showed single charm and bottom distributions which are important to study the nuclear modification factor, R_{AA} and azimuthal anisotropy, v_2 . In the present chapter I will discuss heavy quark pair production through different mechanisms which is important for studying $Q\bar{Q}$ correlations. It is already stated that the heavy quarks (only charm and bottom quarks are considered here) offer several unique advantages, so that one can use it to probe the properties of QGP. The conservation of flavour in strong interaction dictates that they are always produced in pairs ($Q\bar{Q}$). Their large mass ensures that momentum transfer, ' Q^2 ' necessary for their production in any interaction is large enough, so that pQCD techniques can be used. Heavy meson also stands out against the swarm of pions and thus any medium effects on its evolution during partonic phase are clearly reflected in its final spectra.

Their large mass also provides that, even though buffeted by light quarks and gluons during their passage through the quark gluon plasma, the direction of their motion may not change substantially. This should make them a valuable probe for the properties of the plasma which depend on the reaction plane. It is also not yet clearly established that heavy quarks will completely thermalize in the plasma formed at RHIC and LHC energies (see Ref. [6]). However it must be safe to assume that the drag [7] suffered by heavy quarks will mostly

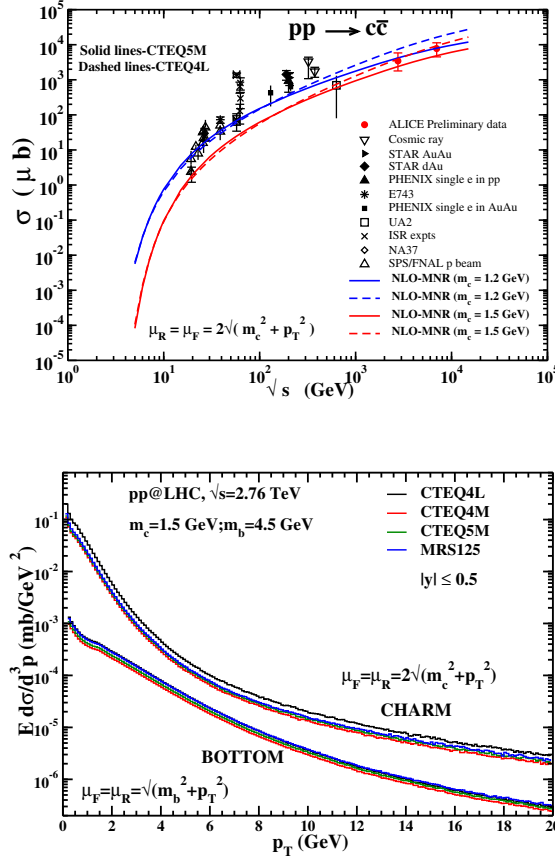


Figure 4.1: Energy dependence of the charm quark production in pp collisions.

slow it down and the diffusion [8] processes will not alter its direction considerably. Thus, the azimuthal correlation of heavy quarks integrated over p_T may be reasonably immune to the energy loss suffered by them.

The heavy quarks could be influenced by the flow [9] generated in heavy ion collisions. If this is true, then a very interesting situation may arise for heavy quarks which is not possible in case of light quarks or gluons. Let us consider a $Q\bar{Q}$ pair produced in a central collision having rapidity, $y = 0$. At leading order, their transverse momenta would be equal in magnitude and would point towards opposite directions. Consider a heavy quark Q is moving away from the centre with momentum \mathbf{p}_T , then its partner \bar{Q} would move with momentum $-\mathbf{p}_T$ towards the centre. Their velocities would be $\mathbf{v}_Q = \pm \mathbf{p}_T / M_T$, where $M_T = \sqrt{p_T^2 + M_Q^2}$, and M_Q is the mass of the heavy quark. Let the radial flow velocity be

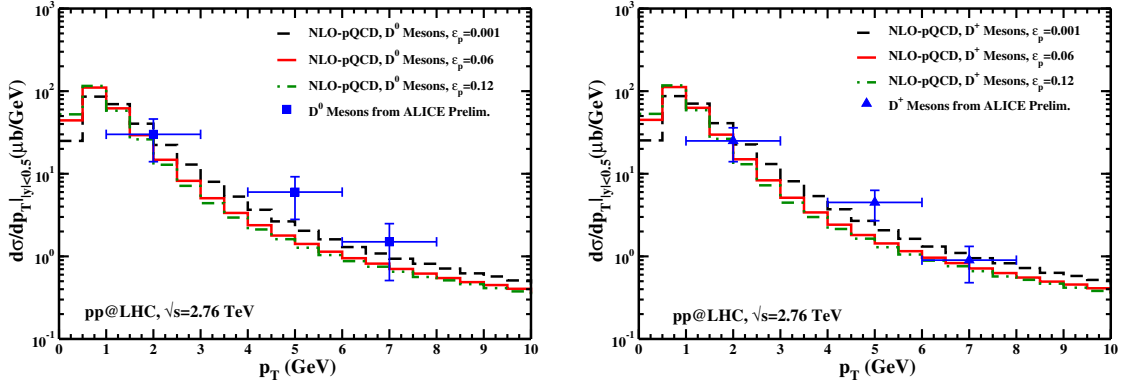


Figure 4.2: (left) Transverse momentum distribution of D^0 -mesons and (right) of D^{+-} -mesons, in pp collisions for $\sqrt{s}=2.76$ TeV.

\mathbf{v}_f . Now if $|\mathbf{v}_f| \geq |\mathbf{v}_Q|$, the \bar{Q} will turn back and start moving away from the centre! Thus the $Q\bar{Q}$ pair, which should have appeared back-to-back would appear as moving in the same direction. This would drastically alter the azimuthal correlation of the pair. A similar change of direction of motion is not possible for light quarks and gluons as they move with the speed of light, (see Ref. [9]).

Now let us consider the QCD processes of charm pair production: $gg \rightarrow Q\bar{Q}$ at leading order and $gg \rightarrow gQ\bar{Q}$ at next-to-leading order. In the absence of any intrinsic transverse momentum, k_T for partons, the quarks from the first process will be produced back-to-back, while those from the second process will be mostly collinear and will additionally be accompanied with a recoiling parton. A comparison of the energy loss suffered by the recoiling parton and the heavy-quarks will allow us to obtain flavour dependence of the energy loss. A considerable richness to this picture is added by the realization that the splitting $g \rightarrow Q\bar{Q}$, would produce collinear heavy quarks, while the process $gg \rightarrow Q\bar{Q}g$, where a gluon is radiated by one of the heavy quarks will essentially give rise to a flat azimuthal correlation.

So far we have discussed only the azimuthal correlation of the heavy quarks. A study of the transverse momentum of the pair and the rapidity-difference of the pair can help us disentangle the LO and the NLO processes. Recall that the transverse momentum of the

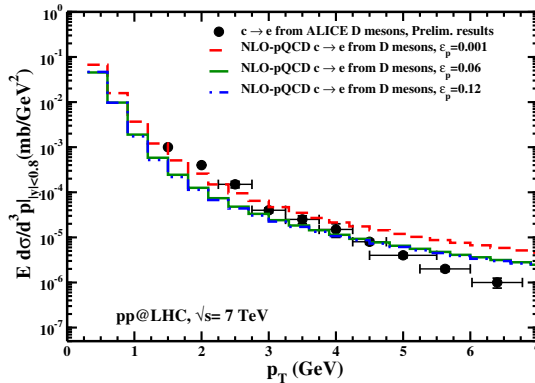


Figure 4.3: Transverse momentum distribution of single electrons from pp collisions at $\sqrt{s} = 7$ TeV.

$Q\bar{Q}$ pair would be identically zero at LO and equal to that of the recoiling parton at NLO. Deviations from the results for pp collisions at the corresponding centre of mass energy in nuclear collisions will provide a measure of medium modifications as usual.

The nuclear modification factor, R_{AA} , is a strong observable for energy loss [10] of jet particles in a medium and thus indicates formation of QGP. However it is suggested in some literatures that it may not be able to discriminate between different mechanisms of energy loss and evolution of the system [11] and the correlation of the leading hadrons may fill up the picture of our understanding of the modification of the particle spectra in the medium [12]. Consider a simple example. We need to know the transverse momentum of heavy quarks in pp collisions in order to have a base-line to estimate the nuclear modifications. The NLO pQCD results for these are easily approximated by a K factor multiplying the results for LO pQCD (see eg. Ref. [13]). Now consider the azimuthal correlations of heavy quarks produced in similar collisions. As we discussed above, the LO pQCD results for the correlation is a delta function around $\Delta\phi = \pi$. However, we shall see that the correlation function estimated at NLO, though still peaking at $\Delta\phi = \pi$ fills up the phase-space from zero to π with an interesting catenary like structure.

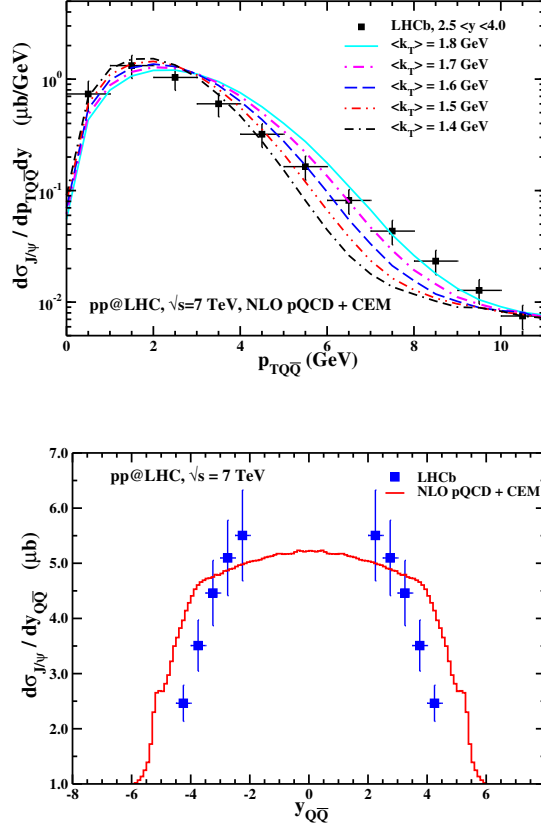


Figure 4.4: Transverse momentum (left panel) and rapidity distribution (right panel) of J/ψ from pp collision at $\sqrt{s}=7$ TeV, using color evaporation model.

The present work aims at investigating azimuthal, momentum, and rapidity correlations for heavy quark-anti quark pairs for pp collisions and setting the stage for the study of the deviations in these due to medium modifications in heavy ion collisions at the corresponding energies. We also discuss the complexities arising from the additional production of heavy quarks due to multiple scatterings [14].

The chapter is organized as follows. In the next section we discuss various correlations for pp collisions using NLO pQCD. In Sect. 3 we discuss the azimuthal correlations in Pb+Pb collisions due to initial production and various secondary mechanisms. Our results for pp and Pb+Pb collisions are discussed in Sect. 4 followed by conclusion in Sect. 5.

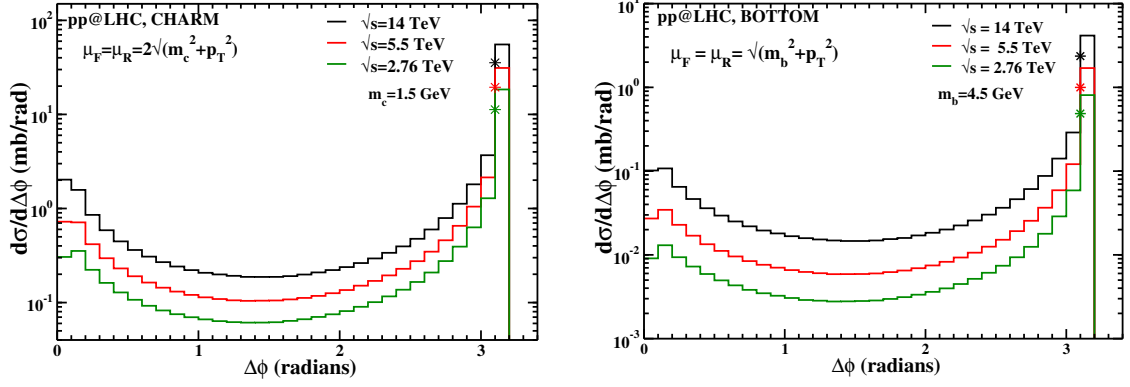


Figure 4.5: Azimuthal correlation of charm (left panel) and bottom (right panel) quarks at 2.76, 5.5 and 7 TeV for pp collisions. The symbols give the LO values for $d\sigma/d\phi = \sigma_{LO}/\delta(\Delta\phi)$ where $\delta(\Delta\phi)$ is the size of ϕ bin.

4.1 Proton on Proton Collision

The results for particle and photon productions in proton on proton, pp collisions serve as a baseline in search for quark-gluon-plasma and other medium effects at the corresponding centre of mass energy/nucleon for collision of heavy nuclei. This paradigm may have to be modified if the recent suggestions for formation of high multiplicity system(perhaps only in high multiplicity events), Ref. [15] in pp collisions turn out to be valid. In the present work any AA collision has been considered as a incoherent superposition of pp collisions.

The correlation of heavy quarks produced in pp collisions is defined in general as:

$$E_1 E_2 \frac{d\sigma}{d^3 p_1 d^3 p_2} = \frac{d\sigma}{dy_1 dy_2 d^2 p_{T1} d^2 p_{T2}} = C, \quad (4.1)$$

where y_1 and y_2 are the rapidities of heavy quark and anti-quark and \mathbf{p}_{T_i} are their transverse momenta.

At the leading order, the differential cross-section for the charm correlation from proton-proton collision can be written as:

$$C_{LO} = \frac{d\sigma}{d^2 p_T dy_1 dy_2} \delta(\mathbf{p}_{T1} + \mathbf{p}_{T2}). \quad (4.2)$$

In the above $\mathbf{p}_{T1} = \mathbf{p}_{T2} = \mathbf{p}_T$ and

$$\begin{aligned} \frac{d\sigma}{dy_1 dy_2 dp_T} &= 2x_a x_b p_T \sum_{ij} \left[f_i^{(a)}(x_a, Q^2) f_j^{(b)}(x_b, Q^2) \frac{d\hat{\sigma}_{ij}(\hat{s}, \hat{t}, \hat{u})}{d\hat{t}} \right. \\ &\quad \left. + f_j^{(a)}(x_a, Q^2) f_i^{(b)}(x_b, Q^2) \frac{d\hat{\sigma}_{ij}(\hat{s}, \hat{u}, \hat{t})}{d\hat{t}} \right] / (1 + \delta_{ij}), \end{aligned} \quad (4.3)$$

where x_a and x_b are the fractions of the momenta carried by the partons from their interacting parent hadrons. These are given by

$$x_a = \frac{M_T}{\sqrt{s}}(e^{y_1} + e^{y_2}); \quad x_b = \frac{M_T}{\sqrt{s}}(e^{-y_1} + e^{-y_2}). \quad (4.4)$$

where M_T is the transverse mass, $\sqrt{m_Q^2 + p_T^2}$, of the produced heavy quark. The subscripts i and j denote the interacting partons, and f_i and f_j are the partonic distribution functions for the nucleons. We shall use CTEQ5M structure function, though we have checked that similar results are obtained for other modern structure functions (see later). The differential cross-section for partonic interactions, $d\hat{\sigma}_{ij}/d\hat{t}$ is given by

$$\frac{d\hat{\sigma}_{ij}}{d\hat{t}} = \frac{|M|^2}{16\pi\hat{s}^2}, \quad (4.5)$$

where $|M|^2$ is the invariant amplitude for different sub-processes as obtained from Ref. [16]. The physical sub-processes included for the leading order, $\mathcal{O}(\alpha_s^2)$ production of heavy quarks are:

$$\begin{aligned} g + g &\rightarrow Q + \bar{Q} \\ q + \bar{q} &\rightarrow Q + \bar{Q}. \end{aligned} \quad (4.6)$$

At next-to-leading order, $\mathcal{O}(\alpha_s^3)$ subprocesses included are as follows

$$\begin{aligned} g + g &\rightarrow Q + \bar{Q} + g \\ q + \bar{q} &\rightarrow Q + \bar{Q} + g \\ g + q(\bar{q}) &\rightarrow Q + \bar{Q} + q(\bar{q}). \end{aligned} \quad (4.7)$$

We show our results for azimuthal correlation $C(\Delta\phi)$, where $\Delta\phi = |\phi_1 - \phi_2|$ as well as for rapidity correlations, $C(\Delta y)$, where $\Delta y = y_1 - y_2$, of produced heavy quarks. We also present

$(\Delta\eta, \Delta\phi)$ correlations in the jet radius parameter, R , where $R = \sqrt{(\Delta\eta)^2 + (\Delta\phi)^2}$ along with the transverse momentum, invariant mass, and rapidity of the pair.

We also show results on the production of J/ψ and charm measured recently.

4.2 Lead Lead Collisions

Let us now move towards lead on lead, Pb+Pb collisions currently under study at the Large Hadron Collider (LHC), CERN. We have discussed that most of the heavy-quarks and as well as quarks and gluons having large transverse momenta are produced in initial hard collisions. At the energies reached at the LHC, the sheer number of quarks and gluons produced in these collisions leads to vehement multiple collisions and gluon multiplication. This, then, leads to a quark-gluon plasma at a very large initial temperature.

As discussed earlier, we would like to know if these initial temperatures are large enough to produce heavy quarks as well (see eg. Ref. [4]). The multiple collisions among the very high momentum quarks and gluons (the so called jet-jet collisions) have been seen earlier to produce substantial number of heavy quarks. These jets, produced at very early times $\tau \approx 1/p_T$ will have to necessarily pass through the QGP which will be formed only after $\tau \approx 0.1$ fm/c. Do these lead to a substantial production of heavy quarks? Some of these questions have been addressed earlier [1, 2, 4].

4.2.1 Prompt Interactions

The basic formulation which gives the correlation of produced heavy quarks from initial fusion of gluons and quark-anti quark annihilation in proton-proton collision is given by Eq. 4.1. Thus the azimuthal distribution of heavy quark for Pb+Pb collision at $b = 0$ is given by

$$E_1 E_2 \frac{dN}{d^3p_1 d^3p_2} = T_{AA} E_1 E_2 \frac{d\sigma_{pp}}{d^3p_1 d^3p_2}. \quad (4.8)$$

For central collisions of lead nuclei, the nuclear thickness function is taken as $T_{AA} = 292 \text{ fm}^{-2}$. In the above \mathbf{p}_1 and \mathbf{p}_2 are the momenta of the heavy quarks produced.

4.2.2 Jet-Jet Interaction

The initial hard scattering will produce massless gluons and light quarks in large numbers. These partons have large transverse momenta. These quarks and gluons may ultimately thermalize because of frequent interactions among themselves and if sufficient energy is available, their interactions may lead to the production of heavy quarks as well. Here we give the formulation for azimuthal distribution of produced heavy quarks pair from jet-jet interaction. Since the jet-jet contribution to the heavy quark production is comparable to that of primary production [1, 2], it should be interesting to see if their azimuthal distributions differ.

As a first step we obtain the distribution of light partons, having $p_T > 2 \text{ GeV}$, from a LO pQCD calculation using CTEQ5M structure function, for pp collisions at 2.76 TeV and 5.5 TeV. We parametrize them as:

$$\begin{aligned} \frac{dN}{dyd^2p_T} &= T_{AA} \frac{d\sigma_{pp}^{\text{jet}}}{d^2p_T dy} \Big|_{y=0} \\ &= K \frac{C}{(1 + p_T/B)^\beta} \end{aligned} \tag{4.9}$$

where the K factor is taken as 2.5 to account for higher order effects and the parameters C , B , and β are given in Table 2 (see Appendix A). The factorization and renormalization scales for $Q\bar{Q}$ are chosen as $\mu_F = \mu_Q = 2\sqrt{p_T^2 + M_Q^2}$.

Now the azimuthal distribution of heavy quarks for collisions having an impact parameter, $b = 0$, due to jet-jet interaction can be written as:

$$\begin{aligned}
E_1 E_2 \frac{dN}{d^3 p_1 d^3 p_2} &= \frac{1}{16(2\pi)^8} \int d^4 x \int \frac{d^3 p_a d^3 p_b}{\omega_a \omega_b} \delta^4(\Sigma p^\mu) \\
&\times \left[\frac{1}{2} g_g^2 f_{\text{jet}}^g(p_{Ta}) f_{\text{jet}}^g(p_{Tb}) |M_{gg \rightarrow Q\bar{Q}}|^2 \right. \\
&\left. + g_q^2 \sum_i \left\{ f_{\text{jet}}^{q_i}(p_{Ta}) f_{\text{jet}}^{\bar{q}_i}(p_{Tb}) |M_{q\bar{q} \rightarrow Q\bar{Q}}|^2 + (q_i \leftrightarrow \bar{q}_i) \right\} \right], \quad (4.10)
\end{aligned}$$

where p_a, p_b are the four momenta of the incoming partons and p_1 and p_2 are the same for the outgoing heavy quarks, and q_i stands for the flavour of the light quarks. The jet distribution function $f_{\text{jet}}(p_T)$ is given by

$$f_{\text{jet}}^i(p_T) = \frac{(2\pi)^3}{g_i \tau \pi R_T^2 p_T} \frac{dN_i}{d^2 p_T dy} \delta(y - \eta) \Theta(\tau_f - \tau) \Theta(\tau - \tau_i). \quad (4.11)$$

This follows the Bjorken space-time correlation used earlier in Refs. [1, 2, 33]. Now the Eq. 4.10 reduces to:

$$\begin{aligned}
E_1 E_2 \frac{dN}{d^3 p_1 d^3 p_2} &= \frac{1}{16(2\pi)^8} \int d^4 x \int d^2 p_{Ta} d^2 p_{Tb} dy_b \frac{\delta(\Sigma E)}{\omega_b} \\
&\times \left[\frac{1}{2} g_g^2 f_{\text{jet}}^g(p_{Ta}) f_{\text{jet}}^g(p_{Tb}) |M_{gg \rightarrow Q\bar{Q}}|^2 + g_q^2 \times \right. \\
&\left. \sum_i \left\{ f_{\text{jet}}^{q_i}(p_{Ta}) f_{\text{jet}}^{\bar{q}_i}(p_{Tb}) |M_{q\bar{q} \rightarrow Q\bar{Q}}|^2 + (q_i \leftrightarrow \bar{q}_i) \right\} \right], \quad (4.12)
\end{aligned}$$

where $d^4 x = \tau d\tau r dr d\eta d\phi_r$ and $d^3 p = p_T dp_T d\phi_p E dy$.

The formation time for the jets (light p_T partons) is taken as $\tau_i = 0.1$ fm/c, as we count those having $p_T > 2$ GeV, as jets, We take $\tau_f \approx R_T$, of the system and perform rest of the integration numerically.

4.2.3 Jet-Thermal Interaction

Now, we consider passage of high energy energy jets through quark gluon plasma and estimate azimuthal dependence of the produced heavy quarks.

Suppose, a light parton is produced at position \mathbf{r} , and moves at an angle α where $\cos \alpha = \hat{r} \cdot \hat{d}$, then the distance d travelled by the jet along the direction \hat{d} , before it reaches the surface is given by:

$$d = -r \cos \alpha + \sqrt{R^2 + r^2 \sin^2 \alpha}, \quad (4.13)$$

Hence the time available for heavy quark production is the minimum of $[\tau_d, \tau_f]$, where τ_d is time taken by the parton to cover the distance d and τ_f is the time when quark gluon plasma hadronizes.

The azimuthal distribution of the produced heavy quark from jet-thermal interaction is given by

$$\begin{aligned} E_1 E_2 \frac{dN}{d^3 p_1 d^3 p_2} &= \frac{1}{16(2\pi)^4 \pi R_T^2} \int r dr d\tau d\eta d\phi_b dy_b \\ &\times \frac{p_{Tb0}}{p_{Ta} [p_{T1} \cos(\phi_1 - \phi_b) + p_{T2} \cos(\phi_2 - \phi_b) - M_{T1} \cosh(y_1 - y_b) - M_{T2} \cosh(y_2 - y_b)]} \\ &\times \left[\frac{1}{2} g_g h_{\text{jet}}^g(p_{Ta}) f_{\text{th}}^g(p_{Tb0}) |M_{gg \rightarrow Q\bar{Q}}|^2 \right. \\ &\left. + g_q \sum_i \left\{ h_{\text{jet}}^{q_i}(p_{Ta}) f_{\text{th}}^{q_i}(p_{Tb0}) |M_{q\bar{q} \rightarrow Q\bar{Q}}|^2 + (q_i \leftrightarrow \bar{q}_i) \right\} \right] \quad (4.14) \end{aligned}$$

which is then evaluated numerically (see Appendix for Mathematical details).

4.2.4 Thermal Interaction

We have discussed earlier that the multiple scatterings among the quarks and gluons leads to the formation of quark gluon plasma at a large initial temperature. Interaction among the thermalized partons may also lead to charm production provided the initial temperature of quark gluon plasma is high. Using the recent results from ALICE at $\sqrt{s}=2.76$ A TeV for central collisions of lead-lead nuclei, we take particle multiplicity density to be $dN/dy=2850$ at $\sqrt{s}=2.76$ TeV/nucleon, [17] and extrapolate it to 3000 for $\sqrt{s} = 5.5$ TeV/nucleon. Now using the relation [19]

$$\frac{2\pi^4}{45\zeta(3)\pi R_T^2} \frac{dN}{dy} = 4aT_0^3 \tau_0 \quad (4.15)$$

and initial formation time for QGP, $\tau_i=0.1$ fm/c, we estimate T_0 to be 653 MeV at 2.76 TeV/nucleon and 664 MeV at 5.5 TeV/nucleon respectively.

Recall also that at RHIC energies, τ_i up to 0.6 fm/c have been used, specially for the part of the evolution which could be described using hydrodynamics. One may imagine τ_i getting smaller at LHC energies, due to increased activity of minijets, etc. Thus for example, the parton saturation models [20] suggest that p_{sat} at LHC energies is close to 2 GeV, which suggests that the initial time τ_i for the plasma would be $\approx 1/p_{\text{sat}}$ or about 0.1 fm/c. We shall discuss the consequences of taking large formation times (see later).

Thus the azimuthal distribution of heavy quarks produced from interactions of thermalized partons is given by

$$\begin{aligned}
E_1 E_2 \frac{dN}{d^3p_1 d^3p_2} &= \frac{1}{16(2\pi)^8} \int d^4x \int d\phi_b dy_b \\
&\times \frac{p_{Tb0}}{[p_{T1} \cos(\phi_1 - \phi_b) + p_{T2} \cos(\phi_2 - \phi_b) - M_{T1} \cosh(y_1 - y_b) - M_{T2} \cosh(y_2 - y_b)]} \\
&\times \left[\frac{1}{2} g_g^2 f_{\text{th}}^g(p_{Ta}) f_{\text{th}}^g(p_{Tb0}) |M_{gg \rightarrow Q\bar{Q}}|^2 \right. \\
&\left. + g_q^2 \sum_i \left\{ f_{\text{th}}^{q_i}(p_{Ta}) f_{\text{th}}^{\bar{q}_i}(p_{Tb0}) |M_{q\bar{q} \rightarrow Q\bar{Q}}|^2 + (q_i \leftrightarrow \bar{q}_i) \right\} \right], \quad (4.16)
\end{aligned}$$

where (the boosted) thermal distribution of partons is approximated as

$$f_{\text{th}}(p_T, y, \eta) = \exp \left[-\frac{p_T}{T} \cosh(y - \eta) \right]. \quad (4.17)$$

The above integration is done numerically, with the temperature varying according to Bjorken's cooling law, i.e. $T^3\tau = \text{constant}$, till the temperature drops to about 160 MeV.

4.3 Results and Discussions

4.3.1 Proton Proton Collisions

In the results to be reported in the following, we shall use the CTEQ5M structure function, though some results are also given for other structure functions. The mass of the charm

quarks is kept fixed at $m_c = 1.5$ GeV, while that for bottom quarks is $m_b = 4.5$ GeV. The factorization and renormalization scales are taken as $C \sqrt{m_Q^2 + p_T^2}$ with factor $C = 2$ for charm quarks and 1 for bottom quarks. The NLO pQCD code (NLO-MNR) developed by Mangano et al. [21, 22] has been used for the initial production of heavy quarks.

Production of heavy quarks, charmed mesons, and J/ψ :

The results for charm production along with recent results obtained at LHC for pp collisions are shown in Fig. 4.1. For the sake of exploration we have also included results for $m_c = 1.2$ GeV and the structure function CTEQ5M. A very good description of the data Ref. [23], without any adjustment of parameters is seen (see also Refs. [13, 24]).

We have given the results of our calculations using several structure functions in Fig. ?? for the production of charm and bottom quarks at central rapidities in pp collisions at 2.76 TeV. We see that use of any of the more modern structure functions gives results which differ by just a few percent from each other.

One may also consider the production of D-mesons by writing schematically:

$$E \frac{d^3\sigma}{d^3p} = E_Q \frac{d^3\sigma(Q)}{d^3p_Q} \otimes D(Q \rightarrow H_Q) , \quad (4.18)$$

where the fragmentation of the heavy quark Q into the heavy-meson H_Q is described by the function D . We have assumed that the shape of $D(z)$, where $z = p_D/p_c$, where p_D is the D meson momentum and p_c is the charm momentum and is identical for all the D -mesons [25],

$$D_D^{(c)}(z) = \frac{n_D}{z[1 - 1/z - \epsilon_p/(1 - z)]^2} , \quad (4.19)$$

ϵ_p is the Peterson parameter and

$$\int_0^1 dz D(z) = 1 . \quad (4.20)$$

The production of a particular D -meson is then obtained by using the fraction for it, determined experimentally [26, 27].

A comparison of our results for D^0 and D^+ production with the preliminary data obtained by ALICE experiment [28] is shown in Fig. 4.2. We give results for $\epsilon_p = 0.001, 0.06, \text{ and } 0.12$ to show the sensitivity of our calculations to this variation. Considering that no parameters have been adjusted, the results seem to be satisfactory. More detailed and accurate data will definitely put stringent constraints on all the inputs.

Note that the semi-leptonic decay of D -mesons has been extensively used to study the production of charm and bottom quarks, as well as the energy loss suffered by them. The electrons coming from charm decay, for example, are obtained by convoluting the distribution of D -mesons (Eq. 5.10) with the electron decay spectrum [29] and accounting for the branching to a particular D -meson [26, 27]. In case the contributions of the B and the D mesons cannot be distinguished, one should use the B and D -meson mixtures, with appropriate branchings, $B \rightarrow e, D \rightarrow e$ and $B \rightarrow D \rightarrow e$. The semileptonic decay of B -mesons becomes important at higher p_T in spite of their reduced production, though the contribution of the $B \rightarrow D \rightarrow e$ channel drops rapidly with increase in p_T (see e.g., Ref. [30]).

The ALICE experiment has, however, obtained the single electrons from the process $c \rightarrow D \rightarrow e$ [31]. The upgrades of STAR and PHENIX experiments at RHIC will also be able to measure this.

In Fig. 4.3, we compare our results for the electrons measured by the ALICE experiment with the decay of charm and a reasonable agreement is seen. In a future publication, we shall report on the consequences of introducing an intrinsic k_T for the partons and also using different parametrization of the decay spectrum of the electrons.

The production of J/ψ in pp collisions is yet another important observable, which is closely related to the production of charm quarks. For example, using the colour evaporation model, one can write:

$$\frac{d\sigma_{J/\psi}}{dy} = F \int_{2m_c}^{2m_D} dM \frac{d\sigma_{c\bar{c}}}{dM dy}. \quad (4.21)$$

where M is the invariant mass of the pair, y is its rapidity, m_D is the mass of D -mesons, and F is the (constant) colour-evaporation factor which should be fixed by evaluation at some energy. There is one small detail which should be mentioned here; the LO pQCD

calculations for heavy quark production produce $c\bar{c}$ pairs with pair-momentum identically equal to zero (though the NLO processes do provide them with a net transverse momentum). This is corrected by imparting an intrinsic k_T to the partons (see e.g. [32]). *Only for these calculations* we impart an intrinsic k_T of 1.5 GeV/ c to the partons.

We show our results for the transverse momentum and the rapidity distribution of J/ψ in Fig. 4.4 along with the experimental results for pp collision at 7 TeV obtained for prompt J/ψ by the LHCb experiment[33]. (Note that the ALICE collaboration has measured the inclusive J/ψ which includes the b-decays [34]. Even though this contribution is of the order of 10%, it is often accounted for by adding the $b \rightarrow J/\psi$ contribution measured by the LHCb experiment.) We have explored the consequences of varying the intrinsic k_T on the p_T distribution of J/ψ and, as expected, the slope of the p_T distribution decreases with increase in k_T . A reasonable description of the distribution of the transverse momentum and the rapidity distribution is seen. An accurate description of the data will involve a more detailed exploration of the parameters. For example, the colour evaporation coefficient is kept fixed in these calculations, to magnify the effect of varying intrinsic k_T . Of-course the change of intrinsic k_T will not affect the rapidity distribution.

It will be interesting to continue with this study for the prompt production of higher resonances of $c\bar{c}$ as well as of $b\bar{b}$, when more accurate and detailed data become available.

Correlations:

Having witnessed a good description of charm production as well as J/ψ production, we now move to the main topic of the present work. In the following we give our results for azimuthal, rapidity-difference, transverse momentum, and jet-radius correlation for charm and bottom quarks at 2.76 and 5.5 TeV for pp collisions. Deviations from these would signal medium modifications in case of nucleus-nucleus collisions.

Fig. 4.5 shows p_T and rapidity integrated $\Delta\phi$ distribution for heavy quarks at $\sqrt{s} = 2.76$ TeV, 5.5 TeV and 14.0 TeV for both leading order and next-to-leading order calculations.

As expected the contribution rises with the energy available in the centre-of-mass system. It is felt that if our argument about heavy quarks not changing direction of their motion due to soft collisions with partons is valid, then drag (or energy loss) alone will not drastically alter this feature. It is needless to repeat that at LO all the heavy quarks will be produced back-to-back resulting in a peak at $\Delta\phi = \pi$. However, *if* the heavy quarks thermalize and flow with the medium, this picture may undergo change. We shall come back to this.

In Fig. 4.6 we show our results for the transverse momentum, rapidity, and invariant mass distribution of charm and bottom quark pairs produced in pp collisions at $\sqrt{s}=2.76$ and 5.5 TeV. Recall that the pair momentum will be balanced by the momentum of the recoiling parton. Thus tagging on a high transverse momentum recoiling parton in the case of heavy ion collisions can give interesting details of how heavy quarks and (mostly) gluons behave in the medium produced in the collision. These results also contain a very interesting situation. Consider a heavy-quark produced in LO pQCD in a nucleus-nucleus collision. They will be produced back-to-back and are most likely to cover different part and length of the system, before they fragment (or coalesce with a light quark) to form a D-meson. Thus they would lose a differing amount of energy and acquire a net-transverse momentum which was initially identically zero. At least the collinear heavy-quarks produced during splitting of an off-shell gluon would, on the other hand, cover similar distances under similar conditions in the plasma, and thus their net transverse momentum will remain largely unaltered. It would be interesting to study such cases in future more detailed experiments.

We show our results for rapidity correlation where, $\Delta y = y_1 - y_2$, of heavy quarks produced in such collisions in Fig. 4.7. We note that this correlation peaks at vanishing rapidity difference. We have also given the LO results for this along with a scaling of the LO results with a factor $\sigma_{\text{NLO}}/\sigma_{\text{LO}}$ to demonstrate that the NLO results cannot, in general, be approximated by a K factor multiplying the LO results, and the inadequacy of this shows up most strongly near Δy equal to zero. It is also likely that the rapidity difference, specially when the two rapidities have opposite signs may encode effects of longitudinal flow in case of nucleus-nucleus collisions.

Fig. 4.8 shows the results of our calculation for the jet-radius, R , correlation, where $R = \sqrt{\Delta\eta^2 + \Delta\phi^2}$. It brings out the interesting differences between results for the leading order and next-to-leading calculations. Thus, while at leading order we do not have any contribution for $R < \pi$, there is a substantial contribution coming from next-to-leading processes for $0 < R < \pi$.

4.3.2 Lead Lead Collisions

Now we proceed to our results for collision of lead nuclei at 2.76 ATeV and 5.5 ATeV. In Fig. 4.9 we show our results for azimuthal distribution of heavy quarks produced from initial (prompt) collision of partons, having transverse momenta of 1–4 GeV and rapidities close to zero. The results for LO calculations, having a peak at $\Delta\phi = \pi$ are given, to demonstrate the importance of using NLO results as a base line for these studies. We see a sharpening of the collinear and back-to-back correlations as the momenta of the quarks increases, while the correlation, with the exception of the peak at $\Delta\phi = \pi$, gets more flat, as NLO processes have a larger role, as the available energy increases. We also find less production of pairs of bottom quarks with smaller $\Delta\phi$ at the same energy, compared to charm quarks, as expected.

We show our results for production of heavy quarks from multiple scattering of jets in Fig. 4.10. We have limited our calculations to contributions from quarks and gluons having $p_T > 2$ GeV. Let us first consider our results for charm quarks. At both the energies, we see that while charm quarks having transverse momenta around 1.5 GeV, show a correlation which rises smoothly as we go from collinear to back-to-back correlations, the charm-quarks having larger transverse momenta give rise to a flat distribution for larger $\Delta\phi$. We also note that the contribution of multiple scattering of the jets, even though smaller at $\Delta\phi \approx \pi$ compared to the contribution of initial production, is rather comparable at smaller angular separations. We note that as the initial and the final times τ_i and τ_f appear only as a multiplicative factor $\ln(\tau_f/\tau_i)$, the shape the correlation will remain unaffected by any change in their value.

The bottom quarks show a very interesting trend. For the lowest momentum considered, the bottom-quarks are seen to be produced with a flat azimuthal correlation, while as their momenta increase, the distribution becomes more and more collinear. The observation about comparable contributions of multiple scattering of jets and initial production at $\Delta\phi < \pi$, seen earlier for charm quarks, applies to them as well.

The results for the angular correlations of heavy quarks produced from the passage of jets through QGP are shown in Fig. 4.11. A very interesting and distinct picture emerges for these heavy quarks. We see that these productions are dominated by collinear contributions, confirming the nomenclature "jet-conversion" (see Ref. [4, 33]) for them. At small $\Delta\phi$ their contribution is similar to that from initial production. The corresponding results for bottom quark-pairs show similar trends, but those are an order of magnitude smaller than the contribution of initial production.

And finally the results for the angular correlation of heavy quarks produced from scattering of thermalized partons is shown in Fig. 4.12. Firstly, these contributions are smaller by more an order of magnitude than the contributions discussed above. However, we still discuss their features as these are quite interesting. The azimuthal correlation of charm as well as bottom quark pairs is rather flat for low transverse momenta but changes steadily to back-to-back at the transverse momentum increases. This, we feel, happens as heavy quarks having large transverse momenta can only come from collisions of partons having large \sqrt{s} . This would be possible for partons having almost equal and opposite momenta, thus leading to heavy quarks which will be predominantly back-to-back.

Recall that we have used a formation time of the plasma as $0.1 \text{ fm}/c$, inspired by the parton saturation model. A larger value for τ_i will leave the jet-jet contribution essentially unchanged, as we discussed earlier. However the jet-thermal and thermal contributions are expected to drop if the initial time is increased. Thus recalling our results from Ref. [2], we estimate that raising the τ_i to $0.5 \text{ fm}/c$ the jet-thermal contribution may decrease by a factor of 2, while the thermal contribution will come down by a factor of about 4.

4.3.3 Effect of Flow

We have suggested earlier that the effect of drag or energy loss of heavy quarks alone may not be enough to change their direction of motion, and thus the p_T -integrated azimuthal correlations discussed in this work may not be affected by the energy loss. It may change for a given p_T due to migration of quarks to the regions of lower p_T and the p_T dependence of the heavy quark production. The flow of the medium can, however, affect the angular correlation considerably, if it is large and if the heavy quarks are thermalized. In order to estimate the effect of the flow on the correlation of the heavy quarks, we use a toy model used earlier by Cuautle and Paic [35], and more recently in Ref. [36], for studying correlations.

In order to do this, we proceed as follows. We first give a random orientation to the quark-pairs from the NLO pQCD calculations (the NLO MNR code, e.g., at LO gives pairs with $p_{x_1} = p_{x_2} = 0$). Then we place them at (x, y) , randomly chosen according to the probability:

$$P = \frac{\int \int dx dy T_A(x, y, b=0) T_B(x, y, b=0)}{T_{AB}(b=0)}, \quad (4.22)$$

where T_i is the transverse density profile of the nucleus i assumed to have a uniform density of radius R , and $T_{AB}(b=0)$ is the nuclear thickness for impact parameter, $b=0$. Assuming a flow, directed away from the centre, we add the flow momentum $\mathbf{p}_{Tf} = p_{Tf} (\mathbf{r}/r)$ to the momentum of the heavy quark \mathbf{p}_T .

We use the blast-model [37] to write p_{Tf} as

$$p_{Tf} = \gamma \beta_r m_Q, \quad (4.23)$$

where

$$\beta_r = \beta_s \times \left(\frac{r}{R_T} \right)^2. \quad (4.24)$$

and $r = \sqrt{x^2 + y^2}$. We give results for $\beta_s = 0, 0.3, \text{ and } 0.6$. We show our results Fig. 4.13 for two ranges of p_T of the charm quarks, $p_T < 4 \text{ GeV}$ and $p_T > 4 \text{ GeV}$. We see that even though the azimuthal correlation is more strongly affected for charm quarks having lower transverse momenta for reasonable values of the flow, the basic nature of the correlation

function remains unchanged. It is likely that if the charm quarks are not completely thermalized, the effective flow velocity for them could be smaller, and then the above observation becomes even more relevant. Note that large values of β_s are normally reached only in the hadronic phase.

4.4 Summary

We have calculated azimuthal, rapidity difference, and transverse momentum correlations of heavy quark pairs produced in pp collisions at several energies relevant for experiments being done at the Large Hadron Collider, using NLO pQCD. Wherever possible, we have discussed how these could change due to final state effects in nucleus-nucleus collisions. These results will act as a base-line for similar studies in the case of $Pb + Pb$ collisions at the corresponding centre of mass energies/nucleon, to determine medium modifications. We have noted that this picture is enriched (or complicated) by multiple collisions among the partons having high energy, which can give very different correlations of a magnitude comparable to that of initial productions considered above. We have argued, but it remains to be verified, that these correlations may not be drastically altered due to the energy loss suffered by heavy quarks, as they may not change the direction of their motion substantially, due to soft scatterings. These aspects will be addressed in the next chapter. These may, however, be affected by a strong flow of the medium, if the heavy quarks are thermalized.

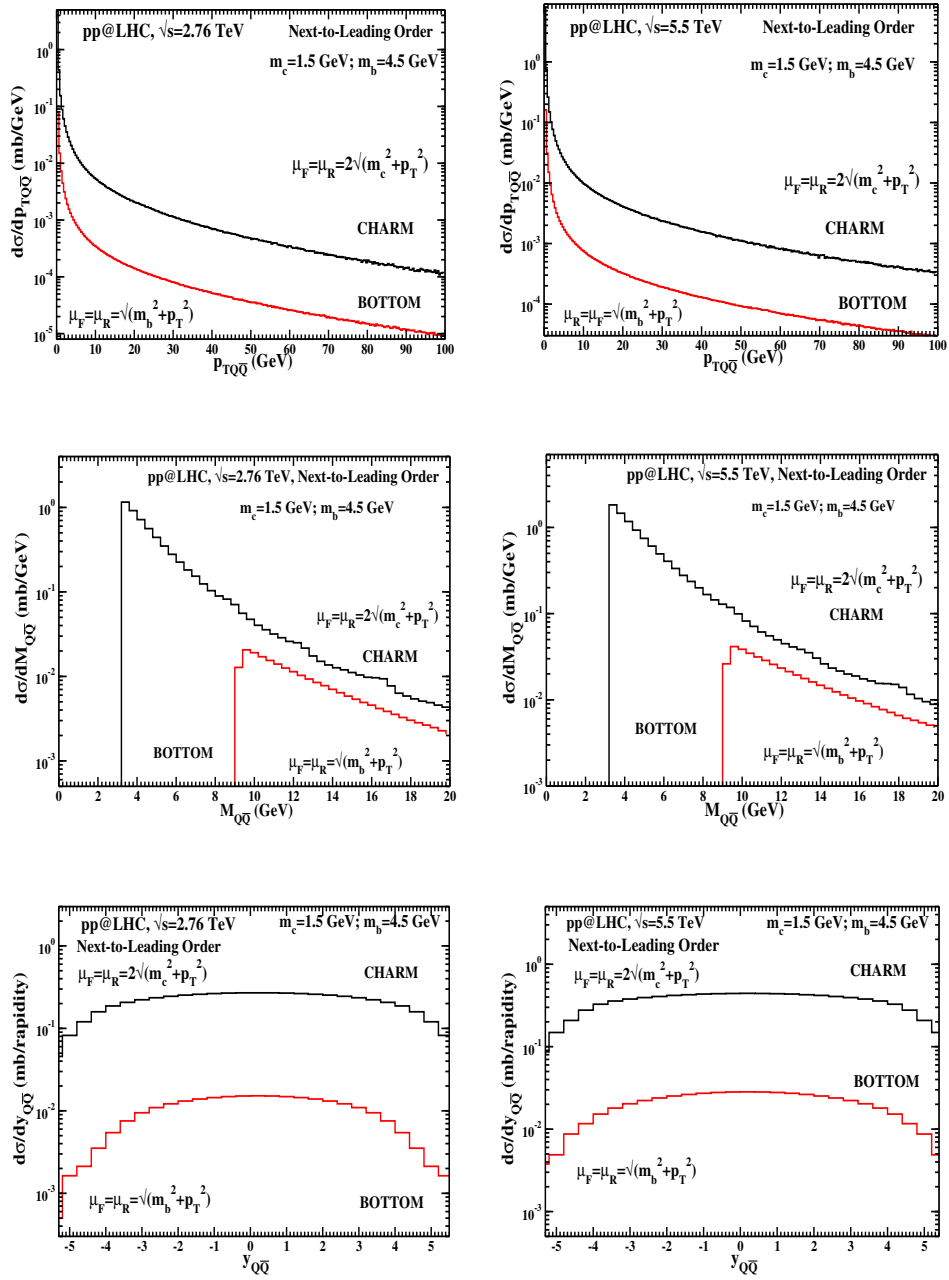


Figure 4.6: Transverse momentum, invariant mass and rapidity distribution of charm and bottom quark pairs at LHC.

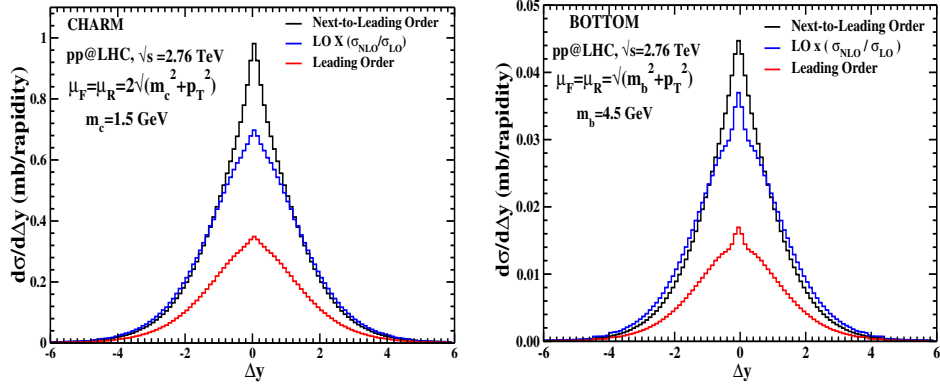


Figure 4.7: Rapidity difference of $\Delta y = y_Q - y_{\bar{Q}}$, of charm and bottom quarks at LO and NLO in pp collisions.

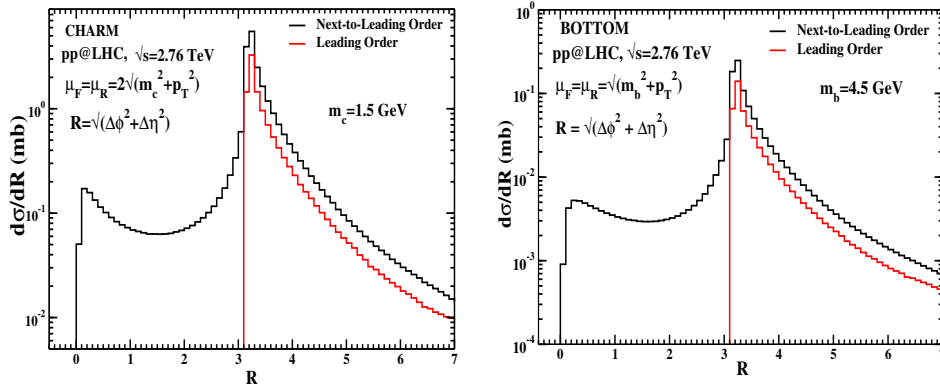


Figure 4.8: $(\Delta\eta, \Delta\phi)$ correlations of heavy quarks produced in pp collisions at $\sqrt{s}=2.76$ TeV and 5.5 TeV at LO and NLO.

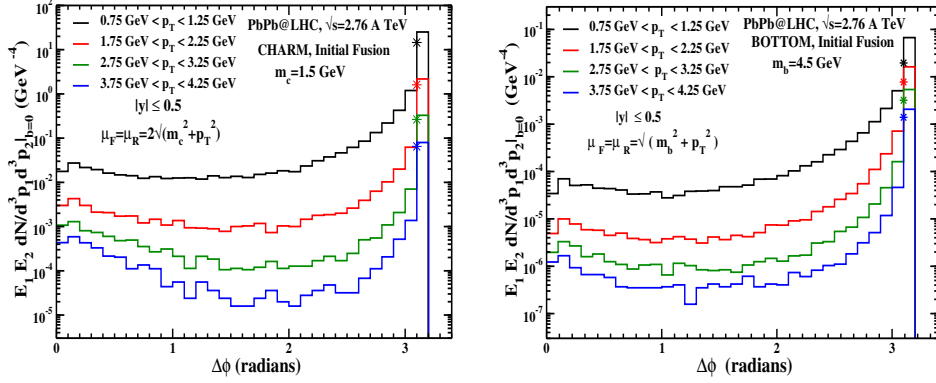


Figure 4.9: Azimuthal correlation of heavy quarks from prompt interaction for lead on lead collisions at LHC, having different transverse momenta and rapidities close to zero. The symbols give the corresponding LO values, with the same bin-size for $\Delta\phi$. The upper panels are for 2.76 ATeV while the lower panels give results for 5.5 ATeV. The left panels give results for charm quarks while the right panels give the results for bottom quarks.

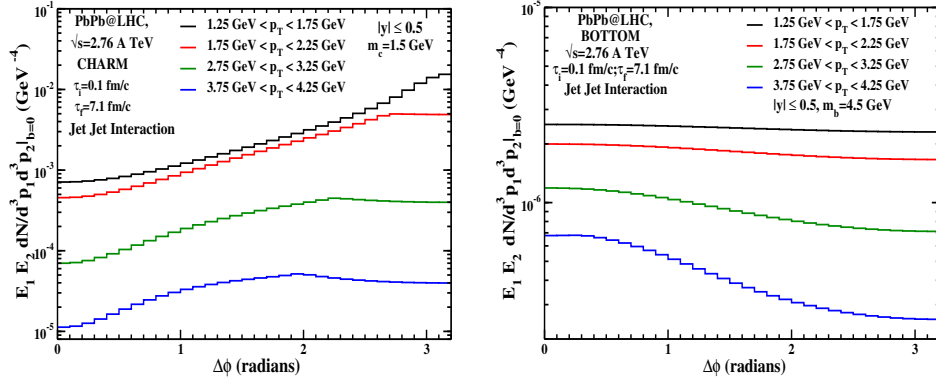


Figure 4.10: Azimuthal correlation of heavy quarks from jet-jet interaction for lead on lead collisions at LHC, for different transverse momenta.

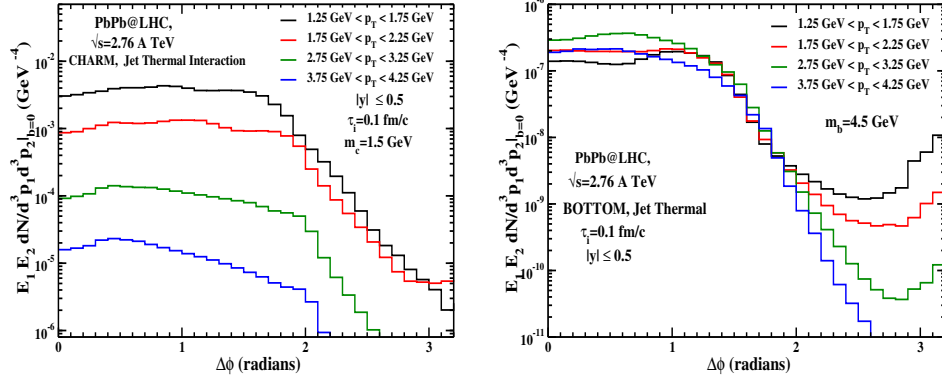


Figure 4.11: Azimuthal correlation of heavy quarks from jet-thermal interaction for lead on lead collisions at LHC, for different transverse momenta.

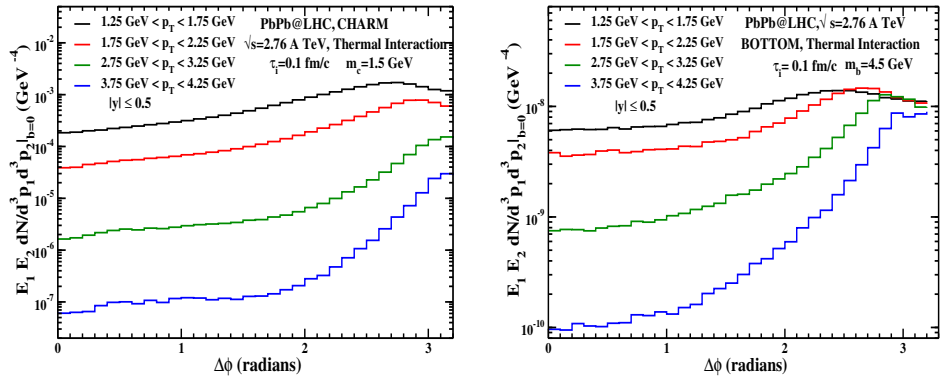


Figure 4.12: Azimuthal correlation of heavy quarks from thermal interaction for lead on lead collisions at LHC, for different transverse momenta.

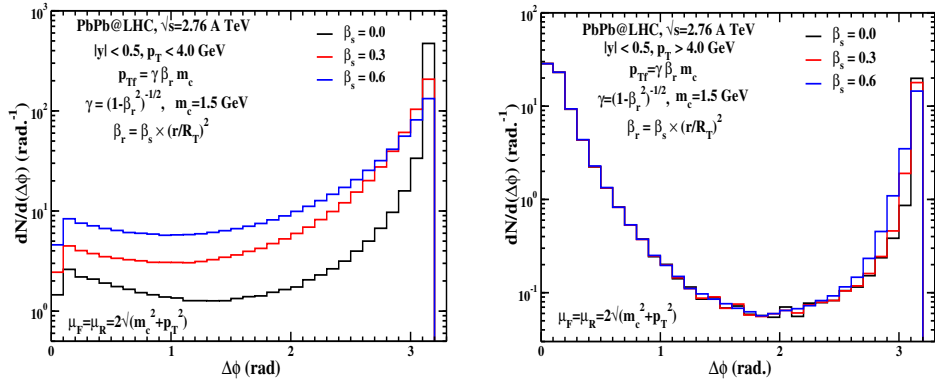


Figure 4.13: Azimuthal correlation of heavy quarks from prompt interaction for lead on lead collisions at LHC, with flow

Bibliography

- [1] Z. W. Lin and M. Gyulassy, Phys. Rev. C **51**, 2177 (1995) [Erratum-ibid. C **52**, 440 (1995)].
- [2] M. Younus, D. K. Srivastava, J. Phys. G Nucl. Part. Phys. **37**, 115006 (2010).
- [3] P. Levai, B. Müller, X. N. Wang, Phys. Rev. C **51**, 6 (1995).
- [4] W. Liu, R. J. Fries, Phys. Rev. C **77**, 054902 (2008), W. Liu, R. J. Fries, Phys. Rev. C **78**, 037902 (2008). A. Shor, Phys. Lett. **B 215**, 375 (1988).
- [5] Y. L. Dokshitzer, V. A. Khoze, S. I. Troian, J. Phys. G **17**, 1602 (1991); Yu. L. Dokshitzer, D. E. Kharzeev, Phys. Lett. **B 519**, 199 (2001); R. Thomas, B. Kampfer, G. Soff, Acta Phys. Hung. **A 22**, 83 (2005); N. Armesto, C. A. Salgado, U. A. Wiedemann, Phys. Rev. D **69**, 114003 (2004); W. C. Xiang, H. Ding, D. Zhou, Chin. Phys. Lett. **22**, 72 (2005).
- [6] H. van Hees and R. Rapp, Phys. Rev. C **71**, 034907 (2005) [arXiv:nucl-th/0412015], P. B. Gossiaux, V. Guiho and J. Aichelin, J. Phys. G **32**, S359 (2006).
- [7] B. Svetitsky, Phys. Rev. D **37**, 2484 (1988), M. G. Mustafa, D. Pal and D. K. Srivastava, Phys. Rev. C **57**, 889 (1998) [Erratum-ibid. C **57**, 3499 (1998)], Santosh K. Das, Jan-e Alam, P. Mohanty, Phys. Rev. C **82**, 014908 (2010).
- [8] R. Rapp, H. van Hees, arXiv:0803.0901v2 [hep-ph], H. van Hees, M. Mannarelli, V. Greco, R. Rapp Phys. Rev. Lett. **100**, 192301 (2008), R. Rapp, H. van Hees, J. Phys. G **G32**, S351 (2006).

- [9] N. Xu, X. Zhu, P. Zhuang, Phys. Rev. Lett. **100**, 152301 (2008), N. Xu, X. Zhu, P. Zhuang, J. Phys. G **36**, 064025 (2009).
- [10] E. Batten, M. H. Thoma, Phys. Rev. D **44**, R2625 (1991), M. G. Mustafa, D. Pal, D. K. Srivastava and M. Thoma, Phys. Lett. B **428**, 234 (1998), M. Djordjevic and M. Gyulassy Nucl. Phys. A **733**, 265 (2004), S. Wicks, W. Harowitz, M. Djordjevic, M. Gyulassy, Nucl. Phys. A **784**, 426 (2007), W. -C. Xiang, H. T. Ding, D. C. Zhou, D. Rohrick Eur. Phys. J **A25**, 75 (2005), N. Armesto, C. A. Salgado, U. A. Wiedemann, Phys. Rev. D **69**, 114003 (2004), M. G. Mustafa, Phys. Rev. C **72**, 014905 (2005), (erratum) Phys. Rev. C **74**, 019902 (2006), S. Peigne, A. Peshier, Phys. Rev. D **77**, 114017 (2008).
- [11] T. Renk, Phys. Rev. C **74**, 034906 (2006).
- [12] X. -N. Wang, Phys. Lett. B **B595**, 165 (2004), A. Mischke, [nucl-ex/1107.5138v1].
- [13] E. Eichten, I. Hinchliffe, K. Lane, C. Quigg, Rev. Mod. Phys. **56**, 4 (1984) U. Jamil, D. K. Srivastava, J. Phys. G Nucl. Part. Phys. **37**, 085106 (2010).
- [14] M. Younus, U. Jamil and D. K. Srivastava J. Phys. G Nucl. Part. Phys. **39**, 025001 (2012).
- [15] S. Vogel, P. B. Gossiaux, K. Werner, J. Aichelin, Phys. Rev. Lett. **107**, 032302 (2011), F. -M. Liu, K. Werner, Phys. Rev. Lett. **106**, 242301 (2011).
- [16] B. L. Combridge Nucl. Phys. B **151**, 429 (1979).
- [17] K. Aamodt et al(ALICE Collaboration), Phys. Rev. Lett. **105**, 252301 (2010).
- [18] Rainer J. Fries, B. Müller, D. K. Srivastava, Phys. Rev. Lett., **90**, 132301 (2003).
- [19] J. D. Bjorken, Phys. Rev. D **27**, 140 (1983).
- [20] K. J. Eskola, H. Honkanen, H. Niemi, P. V. Ruuskanen, S. S. Rasanen, Phys. Rev. C **72**, 044904 (2005). [hep-ph/0506049].

- [21] M. L. Mangano, P. Nason, G. Ridolfi, Nucl. Phys. B **373**, 295 (1992).
- [22] S. Frixione, M. L. Mangano, P. Nason, G. Ridolfi, Adv. Ser. Direct. High Energy Phys. **15**, 609-706 (1998). [arXiv:hep-ph/9702287 [hep-ph]].
- [23] A. Dainese (ALICE Collaboration), Quark Matter 2011, Annecy, France.
- [24] R. Vogt, Acta Phys. Polon. Supp. **1**, 695 (2008), N. Carrer, A. Dainese [hep-ph/0311225].
- [25] C. Peterson, D. Schlatter, I. Schmitt, P. M. Zerwas, Phys. Rev. **D27**, 105 (1983).
- [26] A. Aktas *et al.* [H1 Collaboration], Eur. Phys. J. **C38**, 447-459 (2005). [hep-ex/0408149].
- [27] ZEUS Collaboration, JHEP **07**, 074 (2007).
- [28] A. Dainese, [ALICE Collaboration], Talk given at QM 2011.
- [29] G. Altarelli, N. Cabibbo, G. Corbo, L. Maiani, G. Martinelli, Nucl. Phys. **B 208**, 365 (1982).
- [30] M. Cacciari, P. Nason, R. Vogt, Phys. Rev. Lett. **95**, 122001 (2005).
- [31] A. Mischke, [ALICE Collaboration], arXiv:1106.1011.
- [32] G. T. Bodwin, E. Braaten, J. Lee, Phys. Rev. D **72**, 014004 (2005).
- [33] R. Aaij *et al.*, [LHCb Collaboration], Eur. Phys. J. **bf C 71**, 1645 (2011).
- [34] K. Aamodt *et al.* [ALICE Collaboration], Phys. Lett. **B704**, 442-455 (2011). [arXiv:1105.0380 [hep-ex]].
- [35] E. Cuautle, G. Paic, AIP Conf. Proc. **857**, 175-178 (2006). [hep-ph/0604246].
- [36] G. Tsileidakis, H. Appelshäuser, K. Schweda, J. Stachel, Nucl. Phys. A **858**, 86 (2011), G. Tsileidakis, K. Schweda, Proc. of the ISMD08 Conf., DESY-PROC -2009-001, 2009, p. 214, G. Tsileidakis, Proc. of the 417th WE-Heraeus-Seminar, 2008, (Bad Honnef).

[37] E. Schnedermann, J. Sollfrank, U. W. Heinz, Phys. Rev. **C48**, 2462-2475 (1993).

Chapter 5

Energy Loss Mechanisms of Charm in QGP

The previous two chapters deal with production mechanisms for charm and bottom quarks. Single particle distribution and two particle ($Q\bar{Q}$) azimuthal distribution have been calculated for proton on proton as well as for heavy ion collision at RHIC and LHC energies. Now, we can move over to study the evolution of p_T and $\Delta\phi$ spectra of charm in QGP. This chapter contains the first part of our calculations on charm quark energy loss and is based on multiple scattering of charm quark with QGP partons.

It is often suggested that heavy quarks may lose a smaller amount of energy per unit length during their passage through QGP compared to light quarks, due to the 'dead cone effect' [1]. The experimental results, however, show similar suppression for light and heavy mesons [2]. Some recent calculations (see for eg. Refs. [3]) incorporated the generalized distribution of gluons in $qc \rightarrow qcg$ and $gc \rightarrow gcg$, and calculated a dE/dx for charm quarks which is quite similar to those for light quarks at energies ≥ 10 -15 GeV.

The study of charm quark energy loss provides several unique advantages over those of light partons. The charm mesons easily stand out in the multitude of light mesons. Most of the charm quarks are produced in initial fusion of quarks and anti-quarks ($q\bar{q} \rightarrow c\bar{c}$) and gluons

($gg \rightarrow c\bar{c}$), though a small additional production is expected [4]–[8] from multiple scattering between jets, jets and thermalized partons, and thermalized partons. It is not yet clearly established if the charm quarks thermalize in the QGP [9], though it is expected that due to their small numbers their impact on the bulk properties of the QGP would be negligible. One also expects that due to their large mass, charm quarks will not change their direction as they traverse the plasma, though they will slow down. This makes them excellent probes to check the dependence of azimuthal correlation on the conditions of the thermal system.

There is one additional trait which should help us in getting flavour dependence of energy loss of heavy quarks. While a 'u' or a 'd' or a 's' quark or a gluon can fragment into one of many mesons or baryons, a charm or a bottom quark would mostly fragment into only a D or a B meson or a charm or bottom baryon, respectively. Thus a charm quark after losing energy will appear as a D-meson having lower energy or momentum. We shall see that this would lead to a characteristic enhancement of charmed mesons or single electrons at low p_T .

The chapter contains expressions for calculations of nuclear modification factor- R_{AA} , azimuthal anisotropy coefficient- v_2 , azimuthal correlation for charm pairs, and our model prescription for energy loss. Sec. 3.2 contains discussion of our results, followed by a summary in Sec. 5.4

5.1 Formulation

5.1.1 Charm Production

The energy loss of quarks and gluons is most easily seen via the suppressed production of hadrons measured using nuclear modification factor, R_{AA} :

$$R_{AA}(p_T, y) = \frac{dN_{AA}/d^2p_T dy}{\langle T_{AA} \rangle d\sigma_{pp}/d^2p_T dy} \quad (5.1)$$

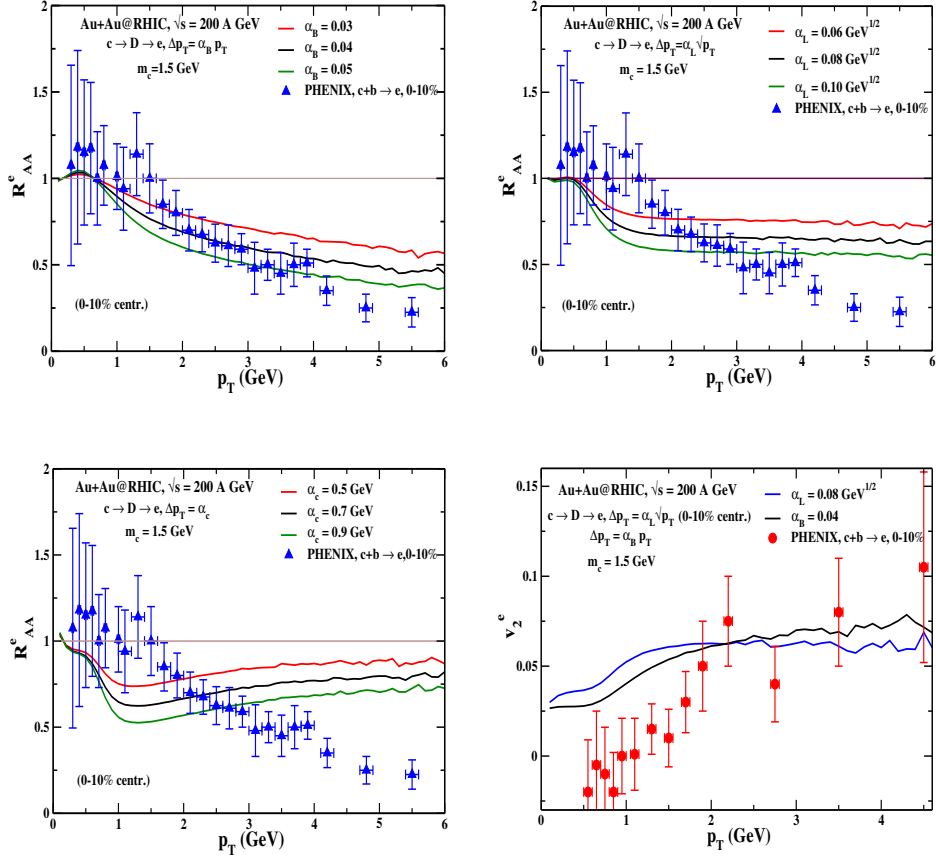


Figure 5.1: R_{AA} and v_2 for non photonic electrons at RHIC. Top: Momentum loss/per collision \propto momentum (left) and \propto square-root of momentum (right). Bottom: Momentum loss per collision = constant (left) and $v_2(p_T)$ for single electrons.

where N_{AA} is the hadron production for the nucleus-nucleus system at a given impact parameter, ' b '. T_{AA} is the corresponding nuclear thickness, and σ_{pp} is the cross-section for the production of hadrons at the corresponding centre of mass energy/nucleon in pp collisions.

One can now calculate

$$\begin{aligned}
 \frac{d\sigma_{pp}}{dy_1 dy_2 d^2p_T} &= 2x_a x_b \sum_{ij} \left[f_i^{(a)}(x_a, Q^2) f_j^{(b)}(x_b, Q^2) \frac{d\hat{\sigma}_{ij}(\hat{s}, \hat{t}, \hat{u})}{d\hat{t}} \right. \\
 &\quad \left. + f_j^{(a)}(x_a, Q^2) f_i^{(b)}(x_b, Q^2) \frac{d\hat{\sigma}_{ij}(\hat{s}, \hat{u}, \hat{t})}{d\hat{t}} \right] / (1 + \delta_{ij}), \quad (5.2)
 \end{aligned}$$

where p_T and $y_{1,2}$ are the momenta and rapidities of produced charm and anti-charm and x_a and x_b are the fractions of the momenta carried by the partons from their interacting parent hadrons. These are given by

$$x_a = \frac{M_T}{\sqrt{s}}(e^{y_1} + e^{y_2}); \quad x_b = \frac{M_T}{\sqrt{s}}(e^{-y_1} + e^{-y_2}). \quad (5.3)$$

where $M_T (= \sqrt{m_Q^2 + p_T^2})$, is the transverse mass of the produced heavy quark. The subscripts i and j denote the interacting partons, and $f_{i/j}$ are the partonic distribution functions for the nucleons. The fundamental processes included for LO calculations are:

$$\begin{aligned} g + g &\rightarrow c + \bar{c} \\ q + \bar{q} &\rightarrow c + \bar{c}. \end{aligned} \quad (5.4)$$

We recall that the above LO pQCD expression reproduces the NLO results [10] when supplemented with a K -factor ≈ 2 (see Ref. [11]).

We have used $T_{AA} = 225 \text{ fm}^{-2}$ for 0-10% centrality for Au+Au collisions at RHIC, as calculated from Glauber formalism. For Pb+Pb collisions at LHC, $T_{AA} = 195 \text{ fm}^{-2}$ for 0-20% centrality has been used. We use CTEQ5M structure function along with EKS98 [12] shadowing function. The factorization, renormalization, and fragmentation scales are chosen as $\sqrt{m_Q^2 + p_T^2}$ and the charm quark mass has been taken as 1.5 GeV. The detailed calculations for charm quark production have been already shown in chapter 3.

5.1.2 Energy Loss

We propose an empirical model for the energy loss for charm quarks which is inspired by a multiple scattering model used earlier by [13] supplemented with considerations of Baier et al [14] for partonic energy loss [15]. We recall once again that the nuclear modification of heavy meson production is similar to those for light mesons.

We perform a Monte Carlo implementation (see also [16]) of our model calculations and estimate the momentum loss of charm quarks and nuclear modification of D-meson and single electron production from semi-leptonic decay of D-mesons. We assume that the energy loss of heavy quarks proceeds via multiple collisions and that the momentum loss per collision is given by, (see for example Ref. [17])

$$(\Delta p)_i = \alpha (p_i)^\beta, \quad (5.5)$$

so that one can write

$$\frac{dp}{dx} = -\frac{\Delta p}{\lambda} \quad (5.6)$$

where α and β are parameters to be determined and λ is the mean free path of the charm quark, taken as 1 fm, in these initial studies. We shall consider charm quarks at central rapidities only and therefore, $p = p_T$. The momentum of the charm quark after n collisions will be given by

$$p_{n+1} = p_n - (\Delta p)_n \quad (5.7)$$

The charm quark can continue to lose energy in collisions as long as the resulting momentum remains positive. We estimate the probability for the charm quark to have n collisions, while covering the path length L from a Poisson distribution

$$P(n, L) = \frac{(L/\lambda)^n}{n!} e^{-L/\lambda}. \quad (5.8)$$

Taking a value for the coefficient α and the exponent β , we estimate the largest number of collisions- N , which the charm quark having momentum p_T can undergo. Next, we sample the number of collisions n , which the charm undergoes from the distribution

$$p(n) = P(n, L) / \sum_{n=1}^N P(n, L) \quad (5.9)$$

to get the final momentum of the charm quark.

Finally we fragment the charm quarks into D-mesons. Thus we have,

$$E \frac{d^3\sigma}{d^3p} = E_Q \frac{d^3\sigma(Q)}{d^3p_Q} \otimes D(Q \rightarrow H_Q) \otimes F(H_Q \rightarrow e), \quad (5.10)$$

where the fragmentation of the heavy quark Q into the heavy-meson H_Q is described by the fragmentation function D . We have assumed that the shape of $D(z)$, where $z = p_D/p_c$, is identical for all the D -mesons, [18] and

$$D_D^{(e)}(z) = \frac{n_D}{z[1 - 1/z - \epsilon_p/(1 - z)]^2}, \quad (5.11)$$

where ϵ_p is the Peterson parameter and

$$\int_0^1 dz D(z) = 1. \quad (5.12)$$

We have kept it fixed at $\epsilon_p=0.13$.

Here $F(H_Q \rightarrow e)$ denotes semileptonic decay of D -mesons and the electron distribution is taken from Ref. [19].

5.1.3 Azimuthal Anisotropy

Non-central collisions of identical nuclei will lead to an oval overlap zone, whose length in and out of the reaction plain would be different. Thus, charm quarks traversing the QGP in and out of the plain will cover different path lengths and lose differing amount of energy. This would lead to an azimuthal dependence in the distribution of resulting charm mesons, whose azimuthal anisotropy could be measured in terms of the v_2 coefficient defined by

$$v_2(p_T) = \frac{\int d\phi \frac{dN}{p_T dp_T d\phi} \cos(2\phi)}{\int d\phi \frac{dN}{p_T dp_T d\phi}} \quad (5.13)$$

We have approximated the colliding nuclei as having a uniform density with radius R in these calculations and also obtained average path-length for the charm quarks along a given ϕ .

5.1.4 Azimuthal Correlation

Next we discuss the effect of charm energy loss via multiple scattering on $D\bar{D}$ azimuthal correlation. $c\bar{c}$ pair will be produced mainly in the pre-equilibrium phase from initial gluon

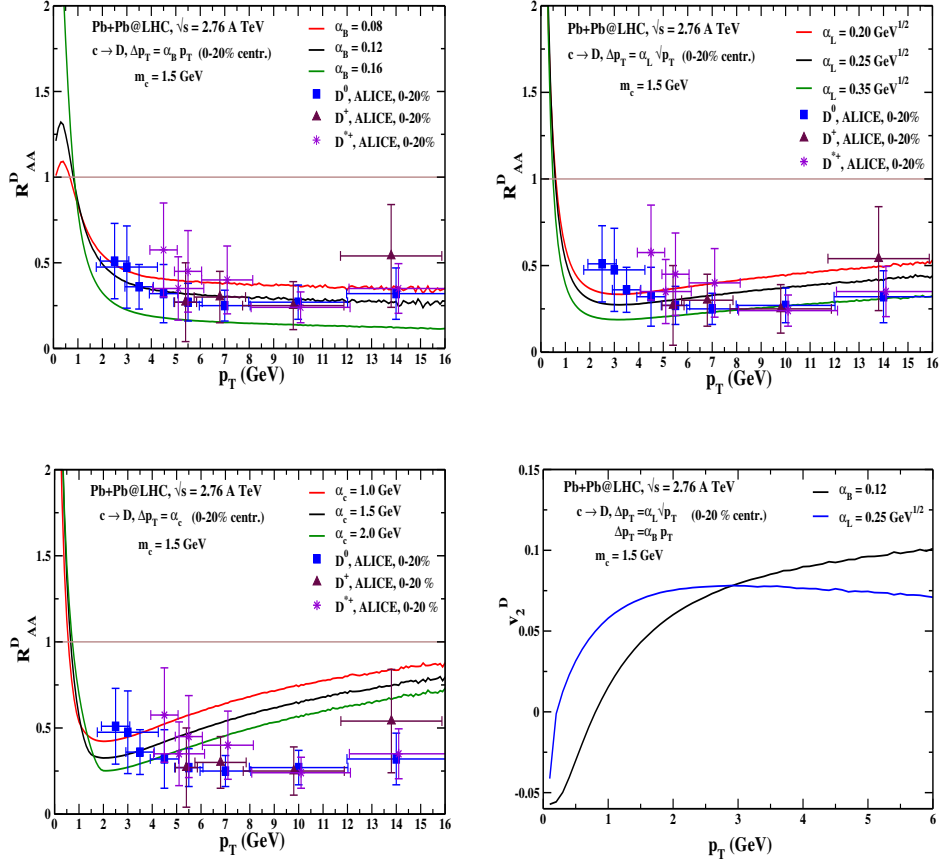


Figure 5.2: R_{AA} and v_2 for D mesons at LHC. Top: Momentum loss per collision \propto momentum (left) and \propto square root of momentum (right). Bottom: Momentum loss per collision = constant (left) and $v_2(p_T)$ for D-mesons (right).

fusion. However the correlation of charm pair may change considerably if it undergoes frequent scattering with thermal partons of QGP. So any change in its final azimuthal spectra might indicate an early development of collective flow of medium particles. On the other hand both the members of $c\bar{c}$ may suffer different energy loss while traveling through QGP and it might be reflected in the correlation distribution of the pair.

The correlation of heavy quarks produced in pp collisions is defined as

$$E_1 E_2 \frac{d\sigma}{d^3p_1 d^3p_2} = \frac{d\sigma}{dy_1 dy_2 d^2p_{T1} d^2p_{T2}} = C, \quad (5.14)$$

where y_1 and y_2 are the rapidities of heavy quark and anti-quark and \mathbf{p}_{T1} are the respective momenta.

At the leading order, the differential cross-section for the charm correlation for proton on proton collision is given by

$$C_{LO} = \frac{d\sigma}{dy_1 dy_2 d^2p_T} \delta(\mathbf{p}_{T1} + \mathbf{p}_{T2}) \quad (5.15)$$

One can now calculate [11]

$$\begin{aligned} \frac{d\sigma_{pp}}{dy_1 dy_2 d^2p_T} &= 2x_a x_b \sum_{ij} \left[f_i^{(a)}(x_a, Q^2) f_j^{(b)}(x_b, Q^2) \frac{d\hat{\sigma}_{ij}(\hat{s}, \hat{t}, \hat{u})}{d\hat{t}} \right. \\ &\quad \left. + f_j^{(a)}(x_a, Q^2) f_i^{(b)}(x_b, Q^2) \frac{d\hat{\sigma}_{ij}(\hat{s}, \hat{u}, \hat{t})}{d\hat{t}} \right] / (1 + \delta_{ij}), \end{aligned} \quad (5.16)$$

where p_T and $y_{1,2}$ are the momenta and rapidities of produced charm and anti-charm and x_a and x_b are the fractions of the momenta carried by the partons from their interacting parent hadrons. These are given by

$$x_a = \frac{M_T}{\sqrt{s}} (e^{y_1} + e^{y_2}); \quad x_b = \frac{M_T}{\sqrt{s}} (e^{-y_1} + e^{-y_2}). \quad (5.17)$$

where $M_T (= \sqrt{m_Q^2 + p_T^2})$, is the transverse mass of the produced heavy quark. The subscripts i and j denote the interacting partons, and $f_{i/j}$ are the partonic distribution functions for the nucleons. The invariant amplitude, $|M|^2$ in differential cross-section $d\hat{\sigma}/d\hat{t}$ is taken from ref. [21].

5.2 Results and Discussions

Let us now discuss our results for nuclear modification factor and azimuthal anisotropy. We consider three values for the exponent β ; 0, 0.5, 1.0 appearing in Eq. 5.5, inspired by the three energy loss mechanisms, namely those applicable in the so-called Bethe-Heitler regime, LPM regime, and complete coherence regimes considered by Baier et al. [14] which lead to energy loss per unit length as proportional to energy, square-root of the energy, and

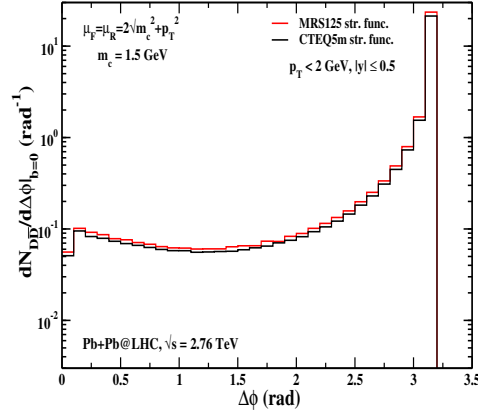


Figure 5.3: Comparison of D mesons azimuthal spectrum for two different structure functions.

independent of the energy for light partons, respectively. Kampfer et al [20] had earlier used this approach to study the effect of charm quark energy loss on the correlated charm decay.

Next we vary α to get a description of the R_{AA} for single electrons at RHIC (Fig. ??) and for D -mesons at LHC (Fig. 5.2).

In Fig. 5.3 we show our results for nuclear modification factor R_{AA} and azimuthal anisotropy v_2 for non photonic electrons at top RHIC energy $\sqrt{s} = 200$ A GeV [21]. Comparing the results of Figs. 5.3, we see that the model assuming momentum loss per collision as proportional to the momentum closely follows the shape of the experimentally determined R_{AA} for single electrons almost over the entire range of p_T under consideration. We add that our theoretical calculations have not included the $b \rightarrow e$ contribution which is contained in the experimental results which can modify the R_{AA} for larger p_T by up to 10% as the produced b quarks are much less in number and also lose much smaller energy [22]. The scenario, where $\Delta p \propto \sqrt{p}$, is only moderately successful in describing the data over a limited p_T range of 2–4 GeV/ c (Fig. 5.3). While the assumption of a constant momentum loss per collision may bracket the R_{AA} over the very limited range of 2–3 GeV/ c , it does not follow the shape of the p_T dependence (Fig. 5.3).

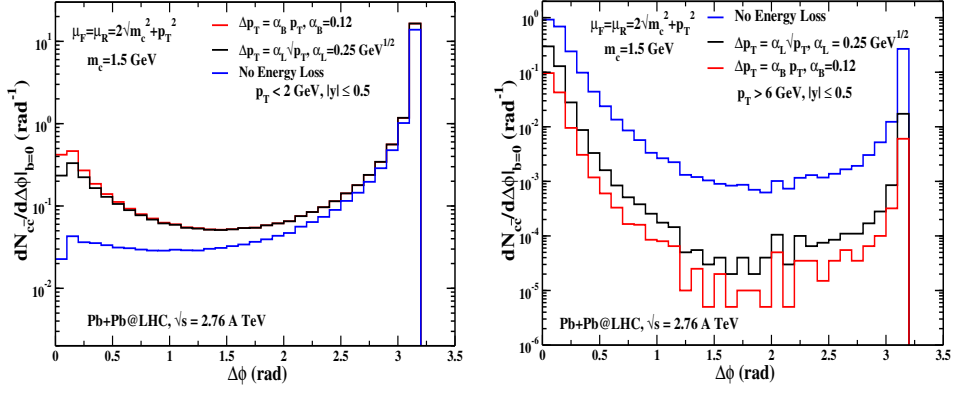


Figure 5.4: $dN/d\Delta\phi$ vs $\Delta\phi$ of $c\bar{c}$ pair for $p_T < 2.0$ GeV, and $p_T > 6.0$ GeV.

The best values of the α determined from the results in Fig. 5.3 are used to estimate v_2 for the single electrons. We see that our calculations provide a reasonable description of $v_2(p_T)$ for $p_T \geq 2$ GeV/ c and overestimate the results for lower p_T . A relaxation of our assumption of a static medium at a constant temperature and a uniform density of the nuclei may improve this agreement.

Similar results are obtained when we apply the model to the R_{AA} measured [23] for the D -mesons at the LHC (Fig. 5.4). We again see that the model using $\Delta p \propto p$ provides a good description of the data over the entire p_T range, while that using $\Delta p \propto \sqrt{p}$ seems to describe the data for $p_T \geq 4$ GeV/ c . The constant momentum transfer collision misses the shape of the p_T distribution completely though it is able to bracket the numerical values over a very narrow p_T range of 3–5 GeV/ c (Fig. 5.4). The predictions for v_2 are given for a ready reference.

Several factors could affect the value of the energy loss coefficient ' α ' for a given mechanism. We have verified that increasing (decreasing) the mean free path, λ , by 0.5 fm results in a decrease (increase) of the coefficient, α_B such that α_B/λ remains unaltered.

We have kept α_s fixed at 0.3 while estimating the initial charm distribution. Taking the renormalization scale as $C\sqrt{p_T^2 + M_Q^2}$, with $C=1$ or 2 leads to a decrease in the value of R_{AA} by 7-10 %, which can then be offset by decreasing α_B by about 12 %.

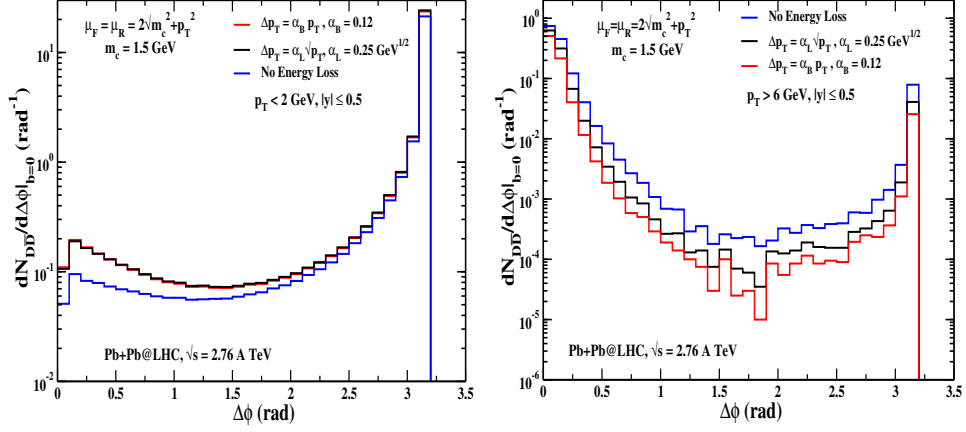


Figure 5.5: same as Fig.5.4, $dN/d\Delta\phi$ vs $\Delta\phi$ of $D\bar{D}$ pair for (left) $p_T < 2.0$ GeV, (right) $p_T > 6.0$ GeV.

We have used NLO-MNR code [25] with CTEQ5M structure function for estimating charm cross-section for all leading and next-to-leading pQCD processes. The scaling factor used is $2\sqrt{m_c^2 + p_T^2}$ with $m_c=1.5$ GeV. The calculation for azimuthal correlation has been done for central collision ($b=0$ fm) and for mid rapidity, $-0.5 \leq y \leq 0.5$

To check the consistency of our results for correlation we have used two different partonic structure functions one of which is CTEQ5M and other an old one MRS125. The comparison is shown in Fig. 5.3, where the difference in the two distributions is very small and the shape almost identical. However more recent structure functions like CTEQ6M and CTEQ6.6 etc. must be used in order to have more up-to-date results. These issues will be addressed in future.

Next, let us recall that LO contribution can be differentiated from NLO contribution with different p_T cuts on charm momentum. Leading order processes give back to back charm pairs which are entirely visible around $\Delta\phi=\pi$, while NLO contribution is distributed from $\Delta\phi=0 - \pi$.

In Fig. 5.4, we show our results for $dN_{c\bar{c}}/d\phi$ for different p_T cuts. Realizing that all heavy quarks now appear with reduced momenta, we see that if we look at $p_T < 2$ GeV, then the back-to-back correlation rise by up to a factor of 10 for $\phi = 0$. The results for $p_T > 6$ GeV

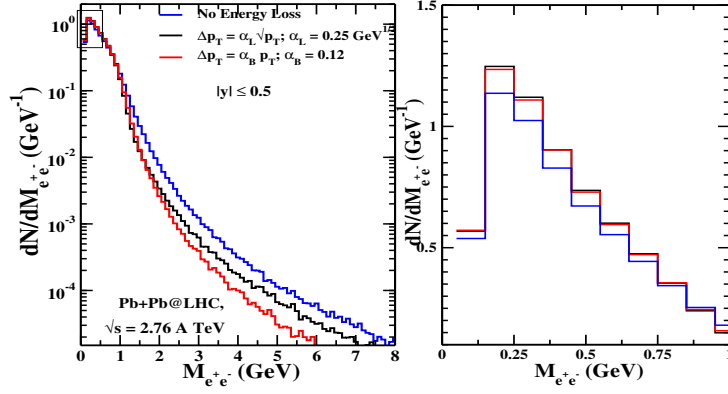


Figure 5.6: Invariant mass distribution for di-electron (inset) Increase in di-electron spectrum for $M_{e^+e^-} < 1.0$ GeV, shown in linear scale.

are more dramatic in the sense that the $\phi=\pi$ correlation now reduces by more than a factor of 10 while that for $\phi=0$ decreases from its value for no energy loss.

We show $dN_{D\bar{D}}/d\Delta\phi$ for $p_T > 6.0$ GeV and $p_T < 2.0$ GeV in Fig. 5.5. Comparing it with Fig. 5.4 for same p_T regions, we observe certain differences which we now discuss. For $p_T < 2.0$ GeV, we observe that D meson distribution is slightly higher than charm spectrum at $\Delta\phi = \pi$, although the order of magnitude remains same. While at $\Delta\phi = 0$, the situation is reversed. Similar observations are noted when figures at $p_T > 6.0$ GeV are compared. We feel that the above differences are caused by fragmentation function, $D(z)$, which changes the p_T distribution of charm into p_T distribution of D mesons with, $0 \leq z \leq 1$. Thus the correlation spectra of charm and D mesons may appear slightly different when we look into particular p_T regions. Here it is worth mentioning that since D-mesons, rather than charms, are observed in the experiments, therefore calculating D-meson correlation and comparing it with that of charm quark will give us a deep insight into the nature of the fragmentation function used in the calculation.

To discuss our simple model of charm quark energy loss, we find that most of the charm pairs not only lose energy to shift to the lower momentum region but also back-to-back correlation for many charm pair is altered to almost collinear pairs. Also, we find that two different

energy loss mechanisms included in our study do not give much different outcomes. Further, investigating at much higher momentum regions might bring out the differences between various energy loss mechanisms. The correlation study can be enriched if expanding medium is included in addition to energy loss by charms.

Next, we move to our results for correlated decay of charm. In Fig. 5.6, we have $dN/dM_{e^+e^-}$ for di-electrons from correlated charm decay. We can recall that there is enhancement in D mesons as well as single non-photonic electrons due to the effects of large drag on charm quark moving through QGP. Here, we find a similar enhancement in di-electron spectrum at midrapidity. For $M_{e^+e^-}$ less than 1 GeV, there is an increase in $dN/dM_{e^+e^-}$ by almost 12% which is quite noteworthy considering our model to be a simple empirical mechanism of energy loss.

It is interesting to recall that a Focker-Planck equation given by

$$\frac{\partial f}{\partial t} = \frac{\partial}{\partial p_i} \left[A_i(\mathbf{p})f + \frac{\partial}{\partial p_j} (B_{ij}(\mathbf{p})f) \right], \quad (5.18)$$

describes the evolution of the distribution 'f', of charm quarks propagating in quark gluon plasma [24] and losing energy due to multiple soft scatterings with light quarks and gluons. This leads to a drag, $A_i(\mathbf{p})$, and a diffusion $B_{ij}(\mathbf{p})$ on the momentum of the charm quark. Assuming that $A_i(\mathbf{p})$ depends on momentum only, we have

$$A_i(\mathbf{p}) = A(p^2) p_i, \quad (5.19)$$

and the energy loss dE/dx can be related to drag coefficient $A(p^2)$ by

$$\frac{dE}{dx} = -A(p^2) p, \quad (5.20)$$

where E is the energy of the charm quark, and p its momentum. Considering the average temperature of the plasma attained at RHIC as ≈ 220 MeV [26], we can read the drag coefficient from Fig. 3(a) of Ref. [27] as ≈ 0.02 fm⁻¹ for p_T up to 5 GeV/ c . We can re-write the above equation as

$$\frac{dp}{dx} = -A(p^2) E, \quad (5.21)$$

Comparing this with one of the ansatzes used for energy loss per collision in the present work, namely $\Delta p = \alpha_B p$, we can write that

$$\frac{dp}{dx} = -\frac{\alpha_B}{\lambda} p, \quad (5.22)$$

Thus the effective drag coefficient ' $A_{\text{eff}}(p^2)$ ', can be written as

$$A_{\text{eff}}(p^2) = \frac{\alpha_B}{\lambda} \frac{p}{E} \quad (5.23)$$

which reduces to α_B/λ for large values of p

We thus note that the effective drag at RHIC energies is about 0.04 fm^{-1} compared to 0.02 fm^{-1} estimated for soft multiple collisions by authors of Ref. [27]. Thus we conclude that at RHIC energies only half of the energy loss could be due to collisions, while the other half could attributed to radiations of gluons. Similarly estimating the average temperature at LHC as about 270 MeV and using the results for drag due to collisions as $\approx 0.04 \text{ fm}^{-1}$ from Ref. [27] at high momentum, we note that the collisions account for only one-third of energy loss at 2.76 TeV/nucleon.

It is of interest to compare our results with other studies on medium modification of charm propagation reported in the literature. Thus Moore and Teaney [28] have calculated the diffusion ' D ' and drag coefficient ' η_D ', (denoted by ' A ' here) using LO pQCD as

$$D \approx \frac{6}{2\pi T} \left(\frac{0.5}{\alpha_s} \right)^2 \quad (5.24)$$

and

$$\eta_D = \frac{T}{M_Q D} \quad (5.25)$$

Taking $\alpha_s \approx 0.3$, this provides $\eta_D \approx 0.06 \text{ fm}^{-1}$ at 220 MeV and $\eta_D \approx 0.09 \text{ fm}^{-1}$ at 270 MeV, which are larger than our values at RHIC and smaller than those at 2.76 TeV/nucleon at LHC.

Recall however, the results of Bass et al. [29] where a description of medium modification as well as v_2 for single electrons at RHIC brackets the diffusion coefficient ' D ' between $1.5/2\pi T$ and $6.0/2\pi T$, when flow and contributions of bottom electrons is included. This

provides a large value for the drag coefficient between 0.17 and 0.68 fm^{-1} . At first these large values may look surprising. However, from Eq. 5.24 we see that these would correspond to values of α_s between ≈ 1.0 and ≈ 0.5 , which are rather large and make the use of perturbative QCD questionable.

In this connection, the studies of Gossiaux et al [30], are also of considerable interest which suggest that the collisional energy loss could be substantially larger if the Debye mass is replaced by hard thermal loop calculation and a running coupling constant is used. We further recall the work of authors of Ref. [31], which suggests that a considerable drag could be produced by the resonant heavy quark-light quark interaction, beyond that determined by LO pQCD interactions.

We have already mentioned that c quarks will materialize mostly as D -mesons. This can have an interesting consequence which is already apparent in the Figs. 5.3 and 5.4. The c quarks after losing energy will pile up at lower energies and this would result in a characteristic increase in the production of D -mesons as well as single electrons having lower transverse momenta (Fig. 5.5). We note that while there is suppression by almost a factor of 2–4 depending on the incident energy (for single electrons) at larger p_T , there is essentially no suppression at lower p_T at RHIC and even an increase by a few percent at LHC where the energy loss is higher and the momentum spectra of c quarks have less steeper slopes. The increase in the case of D -mesons at LHC is rather spectacular. This is different from the normal enhancement of mesons having low p_T due to the so-called Cronin effect, which is expected to be less important at higher incident energies for heavy mesons (see e.g., Ref. [32]). We recall that a similar enhancement in D -meson production at low p_T has been predicted by considering the drag suffered the heavy quarks in the plasma and during their hadronization [33]. In a forthcoming paper we shall show that this can lead to a slight increase in the production of low mass dileptons due to correlated charm decay.

5.3 Summary

At the very minimum the present work describes a simple procedure to implement energy loss of heavy quarks in relativistic collision of heavy nuclei. It will be of interest to explore the energy and centrality dependence of the momentum loss coefficient α .

Bibliography

- [1] Y. L. Dokshitzer, V. A. Khoze, S. I. Troian J. Phys. **G17**, 1602 (1991);
Y. L. Dokshitzer, D. E. Kharzeev Phys. Lett. **B519**, 199 (2001); R. Thomas,
B. Kampfer, G. Soff Acta. Phys. Hung. **A22**, 83 (2001); N. Armesto, C. A. Salgado,
U. A. Wiedemann Phys. Rev. **D69**, 114003 (2004).
- [2] A. Adare *et al.* [PHENIX Collaboration], Phys. Rev. Lett. **98**, 172301 (2007);
B. I. Abelev *et al.* Phys. Rev. Lett. **98**, 192301 (2007); B. Abelev *et al.* [ALICE
Collaboration], arXiv:1203.2160 [nucl-ex], 2012.
- [3] S. Mazumder, T. Bhattacharyya, J. Alam and D. K. Srivastava, Phys. Rev. **C**
84, 044901 (2011); R. Abir, U. Jamil, M. G. Mustafa and D. K. Srivastava,
arXiv:1203.5221 [hep-ph], 2012; T. Bhattacharyya, S. Mazumder, S. Das and J. Alam,
Phys. Rev. **D 85**, 034033 (2012).
- [4] A. Shor, Phys. Lett. **B215**, 375 (1988).
- [5] Z. Lin, M. Gyulassy Phys. Rev. **C51**, 2177 (1995), [Erratum-ibid. **C52**, 440 (1995)].
- [6] P. Levai, B. Müller, X. N. Wang, Phys. Rev. **C51**, 6 (1995).
- [7] M. Younus, D. K. Srivastava J. Phys. **G37**, 115006 (2010).
- [8] J. Uphoff, O. Fochler, Z. Xu and C. Greiner, Nucl. Phys. A **855**, 444 (2011).
- [9] S. Cao and S. A. Bass, Phys. Rev. **C84**, 064902 (2011).
- [10] M. L. Mangano, P. Nason, G. Ridolfi, Nucl. Phys. **B373**, 295 (1992).

- [11] U. Jamil, D. K. Srivastava, J. Phys. **G37**, 085106 (2011).
- [12] K. J. Eskola, V. J. Kolhinen, C. A. Salgado Eur. J. Phys. **C9**, 61 (1998).
- [13] X. -N. Wang, Z. Huang and I. Sarcevic, Phys. Rev. Lett. **77**, 231 (1996) [hep-ph/9605213]; X. -N. Wang and Z. Huang, Phys. Rev. C **55**, 3047 (1997) [hep-ph/9701227].
- [14] R. Baier, Yu. L. Dokshitzer, A. H. Mueller, S. Peigne, D. Schiff, Nucl. Phys. **B483**, 291 (1997); R. Baier, Yu. L. Dokshitzer, A. H. Mueller, S. Peigne, D. Schiff, Nucl. Phys. **B484** 265 (1997).
- [15] S. Jeon, Nucl. Phys. **A830**, 107c (2009).
- [16] M. Younus and D. K. Srivastava, J. Phys. **G: Nucl. Part. Phys.** **39**, 095003 (2012); M. Younus and D. K. Srivastava, J. Phys. **G: Nucl. Part. Phys.** **40**, 065004 (2013).
- [17] B. Muller Phys. Rev. **C67** 061901(R)(2003); G. Wang and H. Z. Huang, Phys. Lett. **B672**, 30 (2009).
- [18] C. Peterson, D. Schlatter, I. Schmitt, P. M. Zerwas, Phys. Rev. **D27**, 105 (1983)
- [19] G. Altarelli, N. Cabibbo, G. Corbo, L. Maiani, G. Martinelli Nucl. Phys. **B208**, 365 (1982)
- [20] B. Kampfer, O. P. Pavlenko and K. Gallmeister, Phys. Lett. B **419**, 412 (1998).
- [21] A. Adare *et al.* [PHENIX Collaboration] Phys. Rev. Lett. **98**, 172301 (2007).
- [22] See e.g., M. Djordjevic, M. Gyulassy, R. Vogt, S. Wicks, Phys. Lett. **B632**, 81 (2006).
- [23] B. Abelev *et al.* [ALICE Collaboration] arXiv:1203.2160 [nucl-ex] 2012, A. Dainese, [ALICE Collaboration] arxiv: 1106.4042v2[nucl. ex.] 2011.
- [24] B. Svetitsky, Phys. Rev. **D37**, 2484 (1988).
- [25] M. L. Mangano, P. Nason and G. Ridolfi, Nucl. Phys. **B373**, 295 (1992).

- [26] A. Adare *et al.* [PHENIX Collaboration], Phys. Rev. Lett. **104**, 132301 (2010).
- [27] M. G. Mustafa, D. Pal, D. K. Srivastava, Phys. Rev. **C57**, 889 (1998); [Erratum-ibid. **C 57**, 3499 (1998)].
- [28] G. D. Moore and D. Teaney, Phys. Rev. **C71**, 064904 (2005).
- [29] S. Cao, G-Y. Qin, S. A. Bass, arXiv:1205.2396v1[nucl-th] 2012.
- [30] P. B. Gossiaux, J. Aichelin, Phys. Rev. **C78**, 014904 (2008).
- [31] H. van Hees, R. Rapp, Phys. Rev. **C71**, 034907 (2005).
- [32] See e.g., G. G. Barnafoldi, P. Levai, G. Fai, G. Papp and B. A. Cole, Int. J. Mod. Phys. **E 16**, 1923 (2007) [hep-ph/0703059 [HEP-PH]].
- [33] M. He, R. J. Fries and R. Rapp, arXiv:1204.4442 [nucl-th] 2012.

Chapter 6

Transport of Heavy Quark-Parton

Cascade Model

Relativistic heavy ion collision at RHIC and the LHC have given rise to a new phase of matter. When two heavy ion collide, the region of their collision consists of deconfined gluons and quarks within a very small region of space. This state of matter, as we know today, is called quark gluon plasma(QGP) [1]–[4].

One of the signals coming out of QGP is quenching of heavy quarks. On other hand high momentum hadron spectra are observed to be highly suppressed relative to those in proton on proton collisions [5, 6], suggesting a quenching effect due to the QGP medium. A similar effect is observed for high p_T charm or beauty quarks with most recent results showing suppression of D or B mesons to same order as that of light partons [7], the focus is now shifted to the accurate theoretical calculations from experimental observations. However, calculations from hydrodynamics give a rough estimate of the ratio of thermalization time for heavy quarks, τ_Q and light partons, $\tau_{q/g}$, [8], $\frac{\tau_Q}{\tau_{q/g}} \sim \frac{M_Q}{T}$. For $M_Q = 1.35\text{--}4.5$ GeV and $T = 300$ MeV, this ratio is found to be ~ 5 and suggests that relaxation time for heavy quarks is larger than that of light quarks and gluons. If thermalization time, $\tau_{q/g}$, is taken to be $\mathcal{O}(1\text{fm}/c)$, and if equilibrium temperature, T_i and freeze-out temperature, T_f are taken as 300 MeV and 170 MeV [9] respectively, then lifetime of QGP can be approximately shown to be

5 fm/c. This might imply that heavy quark relaxation time for $T= 300$ MeV is comparable to QGP lifetime at this condition. Even if heavy quark is subjected to large suppression [7], it may not fully thermalize in QGP.

In last chapter, we discussed the calculations of charm quark energy loss by the mechanism of multiple scattering with medium particles. Other theoretical calculations and phenomenological models of heavy quarks energy loss have also been developed in recent years [10]–[14]. In these literatures, both elastic scattering and inelastic gluon emission off heavy quarks have been suggested as the major mechanisms by which a heavy quark may lose energy in the presence of a thermal medium. In most of these earlier works, collisional energy loss seems to dominate in the lower momentum region while radiative energy loss emerges as the chief mechanism for higher momenta charms.

Transport models can attempt to fully describe a heavy ion collision and the ensuing dynamics. The Parton Cascade Model is one such transport calculations [15, 16, 17]. It is based on Boltzman transport equation and does not include any equilibration assumptions. However the calculations must be well calibrated and validated under controlled conditions before utilizing them fully for heavy quarks.

In this chapter, we will discuss in detail the evolution of charm quark using Parton Cascade Model. In section 6.2., we show our results calculated for a fixed temperature, followed by discussions. In the final section we summarize our results and suggest future lines of inquiry.

6.1 Parton Cascade Model

The Parton Cascade Model VNI/BMS [18, 19, 20] forms the basis for our present study. This model can be used to study the full time evolution of hard probes and a thermal QCD medium. The PCM has been used to study gluons and lighter quarks as hard probes of the QGP. In the current work we use VNI/BMS to study charm quark evolution in an infinite QGP medium for the first time. It is necessary to check the consistency of our calculations within a controlled environment which we will discuss next.

The QGP like medium effect is modeled by taking a box of finite volume with periodic boundary conditions. This provides a system of infinite matter at fixed temperature. The matter inside the box is thermalized quarks and gluons (QGP) and their thermal distributions are used to generate partons at a given temperature and zero chemical potential. We insert a charm with the four momentum $p^\mu = \{0, 0, p_z, E = \sqrt{p_z^2 + M_c^2}\}$, into the box and let it evolve according to the Relativistic Boltzmann Equation given by,

$$p^\mu \frac{\partial F_j(x, \vec{p})}{\partial x^\mu} = \sum_{\text{processes:}i} C_i[F], \quad (6.1)$$

where $F_j(x, \vec{p})$ is the charm single particle phase space distribution and the collision term on r.h.s. is a non-linear functional of phase space distribution terms inside an integral and can be expressed as:

$$\begin{aligned} C_i(F) &= (\pm) \frac{1}{2E_i S_i} \int \prod d\Gamma_j |\mathcal{M}|^2 (2\pi)^4 \delta^4(P_{in} - P_{out}) D(F_j(x, \vec{p})), \\ D(F_j) &= \prod_{in} F_j \prod_{out} [1 \pm F_i] - \prod_{in} [1 \pm F_i] \prod_{out} F_j, \\ \prod d\Gamma_j &= \prod_{i \neq j} \frac{d^3 p_j}{(2\pi)^3 (2E_j)} \end{aligned} \quad (6.2)$$

Here $D(F_j)$ is the quantum statistical distribution factor and S_i is another factor required for averaging over all the particle species excluding 'ith' parton and defined as,

$$S_i = \prod_{j \neq i} K_a^{in}! K_a^{out}!, \quad (6.3)$$

with $K_a^{in,out}$ being the identical partons of species 'a' in the initial or the final process j . We have included the matrix elements for all $2 \rightarrow 2$ binary elastic scattering processes for charm interaction with gluons or light quarks (u, d, s) and $2 \rightarrow n$ process for radiative (brehmsstrahlung) corrections after each scattering. Mathematically $2 \rightarrow n$ process can be shown to be $2 \rightarrow 2$ elements multiplied by a radiative factor,

$$|\mathcal{M}|^2 = |\mathcal{M}_{ab \rightarrow cd}(\hat{s}, \hat{t}, \hat{u}, Q^2)|^2 [T_c(Q^2, \mu_0^2) T_d(Q^2, \mu_0^2)], \quad (6.4)$$

where $T(Q^2, \mu_0^2)$ is the time-like branching or 'Sudakov' radiative factor after each scattering. We will return to this shortly afterwards.

6.1.1 Elastic scattering of charm quark

The matrix elements for elastic ($ab \rightarrow cd$) processes in Eqn. 6.4 are

$$\begin{aligned} gc &\rightarrow gc, \\ q(\bar{q})c &\rightarrow q(\bar{q})c. \end{aligned} \quad (6.5)$$

The corresponding differential scattering cross section is defined to be,

$$\frac{d\hat{\sigma}}{dQ^2} = \frac{1}{16\pi(\hat{s} - M_c^2)^2} \sum |\mathcal{M}|_{ab \rightarrow cd}^2. \quad (6.6)$$

The total cross section is also calculated and used in the calculations to select interacting pairs. The total cross section can be shown to be,

$$\hat{\sigma}_{tot} = \sum_{c,d} \int_{p_{Tmin}^2}^{\hat{s}} \left(\frac{d\hat{\sigma}}{dQ^2} \right)_{ab \rightarrow cd} dQ^2. \quad (6.7)$$

The invariant transition amplitude, $|M|^2$ for elastic scattering which can be calculated or obtained from [21], are shown below for $q(\bar{q})c \rightarrow q(\bar{q})c$,

$$\sum |\mathcal{M}|^2 = \frac{64\pi^2\alpha_s^2 (M_c^2 - \hat{u})^2 + (\hat{s} - M_c^2)^2 + 2M_c^2\hat{t}}{9 (\hat{t} - \mu_D^2)^2}. \quad (6.8)$$

While, for $gc \rightarrow gc$,

$$\sum |\mathcal{M}|^2 = \pi^2\alpha_s^2 [g1 + g2 + g3 + g4 + g5 + g6],$$

where,

$$\begin{aligned} g1 &= 32 \frac{(\hat{s} - M_c^2)(M_c^2 - \hat{u})}{(\hat{t} - \mu_D^2)^2}, \\ g2 &= \frac{64 (\hat{s} - M_c^2)(M_c^2 - \hat{u}) + 2M_c^2(\hat{s} + M_c^2)}{9 (\hat{s} - M_c^2)^2}, \\ g3 &= \frac{64 (\hat{s} - M_c^2)(M_c^2 - \hat{u}) + 2M_c^2(M_c^2 + \hat{u})}{9 (M_c^2 - \hat{u})^2}, \\ g4 &= \frac{16 M_c^2(4M_c^2 - \hat{t})}{9 (\hat{s} - M_c^2)(M_c^2 - \hat{u})}, \\ g5 &= 16 \frac{(\hat{s} - M_c^2)(M_c^2 - \hat{u}) + M_c^2(\hat{s} - \hat{u})}{(\hat{t} - \mu_D^2)(\hat{s} - M_c^2)}, \\ g6 &= -16 \frac{(\hat{s} - M_c^2)(M_c^2 - \hat{u}) - M_c^2(\hat{s} - \hat{u})}{(\hat{t} - \mu_D^2)(M_c^2 - \hat{u})}. \end{aligned} \quad (6.9)$$

In order to regularize the cross sections we have used the thermal mass of QGP medium which is defined as $\mu_D = \sqrt{(2N_c + N_f)/6gT}$, where $g = \sqrt{4\pi\alpha_s}$. N_f , no. of flavours and N_c , no. of colour are taken 4 and 3 respectively. We have kept strong coupling, $\alpha_s=0.3$ for the entire calculation.

The Boltzmann transport equation is then solved numerically via Monte Carlo algorithms, a geometric interpretation of the cross section is used to select which collisions will occur.

6.1.2 Charm Quark Radiation

It is known that collisional loss alone is unable to explain the data showing suppression of non-photonic electrons at RHIC or D mesons at LHC [22]. On one hand hard thermal loop(HTL) approximation [23, 24] predicts a large drag on heavy quark which is much bigger than what experimental data has suggested, while the radiative corrections to heavy quark energy loss when combined with elastic scattering is able to explain the results agreeably [22].

In our calculations, radiative corrections are included in form of time-like branching of the probe charm into a final charm and a shower of radiated partons. The basic idea is that during a binary scattering the outgoing partons may acquire some virtuality. These partons are allowed to radiate a shower of partons until their virtuality decreases to some preassigned cutoff value, μ_0^2 ($\approx M_C^2$ for charm quarks). The probability for time-like branching($b \rightarrow cd$), where a parton of time-like virtual mass, M_b^2 , decays into partons c, d with $M_{c,d}^2 < M_b^2$ and having fractions z and $z(1 - z)$ respectively, of momentum, ' p_b ', of the parent parton and requires to follow the kinematics,

$$M_b^2 = \frac{M_c^2}{z} + \frac{M_d^2}{(1-z)} + \frac{k_\perp^2}{z(1-z)}, \quad (6.10)$$

The time-like branching probability are associated with Altarelli-Parisi splitting function, $P_{b \rightarrow cd}(z)$, which is defined as

$$P_{b \rightarrow cd}(z) \equiv P_{Q \rightarrow Qg}(z) = \frac{4}{3} \frac{1+z^2}{1-z}, \quad (6.11)$$

Finally the Sudakov time-like radiative factor is given by,

$$T_a(Q^2, \mu_0^2) = \exp \left[- \int_t^{Q^{max}} dQ^2 \frac{\alpha_s(Q^2)}{2\pi} \int dz P_{b \rightarrow cd}(z) \right] \quad (6.12)$$

which is then put into Eqn. 6.4 to get the final matrix elements.

Let us now move to another aspect of gluon radiation off heavy quarks. Any quark subjected to multiple collision may radiate a shower of partons as we discussed earlier. However emission of multiple partons within a certain length scale may lead to a reduction of the bremsstrahlung cross-sections which we can briefly discuss here. This reduction in emitted gluon spectrum is known as Landau Pomeranchuk Migdal (LPM) effect [26]. This arises from the fact that if the formation time of an emitted gluon, τ_f , after a $Qq(Qg)$ scattering is larger than the typical mean free path, λ , of the heavy quark itself, then a gluon emitted from the next scattering centre may interact coherently with the initial gluon. This interference of emitted gluons may continue if there are a number of scattering centres before the shower of gluons dissociates itself completely from the emitting parton. This is different from Bethe-Heitler (BH) [27] case where all the emitted gluons are assumed to be incoherent and by construction are independent of each other.

The formation time of an emitted parton is τ_f ,

$$\tau_f = \frac{2\omega}{k_{\perp}^2}. \quad (6.13)$$

If $\tau_f > \lambda$, then the number of coherent scattering centres is found by Baier et al (BDMPS) to be [28]

$$N_{coh} = \frac{\tau_f}{\lambda} \sim \sqrt{\frac{\omega}{\mu^2 \lambda}}, \quad \mu^2 = \langle k_{\perp}^2 \rangle. \quad (6.14)$$

For $\omega \gg \mu^2 \lambda$, $N_{coh} > 1$, it can be shown that

$$\omega \frac{dI_{LPM}}{d\omega dz} = \omega \frac{dI_{BH}}{d\omega dz} \cdot \frac{1}{N_{coh}}. \quad (6.15)$$

This implies a typical suppression of emitted gluon spectrum in case of coherent(LPM) emission when compared to incoherent(BH) gluon distribution. The incoherent gluon distribution is approximately given by,

$$\omega \frac{dI_{BH}}{d\omega dz} \sim \frac{\alpha_s}{\lambda} \quad (6.16)$$

It has been found that there exists a certain critical length, $L_{cr} = \lambda \sqrt{\frac{E}{\mu^2 \lambda}}$, where E is the probe charm energy. For a distance, $L > L_{cr}$, traveled by the charm, the average energy loss by charm can be shown as:

$$\begin{aligned} -\Delta E_{LPM} &= \int dz \int d\omega \frac{dI_{LPM}}{d\omega dz}, \\ &\simeq \frac{\alpha_s L}{\lambda} \sqrt{\frac{\mu^2}{\lambda}} E, \\ &\propto \sqrt{E}. \end{aligned} \tag{6.17}$$

This implies that the average energy loss by a heavy quark in the case of LPM radiative loss is less than that of BH where $\Delta E_{BH} \propto E$ instead.

However for $L < L_{cr}$, the energy loss by the probe is found to be

$$\begin{aligned} -\Delta E_{LPM} &\simeq \int dz \sqrt{\frac{\mu^2}{\lambda} \omega_f}, \quad \omega_f = \frac{\mu^2 L^2}{\lambda} \\ &\propto L^2 \end{aligned} \tag{6.18}$$

which shows a strong quadratic dependence of ΔE on length traversed by probe or system size.

Gluon bremsstrahlung from heavy quarks differ from light quark. Emission of gluons by heavy quarks at very small angles is suppressed compared to light quarks. This phenomenon is commonly called the Dead Cone effect [29]. Mathematically this is given by a certain dead cone factor, which can be obtained from emitted gluon distributions from light(q) and heavy quarks(Q) as:

$$\begin{aligned} \omega \frac{dI_q}{d\omega} &= \frac{\alpha_s C_F}{\pi} \frac{dk_{\perp}^2}{k_{\perp}^2}, \\ \omega \frac{dI_Q}{d\omega} &= \frac{\alpha_s C_F}{\pi} \frac{k_{\perp}^2 dk_{\perp}^2}{(k_{\perp}^2 + \omega^2 \theta_0^2)^2}, \quad \text{where, } \theta_0^2 = \frac{M_Q}{E_Q} \end{aligned} \tag{6.19}$$

Now from ratio of the above two gluon distributions, it can be shown for small angle approximation, $k_{\perp} \approx \omega \theta$ that

$$dI_Q = dI_q \left(1 + \frac{\theta_0^2}{\theta^2}\right)^{-2} \tag{6.20}$$

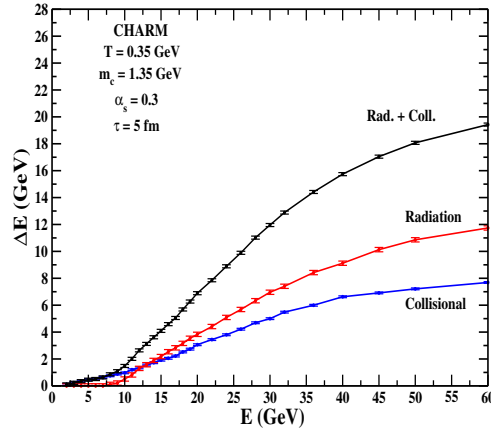


Figure 6.1: Energy loss for different initial energies after 5 fm/c of propagation.

where we may define,

$$\mathcal{D} = \left(1 + \frac{\theta_0^2}{\theta^2}\right)^{-2} \quad (6.21)$$

to be the dead cone factor. The dead cone term is intrinsically present in all $2 \rightarrow 3$ processes namely $Qg \rightarrow Qgg$, $Qq \rightarrow Qqg$ etc., matrix elements as shown earlier by [30].

Radiative energy loss via LPM effect has been calculated earlier for heavy quarks by [30, 31]. The LPM effect in radiative corrections to charm quark energy loss has been utilized to describe the observed suppression of single non-photonic electrons [12].

The Higher-Twist matrix approach for gluon radiations can give LPM effect, too. The HT matrix elements integrate over all the multiple collision interference effects up to the order of process used in the calculations. In VNI/BMS calculations, a leading order approximation of this effect has been assumed and is being treated dynamically. The LPM mechanism has been formulated in terms of Monte Carlo simulation by [32] and has been used by [33] for gluons and light quarks. In the present work similar techniques are used to calculate the energy loss of charm quark via radiation(bremsstrahlung) and added to the collisional(elastic) loss to obtain the average energy loss, momentum broadening per unit length, \hat{q} and energy loss per unit length traversed.

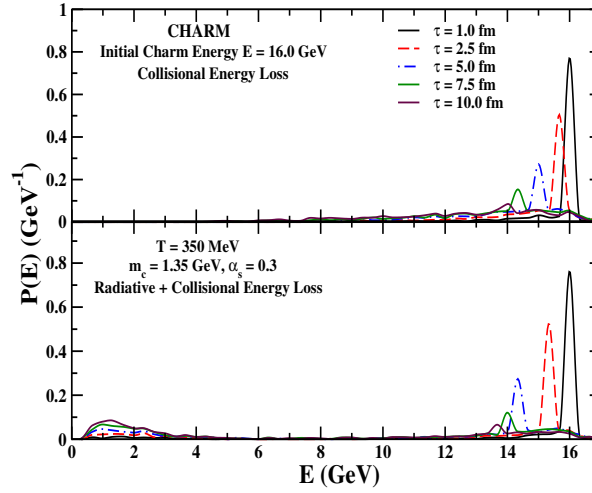


Figure 6.2: Energy profile for 16 GeV charm for different time

6.2 Results and Discussions

In our calculations we have set the strong coupling constant to a fixed value of $\alpha_s = 0.3$ to allow comparison with analytical calculations and other transport models. The temperature is set to $T=350$ MeV, which is roughly the average temperature of the QGP phase attained at RHIC energies. The mass of charm is taken as $M_c = 1.35$ GeV.

In 6.1, we show energy loss, ΔE , of charm quark over a given path length ($\tau \approx L \sim 5fm/c, c \sim 1$ in this case). For discussions on path length dependence of energy loss evolution, other figures in this paper will be referred soon.

Now let us return to 6.1 for specific discussions. The loss due to elastic scattering, gluon radiation and total loss due to both are shown separately in the same figure. We find that collisional loss dominates over radiation up to $7-12$ GeV, and beyond this elastic loss shows a tendency to decrease while radiation enhances and finally dominates the picture. However the radiation too appears to decrease for very high energy charms. We feel that as momentum of charm increases, the no. of elastic scattering tends to saturate so that average collisional energy loss becomes almost constant for all higher energy charms. Also as kinetic energy

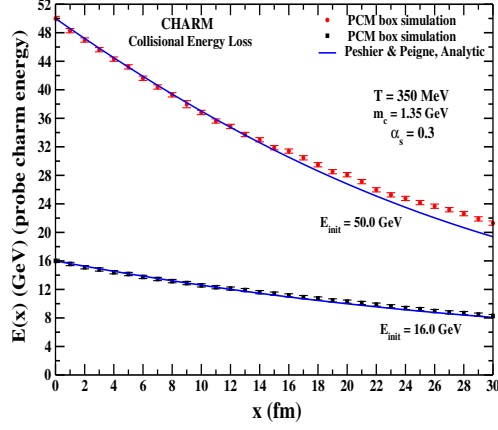


Figure 6.3: Energy of probe charm with distance traveled for elastic scattering only

of charm is increased, medium induced gluon radiation increases, making it the dominant energy loss mechanism at high energies. But let us recall that in our case, radiation takes place only after elastic scattering, and as the no. of scattering saturates ultimately, so does the radiative loss for very high energy charm quarks.

In [8], it has been discussed that for small coupling, α_s , collisional loss tends to dominate for low and intermediate energy charm (for $\gamma v_Q \sim 1$, $\gamma = (1 - \beta^2)^{-1/2}$) while for higher energetic heavy quarks we have bremsstrahlung (for $\gamma v_Q \sim 1/g$, $g = \sqrt{4\pi\alpha_s}$) dominating over collisional energy-loss. Other discussions on the topic are given in [34].

In 6.2 we show the energy profile of a 16 GeV charm after several time intervals of propagation through the thermal medium. Here $P(E)$ can be defined as $= \frac{1}{N} \frac{dN}{dE}$. The energy loss due to collisional and collisional+radiative processes is shown separately in the same figure. The collisional loss (upper panel) shows a shift in the position of the peak with long tail like structure extending towards the low energy regions. A recent study of charm quark energy profile using a Langevin equation along with a hydrodynamical background has instead shown a more Gaussian like distribution [35]. Some other discussions on the differences between Boltzmann and Langevin equations for heavy quark dynamics are also given in [35]. Additionally we find that inclusion of radiative corrections brings about a significant change

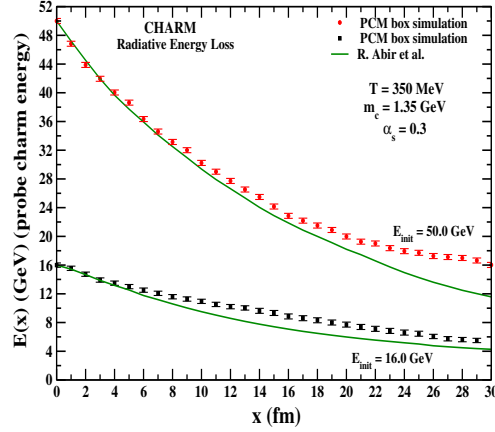


Figure 6.4: Energy of probe charm with distance traveled for radiative energy loss only

in the profile and indicates that for high energy charm quarks the effect of radiative loss is much greater than collisional loss, with the bulk of 16.0 GeV charm quarks ultimately shifting to very low energy (< 2.0 GeV) regions after 10 fm.

Next we study the evolution of charm quark energy as a function of distance traveled through the medium in 6.3 and 6.4. The calculation uses two different initial energies (16 GeV and 50 GeV respectively) for charm. Collisional loss and radiative loss are shown in these two figures separately – the radiative energy-loss figure was obtained by subtracting the elastic energy-loss calculation from the full calculation that included collisional+radiative energy-loss. We would like to elucidate the fact that these two diagrams show energy of charm quark after each ' fm ' of path length traversed and shows the path length behaviour of charm quark. These plots also give the total energy loss of charm and shouldn't be confused with average behaviour shown in 6.1.

Now let us discuss Figs. 6.3 and 6.2 in detail. The curves for the 50 GeV charm quarks show a clear distinction between the radiative and collisional energy-loss mechanisms: whereas the collisional energy-loss shows initially a linear behavior, the radiative energy-loss leads to a much stronger, near quadratic, fall-off in the energy for the first 20 fm/c. For the charm quarks with an initial energy of 16 GeV the differences are far less pronounced, but even

here a ratio between the two curves would yield interesting differences. For both cases, we compare our results to analytical calculations of dE/dx . For collisional loss we have used an analytical form calculated by Peshier and Peigne [36] which can be written as:

$$\frac{dE}{dx} = \frac{4\pi\alpha_s^2 T^2}{3} \left[\left(1 + \frac{N_f}{6}\right) \ln \frac{E_p(x)T}{\mu_D^2} + \frac{2}{9} \ln \frac{E_p(x)T}{M_c^2} + c(N_f) \right] \quad (6.22)$$

Both for our PCM calculation as well as for the analytical expression we have used the following values for the parameters in order to compare the two. They are: a medium temperature of $T=350$ MeV (applicable for RHIC-QGP system), a charm mass of $M_c=1.35$ GeV, no. of flavours and colours, $N_f=4$, $N_c=3$, a fixed coupling strength of $\alpha_s = 0.3$, and a screening mass $\mu_D = \sqrt{(2N_c + N_f)/6gT}$. We find that for the above set of parameters, the PCM results show good agreement to the predictions from the analytical expression, validating our computational setup and approach.

Next we move over to results on charm quark radiative energy loss 6.4. The radiative energy loss is compared to an analytical calculation by R. Abir et al [37] shown below:

$$\begin{aligned} \frac{dE}{dx} &= 24\alpha_s^3 \left(\rho_q + \frac{9}{4}\rho_g \right) \frac{1}{\mu_g} (1 - \beta_1) \\ &\times \left(\frac{1}{\sqrt{(1 - \beta_1)}} [\log(\beta_1)^{-1}]^{1/2} - 1 \right) \mathcal{F}(\delta) \end{aligned}$$

where

$$\begin{aligned}
\mathcal{F}(\delta) &= 2\delta - \frac{1}{2} \log \left(\frac{1 + M_c^2 e^{2\delta/s}}{1 + M_c^2 e^{-2\delta/s}} \right) \\
&\quad - \frac{M_c^2 \cosh \delta/s}{1 + 2M_c^2 \cosh \delta/s + M_c^4/s^2}, \\
\delta &= \frac{1}{2} \log \left[\frac{\log \beta_1^{-1}}{(1 - \beta_1)} \left(1 + \sqrt{1 - \frac{(1 - \beta_1)^{1/2}}{[\log \beta_1^{-1}]^{1/2}}} \right)^2 \right], \\
s &= E^2(1 + \beta_0)^2, \quad \beta_1 = \frac{g^2 T}{C E}, \quad \beta_0 = (1 - M_c^2/E^2)^{1/2}, \\
C &= \frac{3}{2} - \frac{M_c^2}{4ET} + \frac{M_c^4}{48E^2T^2\beta_0} \log \left[\frac{M_c^2 + 6ET(1 + \beta_0)}{M_c^2 + 6ET(1 - \beta_0)} \right]
\end{aligned} \tag{6.23}$$

As in the elastic energy-loss case, we have used identical values for parameters in the PCM calculation and in the analytic case, such as $T = 350$ MeV, $M_c = 1.35$ GeV, $\alpha_s = 0.3$, $N_f = 4$, $N_c = 3$ and $\mu_D = \sqrt{(2N_c + N_f)/6gT}$.

Note, however, that the calculations of [37] is carried out in the Bethe-Heitler limit of radiative energy loss with the effects of the dead-cone formalism being explicitly included in the calculation. The authors of [37] state that the LPM effect if added would only affect a marginal change in the final gluon emission spectrum which is clearly not what our results suggest. The PCM simulation explicitly takes the LPM effect into account as discussed in the previous sections. We do find that our simulation results for coherent gluon emission of charm quarks agrees reasonably well to that of the analytical calculation upto $x = 5$ – 6 fm, supporting the claim that modifications to the heavy-quark emission spectrum due to the LPM effect for this particular medium length, are modest. For $x > 6$ fm, however, the simulation result involving LPM effect and analytical curve in the BH limit move apart from each other. When we change the energy of charm probe, E_c , from 16 GeV to 50 GeV, the differences between BH and LPM radiative mechanisms increase and become more profound and visible. This may be indicative of the rising importance of the coherent gluon emission effects at higher charm quark energies.

Overall we are confident that the comparison and agreement between PCM and the analytical calculations validates the PCM approach to heavy-quark energy loss and allows us to utilize the PCM for observables and calculations that are beyond the scope of analytical approaches, e.g. in the rapidly evolving non-equilibrium domain of ultra-relativistic heavy-ion collisions.

Next let us move over to our calculation of transverse momentum broadening per unit length of charm quarks also known as the transport coefficient \hat{q} [38, 39]. In other words $\langle \hat{q} \rangle$ is a jet-quenching parameter calculated as a measure of momentum broadening within various energy loss models. Also the term 'transverse' refers to the direction perpendicular to the original direction of propagation and consequently for a jet of partons in the medium, the average or mean momentum of the jet remains unchanged while the momenta of each parton show broadening resulting in the redistribution of the transverse momentum spectrum of the jet partons. Some recent calculations have suggested values of this coefficient ranging from 0.5–20 GeV²/fm [40] for light quarks. For heavy quarks, it was calculated in [41] which showed the value of $\hat{q} \sim 0.3\text{--}0.7$ GeV²/fm. More detailed discussions and recent results on \hat{q} of partons and heavy quarks can be found in [42, 43].

Generally, the transport coefficient \hat{q} can be defined as:

$$\frac{d(\Delta p_T^2)}{dx} = \hat{q} = \rho \int d^2q_\perp q_\perp^2 \frac{d\sigma}{d^2q_\perp} \quad (6.24)$$

where $\frac{d\sigma}{d^2q_\perp}$ is the differential scattering cross-section of Q with medium quarks and gluons.

In case of a Monte Carlo simulation this definition can be rewritten as:

$$\hat{q} = \frac{1}{l_x} \sum_{i=1}^{N_{coll}} (\Delta p_{T,i})^2 \quad (6.25)$$

For $T = 350$ MeV and the probe charm energy of 16 GeV, we find \hat{q} to be 1.2 GeV²/fm with an uncertainty of ± 0.2 GeV²/fm, while for charm energy of 50 GeV \hat{q} is calculated to be 1.1 GeV²/fm with ± 0.3 GeV²/fm uncertainty. Due to the rather large statistical uncertainty in our \hat{q} extraction, we cannot make any statements regarding the energy-dependence of \hat{q} at this time. Our results do suggest a range of values for \hat{q} somewhere between 1–1.5 GeV²/fm for the RHIC system.

6.3 Summary

The present work aims to validate the applicability of Parton Cascade Model in case of heavy quark. A benchmark for heavy quark using microscopic Boltzmann transport equation has been set under controlled conditions. However we have to check the consistency of our calculations under stringent conditions before utilizing the model fully for heavy quarks. In the present work we also find that our calculations of Parton Cascade Model give us results which can be statistically improved, for charm quark energy evolution in a infinite QGP like medium at a fixed temperature. The energy loss spectra as calculated from the simulation agree considerably to some recent analytical results. Henceforth we will set out to study charm and bottom quark evolution as well as QGP medium responses at different collider energies. As a next series of calculations, we can take a set of different temperatures, to calculate the effect of heavy quark energy loss on its p_T spectra, correlations, transport coefficients etc. These aspects will be addressed in our future publications.

Bibliography

- [1] J. C. Collins and M. J. Perry, Phys. Rev. Lett. **34**, 1353 (1975); L. D. McLerran and B. Svetitsky, Phys. Lett. **B 98**, 195 (1981).
- [2] K. Kajantie, C. Montonen and C. Pietarinen, Zeit. Phys. **C 9**, 253 (1981); R. Hagedorn and J. Rafelski, Phys. Lett. **B 97**, 180 (1980).
- [3] J. W. Harris and B. Müller, Ann. Rev. Nucl. Part. Sci. **41**, 96 (1996); B. Müller, Rep. Prog. Phys. **58**, 611 (1998).
- [4] S. A. Bass, M. Gyulassy, H. Stöcker and W. Greiner, J. Phys. **G: Nucl. Part. Phys.** **25**, R1 (1999).
- [5] A. Drees, Nucl. Phys. **A 698**, 331 (2002); E. Shuryak, Nucl. Phys. **A 750**, 64 (2005); S. Jeon and G. D. Moore, Phys. Rev. **C 71**, 034901 (2005).
- [6] X-N. Wang, Nucl. Phys. **A 750**, 98 (2005); A. K. Chaudhuri, Phys. Lett. **B 659**, 531 (2008); David d'Enterria and B. Betz, Lect. Notes Phys. **785**, 285 (2010).
- [7] A. Adare et al. (PHENIX Collaboration), Phys. Rev. Lett. **98**, 172301 (2007); B. I. Abelev et al. Phys. Rev. Lett. **98**, 192301 (2007); B. Abelev et al (ALICE Collaboration), arXiv:1203.2160v1[nucl-ex]2012.
- [8] G. Moore and D. Teaney, Phys. Rev. **C 71**, 064904 (2005); S. Cao and S. A. Bass, arXiv:1209.5405v1[nucl-th] 2012.
- [9] S. Mazumder and J. Alam, Phys. Rev. **C 85**, 044918 (2012) and references therein.

- [10] C. M. Ko and W. Liu, Nucl. Phys. A **783**, 23c (2007).
- [11] Y. Akamatsu, T. Hatsuda and T. Hirano, Phys. Rev. C **79**, 054907 (2009).
- [12] S. Mazumder, T. Bhattacharyya, J. Alam, S. K. Das, Phys. Rev. C **84**, 044901 (2011).
- [13] S. Cao and S. A. Bass, J. Phys. G: Nucl. Part. Phys. **40**, 085103 (2013); arXiv:1209.5410[nucl-th]2012; M. Younus and D. K. Srivastava, J. Phys. G: Nucl. Part. Phys. **39**, 095003 (2012).
- [14] P. B. Gossiaux, J. Aichelin, T. Gousset, Acta. Phys. Polon. **B 43**, 655 (2012); A. Meistrenko, A. Peshier, J. Uphoff, C. Greiner, Nucl. Phys. A **901**, 51 (2013).
- [15] K. Geiger and B. Müller, Nucl. Phys. **B 369**, 600 (1992).
- [16] B. Zhang, M. Gyulassy and C. M. Ko, Phys. Lett. **B 455**, 45 (1999).
- [17] C. M. Ko, B-W. Zhang and L-W. Chen, J. Phys. **G 34**, S413 (2007); J. Uphoff, O. Fochler, Z. Xu and C. Greiner, Phys. Rev. C **82**, 024907 (2010); O. Fochler, Z. Xu and C. Greiner, Phys. Rev. C **82**, 044906 (2010).
- [18] S. A. Bass, B. Müller and D. K. Srivastava, J. Phys. G: Nucl. Part. Phys., **30**, S1283 (2004); D. Y. Chang, S. A. Bass and D. K. Srivastava, J. Phys. G: Nucl. Part. Phys., **31**, S1005 (2005).
- [19] G. R. Shin, S. A. Bass, B. Müller, J. Phys. G :Nucl. Part. Phys. **37**, 105112 (2010); C. E. Coleman-Smith, G-Y. Qin, S. A. Bass, arXiv:1108.5662v1[hep-ph]2011.
- [20] C. E. Coleman-Smith, B. Müller, arXiv:1210.3377v1[hep-ph] 2012.
- [21] B. L. Combridge, Nucl. Phys. **B 151**, 429 (1979); B. Svetitsky, Phys. Rev. **D 37**, 2484 (1988).
- [22] N. Armesto et al., Phys. Lett. **B 637**, 362 (2006); H. Van Hees, V. Greco and R. Rapp, Phys. Rev. C **73**, 034913 (2006); J. Uphoff, O. Fochler, Z. Xu and C. Greiner, Acta. Phys. Pol. **B 5**, 555 (2012).

- [23] M. Thoma and M. Gyulassy, Nucl. Phys. **B 351**, 491 (1991).
- [24] P. B. Gossiaux and J. Aichelin, arXiv:0802.2525v2[hep-ph] 2008.
- [25] G. Altarelli and G. Parisi, Nucl. Phys. **B 126**, 298 (1997); G. Altarelli, Phys. Rep. **81**, 1 (1982); M. Bengtsson and T.Sjöstrand, Nucl. Phys. **B**, 289, 810 (1987).
- [26] L. D. Landau and I. Pomeranchuk, Dokl. Akad. Nauk. Ser. Fiz. **92**, 535 (1953); Dokl. Akad. Nauk. Ser. Fiz. **92**, 735 (1953)(In Russian); A. B. Migdal, Phys. Rev. **103**, 6 (1956).
- [27] H. Bethe and W. Heitler, Proc. Royal Soc. London, series A, **46**, 83 (1934); L. I. Schiff, Phys. Rev. **83**, 252 (1951); R. Baier, Y. L. Dokhshitzer, S. Peigne and L. I. Schiff, Phys. Lett. **B 345**, 277 (1995).
- [28] R. Baier, Y. L. Dokhshitzer, A. H. Mueller, S. Peigne, and D. Schiff, Nucl. Phys. **B 478**, 577 (1996); R. Baier, Y. L. Dokhshitzer, A. H. Mueller, S. Peigne, and D. Schiff, Nucl. Phys. **B 483**, 291 (1997).
- [29] Y. L. Dokhshitzer and D. E. Kharzeev, Phys. Lett. **B 519**, 199 (2001); R. Thoma, B. Kämpfer and G. Soff, arXiv:hep-ph/0465189v1, 2004.
- [30] R. Abir, C. Greiner, M. Martinez, M. G. Mustafa and J. Uphoff, Phys. Rev. D **85**, 054012 (2012).
- [31] B-W. Zhang, E. Wang and X-N. Wang, Phys. Rev. Lett. **93**, 072301 (2004); M. G. Mustafa, D. Pal, D. K. Srivastava and M. Thoma, Phys. Lett. B **428**, 234 (1998).
- [32] K. C. Zapp, J. Stachel, U. A. Wiedemann, Nucl. Phys. **A 830**, 171c (2009).
- [33] C. E. Coleman-Smith, S. A. Bass, D. K. Srivastava, Nucl. Phys. **A 862**, 275 (2011).
- [34] P. B. Gossiaux, J. Aichelin, T. Gousset and V. Guiho, J. Phys. G **37**, 094019 (2010); J. D. Jackson, Classical Electrodynamics, 3rd Ed., John Wiley and Sons Pvt. Ltd. (2007).

- [35] S. Cao, G-Y. Qin, S. A. Bass and B. Müller, Nucl. Phys. **A 904**, 653c (2013).
- [36] S. Peigné and A. Peshier, arXiv:0802.4362v1[hep-ph] 2008.
- [37] R. Abir, U. Jamil, M. G. Mustafa, D. K. Srivastava, Phys. Lett. **B 715**, 183 (2012).
- [38] R. Baier and Y. M-Tani, Phys. Rev. **C 78**, 064906 (2008).
- [39] T. Renk, arXiv:1004.0809v1[hep-ph] 2010; C. E. Coleman-Smith and B. Müller, arXiv:1209.3328v1 [hep-ph] 2012.
- [40] F. Arleo, JHEP **09**, 015 (2006); R. Baier and D. Schiff, JHEP **09**, 059 (2006).
- [41] P. Romatschke, Phys. Rev. **C 75**, 014901 (2007).
- [42] M. Gyulassy, P. Levai and I. Vitev, Phys. Rev. Lett. **85**, 26 (2000); Nucl. Phys. **B 571**, 197 (2001); Nucl. Phys. **B 594**, 371 (2001); N. Armesto, C. A. Salgado and U. A. Wiedemann, Phys. Rev. **D 69**, 114003(2004); F. D'Eramo, H. Liu and K. Rajagopal, Phys. Rev. **D 84**, 06015 (2011); A. Majumder, B. Müller and S. Mrówczyński, Phys. Rev. **D 80**, 125020 (2009); R. Baier, D. Schiff and B. G. Zakharov, Annu. Rev. Nucl. Part. Sci. **50**, 37 (2000); A. Kovner and U. A. Wiedemann, arXiv:hep-ph/0304152v1 2003; P. Arnold and W. Xiao, Phys. Rev. **D 78**, 125008 (2008).
- [43] U. A. Wiedemann, arXiv:0908.2306v1[hep-ph] 2009; A. Majumder and M. Van Leeuwen, Prog. Part. Nucl. Phys. **66**, 41 (2011); S. Mazumder, T. Bhattacharyya and J. Alam, Phys. Rev. **D 89**, 014002 (2014).

Chapter 7

Summary and Outlook

In this final chapter I will talk about general outlook and future prospects with heavy quarks before winding up my writing. This thesis aims to provide a study of heavy quark dynamics in relativistic heavy ion collision using some simple and basic mathematical models. To begin with, in the chapters 1 and 2, I have tried to explain briefly the basic concepts of Quantum Chromodynamics and Quark Gluon Plasma. These two chapters serve as the motivation for studying heavy quark dynamics.

In chapter-3, detail calculations and results on single particle transverse momentum distribution of heavy quarks produced in heavy ion collision were shown. Various mechanisms of heavy quark production such as prompt production, production from interaction of jet partons among themselves, or from interaction of jet with the thermally equilibrated medium or from interaction among thermally equilibrated system, have been discussed. Another extreme case shown in the chapter is heavy quarks production from interaction among free streaming partons, where we have excluded the condition of thermal equilibration. We also studied these production schemes with two different set of parameters, one with very early thermalization of $\tau_i < 0.1$ fm/c and another with thermalization time, 0.5 fm/c and also undertook two different final times upto which jet-jet interaction can take place, one with $\tau_f \sim 0.5$ fm/c, which gives the proper preequilibrium contribution and another an extreme case when interaction jets reach the surface of the system given by $\tau_f \sim R_T/c$, R_T being

the system size. Calculations were done for both top RHIC and LHC energies. In any case prompt production of heavy quark seems to be the dominant mechanism. Only jet-jet production can match with the prompt production at the top LHC energy. However, the results were shown only for most central collision and hence the centrality dependence of these production mechanisms must be checked. Again the calculations were done assuming that the medium doesn't expand in the transverse direction. So the transverse expansion of the medium must also be included to obtain a more realistic scenario.

The single particle distributions of heavy quark is particularly important in understanding any medium effect on its spectra observed generally through nuclear modification factor, ' R_{AA} ' and elliptic flow, ' v_2 '. Any suppression of jet p_T spectra observed through R_{AA} indicates the formation of hot and dense partonic system.

Chapter 4 also deals with heavy quark production mechanisms but through the study of $Q\bar{Q}$ correlation of quark pair azimuthal angle difference, $\Delta\phi$ in transverse momentum plane, or correlation in pair rapidity difference, Δy or pair transverse momentum distribution, $p_{TQ\bar{Q}}$ etc. Correlation study is emerging as a vital observable since it clearly reflects the differences between leading order and next-to-leading order processes in the particle spectra. Again any change in these correlation spectra especially azimuthal correlation due to passage of $Q\bar{Q}$ through medium can be treated as a definite signal of QGP.

Both chapter 3 and chapter 4 show the calculations of $Q\bar{Q}$ cross-sections using only CTEQ51 and CTEQ5M structure functions. More recent parton distributions functions like CTEQ6M or CTEQ6.6 etc. must be used for up-to-date results. Again more recent nuclear shadowing functions such as EPS09 must be used.

Chapter 5 shows the calculations of energy loss of charm quark via momentum loss per collision based on a recent model of multiple scattering of probe parton with the medium partons. The calculations were done in detail and suppression of heavy quarks calculated and shown through R_{AA} of single non-photonic electrons and D mesons at both RHIC and LHC energies. Similarly the calculations were extended to calculate azimuthal anisotropy, v_2 and azimuthal correlation of $D\bar{D}$. Three different mechanisms of momentum loss per

collision were studied with first one corresponds to momentum loss which is always constant for any initial charm momentum, the second one corresponds to momentum loss proportional to momentum of charm (analogous to Bethe-Heitler energy loss) and third one corresponds to momentum loss proportional to square-root of the initial charm momentum (analogous to Landau-Pomeranchuk-Migdal (LPM) type energy loss). The three mechanisms showed different nature of spectra of R_{AA} and v_2 . Bethe-Heitler (BH) type mechanism showed an agreement with experimental data up to mid- p_T range. On other hand the rising trend in the R_{AA} at high momentum region can be explained using LPM type energy loss mechanism. The differences between BH and LPM types of energy loss can be observed in azimuthal correlation spectra shown in the chapter. Also transport coefficient corresponding to drag experienced by charm in QGP was calculated using our model and compared with some literatures where only soft collisions of charm quark with QGP partons were considered. Our calculations showed almost 2–4 times increase in the effective drag coefficient when compared with only soft collisions.

Now let us move over to chapter 6, where I studied charm quark dynamics using Parton Cascade Model which is based on Boltzman Transport Equation. The scattering cross-sections are based on pQCD calculations of charm quark interaction with gluons or light quarks matrix elements. An debye screened cross-section are used to regulate infrared divergences. Both collisional and radiative energy loss of charm quark are included. The calculations serve to study charm quark evolution in QGP like infinite medium at fixed temperatures. The advantage of using transport equation is that in such scheme probe quark dynamics can be studied without assuming any equilibration condition. The probe's space-time evolution can be tracked and its energy loss, momentum broadening and other transport coefficients can be evaluated. However the calculations were done for charm evolution in infinite thermal medium at fixed temperatures. Here we need an scheme for expanding medium to be included in our formalism to get more realistic picture.

Appendix A:

The general expression for the production of a heavy quark at central rapidity is given by:

$$\begin{aligned}
 E \frac{d^3 N}{d^3 p} \Big|_{y=0} &= \int d^4 x \int \frac{1}{16(2\pi)^8} \frac{d^3 p_1 d^3 p_2 d^3 p'}{\omega_1 \omega_2} \\
 &\times \delta^4 \left(\sum p^\mu \right) / E' \\
 &\times |M|^2 F(\vec{x}, \vec{p}_1, t) F(\vec{x}_2, \vec{p}_2, t)
 \end{aligned}
 \tag{A.1}$$

where $\sum p^\mu = p_1 + p_2 - p - p'$, p_1 and p_2 are the four-momenta of the incoming partons and p and p' are the same for outgoing heavy quark and anti-quark. $F(\vec{x}, \vec{p}, t)$ gives the phase space distribution function for the incoming partons.

we can perform the following simplifications:

Writing $d^3 p_i / \omega_i = p_{T_i} dp_{T_i} d\phi_i dy_i$ and integrating over $d^3 p'$, we get for $y=0$ ($p_z=0$, and $p_T=p$):

$$\begin{aligned}
 &\int \frac{d^3 p_1 d^3 p_2 d^3 p'}{\omega_1 \omega_2 E'} \delta^4 \left(\sum p^\mu \right) |M|^2 F(\vec{x}, \vec{p}_1, t) F(\vec{x}, \vec{p}_2, t) \\
 &= \int dy_1 dy_2 d\phi_1 d\phi_2 p_{T2} dp_{T2} p_{T1} dp_{T1} \frac{\delta(\sum E)}{E'} |M|^2 \\
 &\quad \times F(\vec{x}, p_{T1}, \phi_1, y_1, t) F(\vec{x}, p_{T2}, \phi_2, y_2, t) ,
 \end{aligned}
 \tag{A.2}$$

where

$$\frac{\delta(\sum E)}{E'} = \frac{\delta(p_{T1} - p_{T1,0})}{[p_{T2}(\cosh(y_1 - y_2) - \cos(\phi_1 - \phi_2)) - (E \cosh y_1 - p \cos \phi_1)]} ,$$

and we have

$$p_{T1,0} = \frac{p_{T2}(E \cosh y_2 - p \cos \phi_2)}{[p_{T2}(\cosh(y_1 - y_2) - \cos(\phi_1 - \phi_2)) - (E \cosh y_1 - p \cos \phi_1)]}.$$

Now we proceed to evaluate individual contributions.

Jet-Jet interaction of partons

$$F(\vec{x}, \vec{p}, t) = f_{\text{jet}}(\vec{x}, \vec{p}, t), \quad (\text{A.3})$$

where

$$f_{\text{jet}}^i(\vec{x}, \vec{p}, t) = \frac{(2\pi)^3}{g_i \tau \pi R_T^2 p_T} \frac{dN_i}{dy d^2 p_T} \delta(y - \eta) \Theta(\tau_f - \tau) \Theta(\tau - \tau_i), \quad (\text{A.4})$$

with $p_T > 2 \text{ GeV}$.

Thus we have,

$$\frac{dN}{dy d^2 p_T} = T_{\text{AA}} \frac{d\sigma^{\text{jet}}}{d^2 p_T dy} \Big|_{y=0} = K \frac{C}{(1 + p_T/B)^\beta}, \quad (\text{A.5})$$

and

$$h_{\text{jet}}^i(p_T) = \frac{1}{g_i} \frac{dN}{d^2 p_T dy} \Big|_{y=0}, \quad (\text{A.6})$$

where K , C , B , and β are taken from reference

Now taking

$$d^4 x = \tau d\tau r dr d\eta d\phi_r, \quad (\text{A.7})$$

we can perform the integration over r , ϕ_r and τ . Thus the p_T distribution of open heavy quark production from jet-jet interaction, Eqn. A.2 can be written as

$$\begin{aligned} E \frac{d^3 N}{d^3 p} \Big|_{y=0} &= \frac{\ln(\tau_f/\tau_i)}{16(2\pi)^2(\pi R_T^2)} \int d\eta dp_{T2} d\phi_1 d\phi_2 \\ &\times \left[\frac{1}{p_{T2}(1 - \cos(\phi_1 - \phi_2)) - (E \cosh \eta - p \cos \phi_1)} \right] \\ &\times \left[\frac{1}{2} g_g^2 h_{\text{jet}}^g(p_{T1,0}) h_{\text{jet}}^g(p_{T2}) |M|_{gg \rightarrow Q\bar{Q}}^2 \right. \\ &\quad \left. + g_q^2 N_f h_{\text{jet}}^q(p_{T1,0}) h_{\text{jet}}^q(p_{T2}) |M|_{q\bar{q} \rightarrow Q\bar{Q}}^2 \right], \quad (\text{A.8}) \end{aligned}$$

We note that the use of Bjorken correlations $\delta(y_1 - \eta)$ and $\delta(y_2 - \eta)$ in Eqs. A.3 and A.3 leads to

$$\frac{\delta(\sum E)}{E'} = \frac{\delta(p_{T1} - p_{T1,0})}{p_{T2}(1 - \cos(\phi_1 - \phi_2)) - (E \cosh \eta - p \cos \phi_1)}. \quad (\text{A.9})$$

and

$$p_{T1,0} = \frac{p_{T2}(E \cosh \eta - p \cos \phi_2)}{p_{T2}(1 - \cos(\phi_1 - \phi_2)) - (E \cosh \eta - p \cos \phi_1)}, \quad (\text{A.10})$$

Numerical integration of the Eq. A.8 gives pre-thermal heavy quark production

Thermal Interaction:

We take the phase space distribution for the thermalized quarks and gluons as,

$$f_{th}^i(p_T, y, \eta) = \exp[-p_T \cosh(y - \eta)/T]. \quad (\text{A.11})$$

Thus the transverse momentum distribution of thermally produced charm using Eqn. A.2 given by

$$\begin{aligned} E \frac{d^3 N}{d^3 p} \Big|_{y=0} &= \frac{\pi R_T^2}{16(2\pi)^8} \int \tau d\tau d\eta dp_{T2} d\phi_1 d\phi_2 dy_1 dy_2 \\ &\times \frac{(p_{T2} p_{T1,0})}{[p_{T2}(\cosh(y_1 - y_2) - \cos(\phi_1 - \phi_2)) - (E \cosh y_1 - p \cos \phi_1)]} \\ &\times [f_{th}(p_{T1,0}, y_1, \eta) f_{th}(p_{T2}, y_2, \eta)] \times \left[\frac{1}{2} g_g^2 |M_{gg \rightarrow \bar{Q}Q}|^2 + g_q^2 N_f |M_{q\bar{q} \rightarrow \bar{Q}Q}|^2 \right] \end{aligned} \quad (\text{A.12})$$

Just as in pre-thermal case, we calculate the final charm production at $y=0$ or central rapidity and thus $p_z = 0$ and $p_T = p$. We now have the kinematical constraint;

$$\frac{\delta(\sum E)}{E'} = \frac{\delta(p_{T1} - p_{T1,0})}{[p_{T2}(\cosh(y_1 - y_2) - \cos(\phi_1 - \phi_2)) - (E \cosh y_1 - p \cos \phi_1)]}$$

and

$$p_{T1,0} = \frac{(p_{T2}(E \cosh y_2 - p \cos \phi_2))}{[p_{T2}(\cosh(y_1 - y_2) - \cos(\phi_1 - \phi_2)) - (E \cosh y_1 - p \cos \phi_1)]}$$

Numerical integration of the Eq. A.12 for different initial conditions gives us the contribution from thermalized QGP.

Free Streaming:

As an extreme, we consider free-streaming partons, as a model of evolution of the system of deconfined quarks and gluons, which completely relaxes the condition of thermalization. The initial distribution at $t = \tau_0$ and $z = 0$ is obtained by assuming maximum entropy, so that

$$f(p, x) = \frac{dN}{d^3p d^3x} = \exp\left(-\frac{E}{T_o}\right), \quad (\text{A.13})$$

and the condition that needs to be satisfied is

$$p^\mu \frac{\partial f(x, p)}{\partial x^\mu} = 0. \quad (\text{A.14})$$

We assume boost invariance along the z-axis with

$$f(p, x) = f(p_T, p_z t - E z). \quad (\text{A.15})$$

The solution which satisfies the differential Eq. A.14 is

$$f(p, x) = \exp\left[-\frac{\sqrt{p_T^2 + (p_z t - E z)^2/\tau_0^2}}{T_0}\right]. \quad (\text{A.16})$$

Now using

$$\begin{aligned} p_z &= p_t \sinh y, \quad E = p_t \cosh y, \\ z &= \tau \sinh \eta, \quad t = \tau \cosh \eta, \end{aligned} \quad (\text{A.17})$$

Eq. A.16 becomes

$$f(p_T, \eta, y) = \exp\left[-\frac{p_T \sqrt{1 + \tau^2 \sinh^2(y - \eta)/\tau_0^2}}{T_0}\right]. \quad (\text{A.18})$$

Thus the final integration to calculate p_T distribution for heavy quark production using Eqn. A.2 from free streaming partons is given by

$$\begin{aligned}
E \frac{d^3 N}{d^3 p} \Big|_{y=0} &= \frac{\pi R_T^2}{16(2\pi)^8} \int \tau d\tau d\eta dp_{T2} d\phi_1 d\phi_2 dy_1 dy_2 \\
&\times \frac{(p_{T2} p_{T1,0})}{[p_{T2}(\cosh(y_1 - y_2) - \cos(\phi_1 - \phi_2)) - (E \cosh y_1 - p \cos \phi_1)]} \\
&\times [f(p_{T1,0}, \eta_1, y_1) f(p_{T2}, \eta_2, y_2)] \times \left[\frac{1}{2} g_g^2 |M_{gg \rightarrow \bar{Q}Q}|^2 + g_q^2 N_f |M_{q\bar{q} \rightarrow \bar{Q}Q}|^2 \right]
\end{aligned} \tag{A.19}$$

The initial conditions for the free-streaming case are taken to be same as that for the thermal production, whereas the final time is taken as R_T/c , the transverse radius of the nuclei, after which the system would surely expand rapidly along the transverse direction as well and disintegrate.

The parameters ' C ', ' B ' and ' β ' in the parametrized form of the jet parton distribution given by,

$$\frac{dN}{dy d^2 p_T} = T_{AA} \frac{d\sigma^{\text{jet}}}{d^2 p_T dy} \Big|_{y=0} = K \frac{C}{(1 + p_T/B)^\beta}, \tag{A.20}$$

are given in the tables

Table 7.1: Parametrization of the quark and gluon distributions from initial scattering of partons at 200 GeV and 5.5 TeV in pp collisions, using LO pQCD and CTEQ5L structure functions, for $p_T > 2$ GeV.

\sqrt{s} [TeV]		C [1/GeV ²]	B [GeV]	β
0.2	u	9.113×10^2	1.459	7.679
	d	9.596×10^2	1.467	7.662
	s	1.038×10^2	1.868	8.642
	\bar{u}	2.031×10^2	1.767	8.546
	\bar{d}	2.013×10^2	1.759	8.566
	g	4.455×10^3	1.7694	8.610
5.5	u	2.209×10^4	0.5635	5.240
	d	2.493×10^4	0.5522	5.223
	s	1.662×10^3	2.174	0.9064
	\bar{u}	4.581×10^3	0.7248	5.437
	\bar{d}	4.317×10^3	0.7343	5.448
	g	1.229×10^5	0.7717	5.600

Table 7.2: Parametrization of the quark and gluon distributions from initial scattering of partons at 2.76 and 5.5 TeV in pp collisions, using LO pQCD and CTEQ5M structure functions, for $p_T > 2$ GeV.

\sqrt{s} [TeV]		C [1/GeV ²]	B [GeV]	β
2.76	u	1.078×10^3	1.127	5.615
	d	1.279×10^3	1.099	5.579
	s	1.395×10^2	1.899	6.432
	\bar{u}	3.371×10^2	1.434	5.999
	\bar{d}	3.734×10^2	1.401	5.953
	g	2.947×10^3	1.892	6.523
5.5	u	7.961×10^2	1.293	5.580
	d	9.478×10^2	1.254	5.539
	s	1.228×10^2	2.174	6.418
	\bar{u}	2.659×10^2	1.663	5.966
	\bar{d}	2.908×10^2	1.624	5.924
	g	2.449×10^3	2.192	6.519

Appendix B:

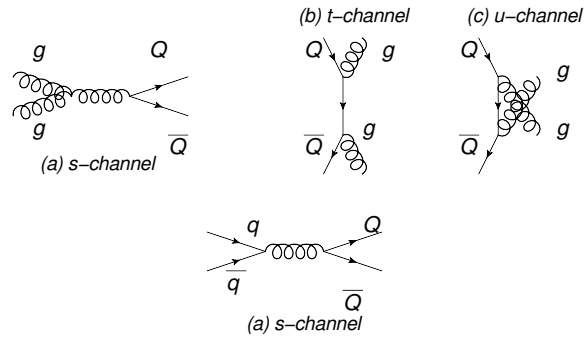


Figure B.1: Invariant Matrix elements:(top) $gg \rightarrow Q\bar{Q}$ (bottom) $q\bar{q} \rightarrow Q\bar{Q}$

The Matrix elements for heavy quark production from gluon fusion and quark-anti-quark annihilations are calculated and given $q\bar{q} \rightarrow Q\bar{Q}$

$$|\mathcal{M}|_{q\bar{q} \rightarrow Q\bar{Q}}^2 = \frac{64\pi^2\alpha_s^2}{9} \left[\frac{(M^2 - \hat{t})^2 + (M^2 - \hat{u})^2 + 2M^2\hat{s}}{\hat{s}^2} \right], \quad (\text{B.1})$$

and for $gg \rightarrow Q\bar{Q}$,

$$\begin{aligned}
|M|_{gg \rightarrow Q\bar{Q}}^2 = \pi^2 \alpha_s^2 & \left[\frac{12}{\hat{s}^2} (M^2 - \hat{t})(M^2 - \hat{u}) \right. \\
& + \frac{8}{3} \frac{(M^2 - \hat{t})(M^2 - \hat{u}) - 2M^2(M^2 + \hat{t})}{(M^2 - \hat{t})^2} \\
& + \frac{8}{3} \frac{(M^2 - \hat{t})(M^2 - \hat{u}) - 2M^2(M^2 + \hat{u})}{(M^2 - \hat{u})^2} \\
& - \frac{2}{3} \frac{M^2(\hat{s} - 4M^2)}{(M^2 - \hat{t})(M^2 - \hat{u})} \\
& - 6 \frac{(M^2 - \hat{t})(M^2 - \hat{u}) + M^2(\hat{u} - \hat{t})}{\hat{s}(M^2 - \hat{t})} \\
& \left. - 6 \frac{(M^2 - \hat{t})(M^2 - \hat{u}) + M^2(\hat{t} - \hat{u})}{\hat{s}(M^2 - \hat{u})} \right]. \tag{B.2}
\end{aligned}$$

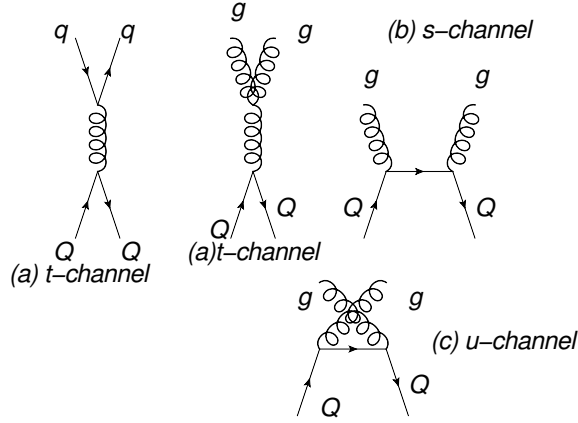


Figure B.2: Invariant matrix elements:(left) $Qq(\bar{q}) \rightarrow Qq(\bar{q})$ (right) $Qg \rightarrow Qg$

The invariant transition amplitude, $|M|^2$ for elastic scattering of heavy quark using QCD Feynman diagrams can be calculated, are shown below for $q(\bar{q})c \rightarrow q(\bar{q})c$,

$$\sum |\mathcal{M}|^2 = \frac{64\pi^2 \alpha_s^2}{9} \frac{(M_c^2 - \hat{u})^2 + (\hat{s} - M_c^2)^2 + 2M_c^2 \hat{t}}{(\hat{t} - \mu_D^2)^2}. \tag{B.3}$$

While, for $gc \rightarrow gc$,

$$\sum |\mathcal{M}|^2 = \pi^2 \alpha_s^2 [g1 + g2 + g3 + g4 + g5 + g6],$$

where,

$$\begin{aligned}
g1 &= 32 \frac{(\hat{s} - M_c^2)(M_c^2 - \hat{u})}{(\hat{t} - \mu_D^2)^2}, \\
g2 &= \frac{64}{9} \frac{(\hat{s} - M_c^2)(M_c^2 - \hat{u}) + 2M_c^2(\hat{s} + M_c^2)}{(\hat{s} - M_c^2)^2}, \\
g3 &= \frac{64}{9} \frac{(\hat{s} - M_c^2)(M_c^2 - \hat{u}) + 2M_c^2(M_c^2 + \hat{u})}{(M_c^2 - \hat{u})^2}, \\
g4 &= \frac{16}{9} \frac{M_c^2(4M_c^2 - \hat{t})}{(\hat{s} - M_c^2)(M_c^2 - \hat{u})}, \\
g5 &= 16 \frac{(\hat{s} - M_c^2)(M_c^2 - \hat{u}) + M_c^2(\hat{s} - \hat{u})}{(\hat{t} - \mu_D^2)(\hat{s} - M_c^2)}, \\
g6 &= -16 \frac{(\hat{s} - M_c^2)(M_c^2 - \hat{u}) - M_c^2(\hat{s} - \hat{u})}{(\hat{t} - \mu_D^2)(M_c^2 - \hat{u})}.
\end{aligned} \tag{B.4}$$

where the thermal mass, μ_D , of QGP medium is defined as $\mu_D = \sqrt{(2N_c + N_f)/6gT}$.